TRW

NONLINEAR OPTICS TECHNOLOGY PHASE III FINAL REPORT

VOLUME 1: SOLID STATE LASER TECHNOLOGY

J. Brock, R. Chan, L. Lembo, J. Ho, H. Injeyan, J. Machan, R. St. Pierre, R. Wagner, B. Zukowski

Sponsored By

Defense Advanced Research Projects Agency

Monitored By

Office Of Naval Research
Contract # N00014-88-C-0228

The views and the conclusions contained in this document are those of the authors and should not be interpreted as necessarily representing the official policies, either expressed or implied, of the Defense Advanced Research Projects Agency or the U.S. Government.

TRW Space And Technology Group
Applied Technology Division
One Space Park Redondo Beach, CA 90278

NONLINEAR OPTICS TECHNOLOGY PHASE III FINAL REPORT

VOLUME 1: SOLID STATE LASER TECHNOLOGY

J. Brock, R. Chan, L. Lembo, J. Ho, H. Injeyan, J. Machan, R. St. Pierre, R. Wagner, B. Zukowski

Sponsored By

Defense Advanced Research Projects Agency

Monitored By

Office Of Naval Research
Contract # N00014-88-C-0228

TRW Space And Technology Group
Applied Technology Division
One Space Park Redondo Beach, CA 90278

UNCLASSIFIED

SECURITY CLASSIFICATION OF THIS PAGE

REPORT DOCUMENTATION PAGE

1a. REPORT SECURITY CLASSIFICATION: Unclassified	1b. RESTRICTIVE MARKINGS
2a. SECURITY CLASSIFICATION AUTHORITY	3. DISTRIBUTION/AVAILABILITY OF REPORT: Unclassified/unlimited
2b. DECLASSIFICATION/DOWNGRADING SCHEDULE	
4. PERFORMING ORGANIZATION REPORT NUMBER(S)	5. MONITORING ORGANIZATION REPORT NUMBER(S)
6a. NAME OF PERFORMING ORGANIZATION: TRW-Space & Technology Group; 6b. OFFICE SYMBOL (If applicable):	7a. NAME OF MONITORING ORGANIZATION: Office of Naval Research
6c. ADDRESS (City, State and ZIP Code): One Space Park, Redondo Beach, CA. 90278	7b. ADDRESS (City, State and ZIP Code): NOSC Code 843, 271 Catalina Boulevard, San Diego, CA 92152
8a. NAME OF FUNDING/SPONSORING ORGANIZATION: DARPA; 8b. OFFICE SYMBOL (If applicable): DEO	9. PROCUREMENT INSTRUMENT IDENTIFICATION NUMBER: N00014-88-C-0228
8c. ADDRESS (City, State and ZIP Code): 1400 Wilson Boulevard, Arlington, VA 22209-2308	10. SOURCE OF FUNDING NOS. — PROGRAM ELEMENT NO.; PROJECT NO.; TASK NO.; WORK UNIT NO.
11. TITLE (Include Security Classification): NLOT Phase III Final Report: Vol. 1: Solid State Laser Technology (U)	
12. PERSONAL AUTHOR(S): D. Brock, H. Injeyan, R. Chan, L. Lembo, J. Machan, R. St. Pierre, R. Wagner & B. Zukowski	
13a. TYPE OF REPORT: Final; 13b. TIME COVERED: FROM 3/88 TO 11/90	14. DATE OF REPORT (Yr., Mo., Day): 01/12/91; 15. PAGE COUNT
16. SUPPLEMENTARY NOTATION	

17 COSATI CODES			18. SUBJECT TERMS (Continue on reverse if necessary and identify by block number)
FIELD	GROUP	SUB. GR.	solid state lasers, solid state amplifiers, phase conjugation, regenerative amplifiers, stimulated Brillouin scattering, etalon-coupled cavity

19. ABSTRACT (Continue on reverse if necessary and identify by block number)

A novel regenerative amplifier concept, suitable for extraction from low gain, high saturation fluence, solid state media has been investigated. The concept is called multipass etalon-coupled conjugated amplifier (MECCA) and uses an etalon and a SBS cell or other frequency shifting medium to form a regenerative amplifier cavity. The beam is injected into the cavity through a transmission window of the etalon and is trapped in the cavity when the frequency is shifted. The beam is extracted by encountering another transmission window after a predetermined number of round trips as it marches in frequency space.

Two MECCA configurations were tested. One uses SBS to provide the frequency shift the other uses an acousto-optic modulator. Using the SBS medium in a multipass configuration with short pulses caused rapid degradation of the SBS reflectivity and fidelity due to the thermalization of the SBS grating between pulses, which resulted in poor extraction and beam quality. Both extraction and beam quality were improved when the cavity was shortened to provide partial beam overlap in the SBS cell and sustained driving fields. Overall amplifications of a factor of 30 and beam quality of 1.8 x D.L. was obtained with beams which have

20. DISTRIBUTION/AVAILABILITY OF ABSTRACT: UNCLASSIFIED/UNLIMITED ☐ SAME AS RPT ☐ DTIC USERS ☐	21. ABSTRACT SECURITY CLASSIFICATION: Unclassified
22a. NAME OF RESPONSIBLE INDIVIDUAL: Dr. V. Smiley	22b. TELEPHONE NUMBER (Include Area Code): (619)553-6128; 22c. OFFICE SYMBOL: ONR

DD FORM 1473, 83 APR EDITION OF 1 JAN 73 IS OBSOLETE.

SECURITY CLASSIFICATION OF THIS PAGE

approximately 25% overlap. The corresponding model predicted values were a factor of 125 and 1.2 x D.L. respectively. Further performance improvements are projected if the degree of overlap is increased and the pulse lengths become much longer than the cavity round trip time.

An alternate configuration MECCA (AC MECCA) was also tested using an acousto-optic modulator as the frequency shifted medium. The beam was coupled into the cavity through a transmission window of the etalon, extracted after a predetermined number of round trips and reinjected into the cavity after phase conjugation to retrace its path. This technique eliminated SBS in a multipass configuration and provided moderate gains (a factor of 40) with good beam quality (1.3 x D.L.).

PREFACE

This document is one of three volumes which constitute the final report for the program entitled "Nonlinear Optics Technology (NLOT), Phase III", performed by TRW under contract No. N00014-88-C-0228 with the Office of Naval Research. This program was devoted to the development of nonlinear optics technology for tactical applications of directed energy. Volume 1 covers the development of phase conjugated, solid state regenerative amplifiers and is titled "Solid State Laser Technology". Volume 2 covers the development of phase conjugated atmospheric optical communication links using four wave mixing and is titled "Phase Conjugated Optical Communication Link". Volume 3, entitled "Directed Energy Utility Study" is classified and investigates the utility of directed energy systems on tactical missions.

The program was performed by TRW Space and Technology Group, Applied Technology Division, Redondo Beach, CA. The program manager was J. Brock, the contract administration was handled most efficiently by L. Meisenholder, and project control was performed by L. Tomich and A. Mittra.

The work described in this volume was conducted under the technical direction of H. Injeyan. Other personnel making important contributions to the technical effort included J. Brock, R. Chan, L. Lembo, J. Ho, J. Machan, R. St. Pierre, R. Wagner, and B. Zukowski. The technical and managerial guidance of L. Marabella and J. Berg is gratefully acknowledged; so is the superb secretarial support of P. Bessenbacher. The authors also acknowledge many useful technical discussions with M. Valley, J. Munch, and C. Clendening.

This work was administered by S. Shey and L. N. Durvasula of the DARPA Directed Energy Office and monitored by V. Smiley of the Office of Naval Research. Their support and assistance contributed greatly to the success of the program.

TABLE OF CONTENTS

1. Introduction and Summary 1
2. MECCA Concept Description 8
2.1 Concept Description 8
2.2 Requirements 8
2.3 Parameter Space 14
3. Modeling and Projected Performance 17
3.1 METALON Extraction Model 17
3.2 METALON Performance Predictions 19
3.3 BRIWON Beam Quality Model 23
3.4 BRIWON Performance Prediction 23
4. MECCA experiments 28
4.1 MECCA Cavity Demonstration 28
4.2 MECCA Experiments With Gain 32
4.3 SBS Physics and Material Considerations 42
4.3.1 Description of Stimulated Brillouin Scattering 42
4.3.2 Competing Processes 44
4.3.3 Candidate Media 46
4.3.4 Dynamic Range Measurements 47
4.4 MECCA characterization 56
4.4.1 Preliminary experiments with Freon as an SBS Medium 56
4.4.2 MECCA Cavity Characterization 60
4.4.3 MECCA Extraction 72
5. Alternate Configuration MECCA 75
5.1 Concept Description and Assessment 75
5.1.1 Design Criteria 75
5.1.2 Concept Description 76
5.3.2 Concept Assessment 76
5.2 AC MECCA Modeling And Projected Performance 81
5.3 Experiments 82
5.3.1 Modulator characterization 82
5.3.2 Cavity Description and Diagnostics 88
5.3.3 AC MECCA Demonstration and Extraction Experiments 88
6. Conclusions and recommendations 96
7. References 97

TABLE OF FIGURES

Figure 1.1	Schematic layout of several extraction techniques used with low gain, high saturation fluence media. a) Multiple stage phase conjugated MOPA, b) four pass polarization coupled phase conjugated MOPA, c) phase conjugated electro-optically switched ring regenerative amplifier.	2
Figure 1.2	Multipass etalon-coupled conjugated amplifier (MECCA) schematic layout and frequency evolution (conventional MECCA)	3
Figure 1.3	Alternate configuration MECCA (AC MECCA) schematic layout	5
Figure 2.1	Slab amplifier gain profile. The master oscillator beam samples the central 1 cm region of the slab	11
Figure 2.2	Slab amplifier gain as a function of master oscillator pulse delay time	11
Figure 2.3	Rod amplifier gain as a function of master oscillator pulse delay time	12
Figure 2.4	SBS frequency shift measurement optical layout	15
Figure 2.5	MECCA characterization parameter space	16
Figure 3.1	Summary of METALON model components and capabilities	18
Figure 3.2	Extraction efficiency of a 7 ns FWHM, temporally gaussian MO pulse as a function of the finesse in a lossless MECCA cavity (SBS reflectivity of 1)	20
Figure 3.3	METALON prediction of MECCA pulse evolution. a) intracavity pulse train immediately downstream of the etalon, b) extracted pulse train immediately upstream of the etalon	21
Figure 3.4	Summary of METALON predicted MECCA extraction efficiency. a) as a function of round trips for several single pass amplifier gains, b) as a function of round trips for several SBS reflectivities.	22
Figure 3.5	Summary of BRIWON model components and capabilities	24
Figure 3.6	BRIWON predicted three round trip MECCA output beam characteristics under a variety of conditions. a) truncated, unaberrated gaussian beam propagating between the lens and SBS medium, b) same as a) but with three meters of propagation, c) short cavity with approximately one wave of wavefront aberrations, d) one wave aberrations with 3 m propagation.	25
Figure 4.1	Optical layout for the MECCA cavity demonstration	29
Figure 4.2	SBS reflectivity and threshold in methane	30
Figure 4.3	MECCA cavity demonstration. a) intracavity oscillation, b) reference pulse reflected from the etalon and extracted pulse after four round trips	31
Figure 4.4	Summary of preliminary experiments and major results	32

Figure 4.5	Intracavity MECCA pulse train with gain using methane as the SBS medium. The pulse trains are measured in front of the SBS cell, the reflections from the SBS cell are time delayed and added to the input train so that each input pulse has its reflection next to it.	33
Figure 4.6	SBS reflectivity and threshold in acetone	35
Figure 4.7	Nearfield intensity distribution of the extracted pulse as function of the number of round trips with acetone as the SBS medium	35
Figure 4.8	Optical layout of MECCA cavity with the rod amplifier and modified to include image relaying telescopes	36
Figure 4.9	Schematic diagram of the ethane distillation apparatus	37
Figure 4.10	SBS reflectivity and threshold in ethane	39
Figure 4.11	Overall amplification using the MECCA layout shown in Figure 4.8. a) Intracavity pulse train, b) extracted pulses; the first major pulse is calibrated to match the input pulse, the second pulse is the pulse extracted after three round trips.	40
Figure 4.12	Nearfield intensity distribution of the pulse extracted after three round trips using the MECCA layout shown in Figure 4.8	41
Figure 4.13	Table of SBS media tested for MECCA and their characteristics	46
Figure 4.14	Optical layout for measuring the SBS reflectivity and fidelity dynamic range in nitrogen	48
Figure 4.15	SBS reflectivity and threshold in nitrogen	50
Figure 4.16	SBS reflectivity in nitrogen for several f/#s	50
Figure 4.17	SBS fidelity in nitrogen for several f/#s	51
Figure 4.18	SBS fidelity in nitrogen using a distributed phase plate for several amplifier rep-rates (different levels of induced aberrations)	52
Figure 4.19	Optical layout for measuring the SBS reflectivity and fidelity dynamic range in freon 113	53
Figure 4.20	SBS reflectivity in freon for two f/#s	55
Figure 4.21	SBS fidelity in freon for two f/#s	55
Figure 4.22	Optical layout for MECCA experiments using freon as the SBS medium	58
Figure 4.23	Input and reflected pulse trains from the SBS cell using the MECCA layout shown in Figure 4.23. The reflected pulses are time delayed and added to the input pulses so that each input pulse has the SBS return next to it.	59

Figure 4.24 Same data as in Figure 4.24 but with a 400 μm pinhole inserted in the vacuum spatial filter 59

Figure 4.25 Optical layout for MECCA cavity characterization 61

Figure 4.26 Effect of freon aging due to optical breakdown. a) intracavity pulse train with freon subjected to optical breakdown for several hours, b) intracavity pulse train with a fresh load of freon under identical conditions 63

Figure 4.27 Input and scattered pulse trains from the SBS cell. The scattered pulse trains have been delayed so that each input pulse train has the corresponding scattered pulse next to it with a nominal net gain of 1. a) injected energy of 5 mJ, b) injected energy of 10 mJ. 64

Figure 4.28 Input and reflected pulse trains from the SBS cell using the MECCA layout shown in Figure 4.23 without an amplifying medium. The reflected pulses are time delayed and added to the input pulses so that each input pulse has the SBS return next to it. 65

Figure 4.29 Optical layout of the two cell experiment 67

Figure 4.30 Input and reflected pulse trains from the SBS cell using the MECCA layout shown in Figure 4.23 without an amplifying medium. a) cavity round trip time 13 ns, b) cavity round trip time 10 ns 68

Figure 4.31 Reflectivity of the third pulse as a function of cavity round trip time 69

Figure 4.32 Input and scattered pulse trains from the SBS cell using the MECCA layout shown in Figure 4.23 without an amplifying medium. a) cavity round trip time 13 ns, b) cavity round trip time 10 ns 70

Figure 4.33 Optical drawing showing the effect of misaligning the etalon on beam path 71

Figure 4.34 Far-field profiles of the extracted pulse under aligned (a) and misaligned (b) etalon conditions 72

Figure 4.35 Input and reflected pulse trains from the SBS cell using the MECCA layout shown in Figure 4.23 with a nominal round trip gain of five and cavity round trip time of 12 ns. 74

Figure 4.36 Near-field intensity distribution of the 12 ns round trip cavity extracted pulse with a factor of 30 amplification 74

Figure 5.1 Schematic layout of the alternative configuration MECCA (AC MECCA) concept 77

Figure 5.2 Optical layout of a linear AC MECCA demonstration cavity 79

Figure 5.3 AC MECCA extraction efficiency as a function of AO modulator scattering efficiency in a six round trip cavity (three for each cycle) with a finesse of six and single pass amplifier gain of 4 81

Figure 5.4 Schematic layout of AO modulator characterization apparatus 83

Figure 5.5 Schematic diagram of the AO modulator driver electronics 84

Figure 5.6 Modulator diffraction efficiency as a function of peak power for several RF frequencies 86

Figure 5.7 Thermal effects in the modulator. a) far-field profile of a beam making a double pass through the modulator operating with a peak power of 80 W and average power of 1.6 W. b) same conditions as a) after the modulator is allowed to cool for five minutes. c) same conditions as a) but using a SBS cell instead of a retro-mirror to correct the induced aberrations. 87

Figure 5.8 Schematic diagram of the linear AC MECCA cavity demonstration layout 89

Figure 5.9 Intracavity optical train in the first cycle of the AC MECCA cavity shown in Figure 5.8 without gain. a) cavity is tuned for optimum injection, b) cavity is tuned for optimum extraction after the third round trip. 91

Figure 5.10 Far field intensity profile of pulses extracted from the AC MECCA cavity which is misaligned to prevent parasitic oscillations. The upper spot is a superposition of the input and the final extracted pulse, the lower spot is the pulse extracted after the first cycle 92

Figure 5.11 Amplification in AC MECCA ; the large pulse is the extracted pulse and on the far left, barely noticeable, is the reference pulse calibrated to match the input from the master oscillator 93

Figure 5.12 Far-field intensity distribution of the amplified pulse which corresponds to a beam quality of 1.3 x D.L. 94

1. INTRODUCTION AND SUMMARY

The work described in this report addresses the development of regenerative amplifier concepts suitable for low gain, high saturation fluence solid state media such as Nd:glass, Cr:alexandrite and others with emission cross-sections typically a factor ≥ 3 smaller than that of Nd:YAG. Efficient extraction from such media has traditionally been difficult typically resulting in multiple amplifier stages, each with modest gain (~ 3). In addition, such systems are susceptible to significant phase aberrations resulting from thermally induced medium inhomogeneities and the surface figure of the optical components. Phase conjugation has been shown to significantly improve the beam quality produced by such amplifier systems, and configurations where phase conjugation can be readily implemented provide a significant advantage.

Figure 1.1 shows schematic layouts of several extraction techniques used with low gain systems listing the advantages and disadvantages of each. All three shown incorporate phase conjugation to provide good beam quality. Figure 1.1a is a standard phase conjugated master oscillator power amplifier (PC MOPA) and is typically very bulky because it requires many amplifier stages. The configuration shown in Figure 1.1b is limited to four passes through the amplifying medium and requires a Faraday rotator for extraction. It can be adequate for some applications but is limited in practicality and is not readily scalable. Figure 1.1c is a concept developed and used by Lawrence Livermore National Laboratory (LLNL) and is the most flexible of the ones tested to date. It is therefore used as the standard of comparison for the concepts described in this report. It consists of a regenerative ring amplifier in which an electro-optic (EO) switch is employed to trap an injected master oscillator pulse inside the ring for a predetermined number of passes. The beam is extracted to a stimulated Brillouin Scattering (SBS) cell using another EO switch and the phase conjugated beam is then sent back into the ring for an equal number of trips before it is extracted using the EO switch. Since this concept is used as the standard, it follows that alternatives to this concept must provide significant advantages or added flexibility in order to be viable.

The multipass etalon-coupled conjugated amplifier (MECCA) concepts described in this report and shown schematically in Figures 1.2 and 1.3, consist of regenerative amplifier systems which provide several key advantages to the regenerative ring amplifier described above. Figure 1.2 which hereafter is called the "conventional" MECCA uses an etalon and a SBS cell to form a cavity. The input master oscillator beam is injected into the cavity by tuning it to a transmission window of the etalon and is trapped in the cavity

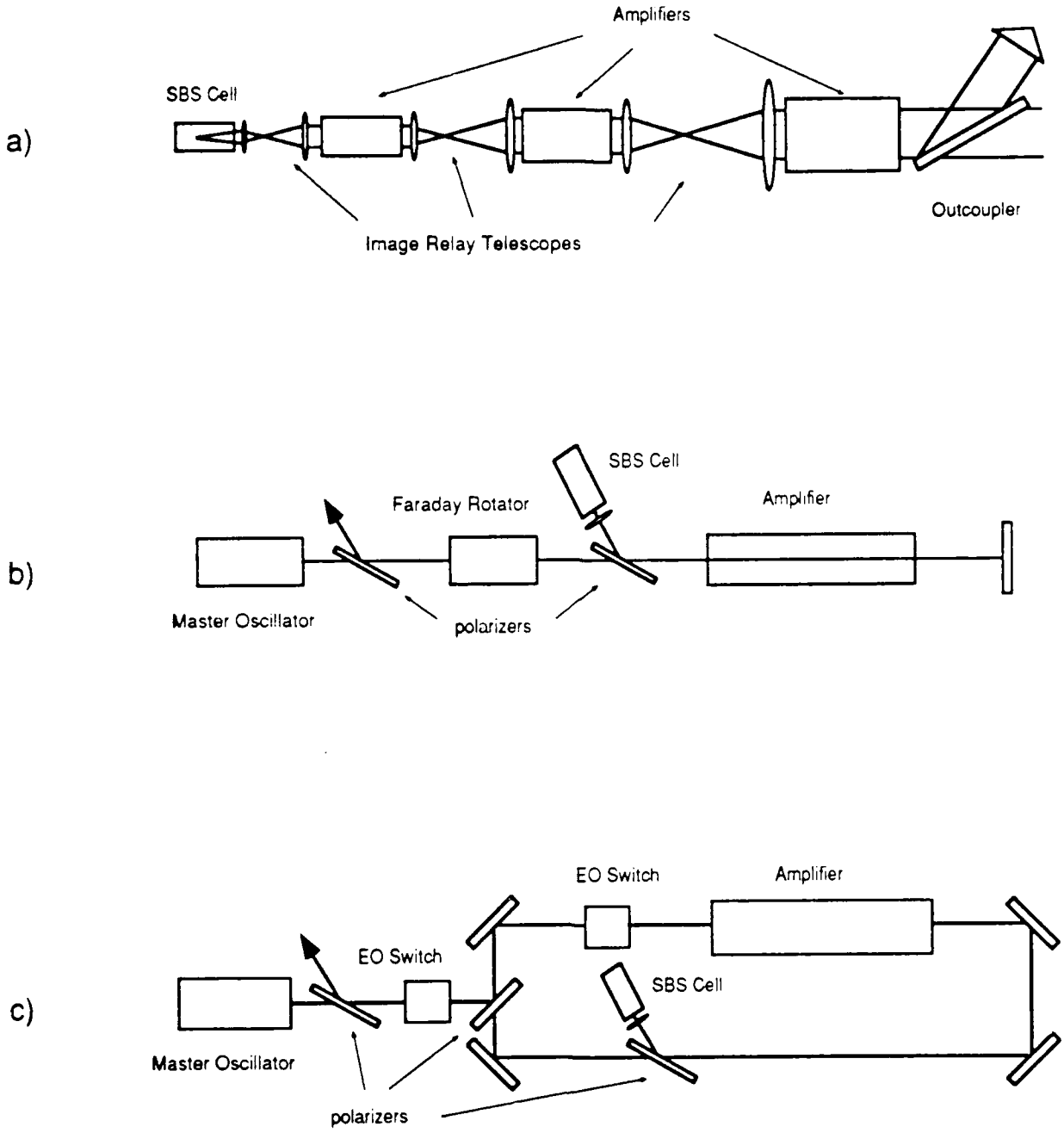

Figure 1.1 Schematic layout of several extraction techniquesused with low gain, high saturation fluence media. a) Multiple stage phase conjugated MOPA, b) four pass polarization coupled phase conjugated MOPA, c) phase conjugated electro-optically switched ring regenerative amplifier.

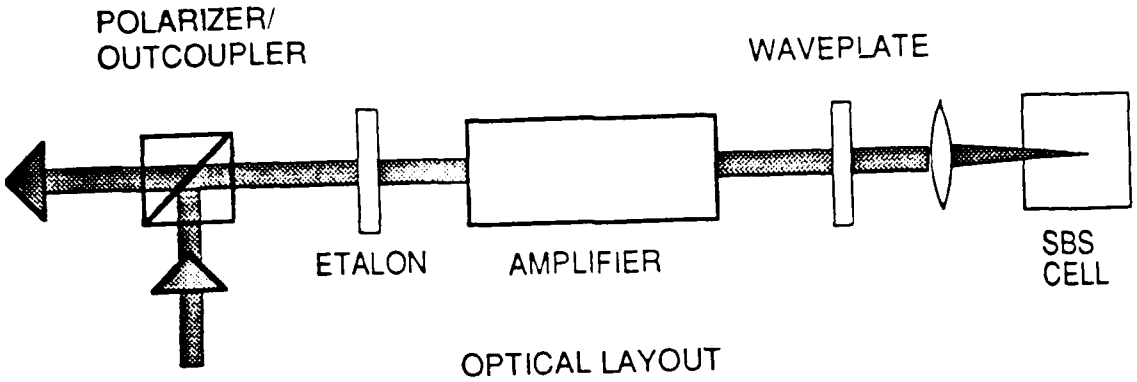

OPTICAL LAYOUT

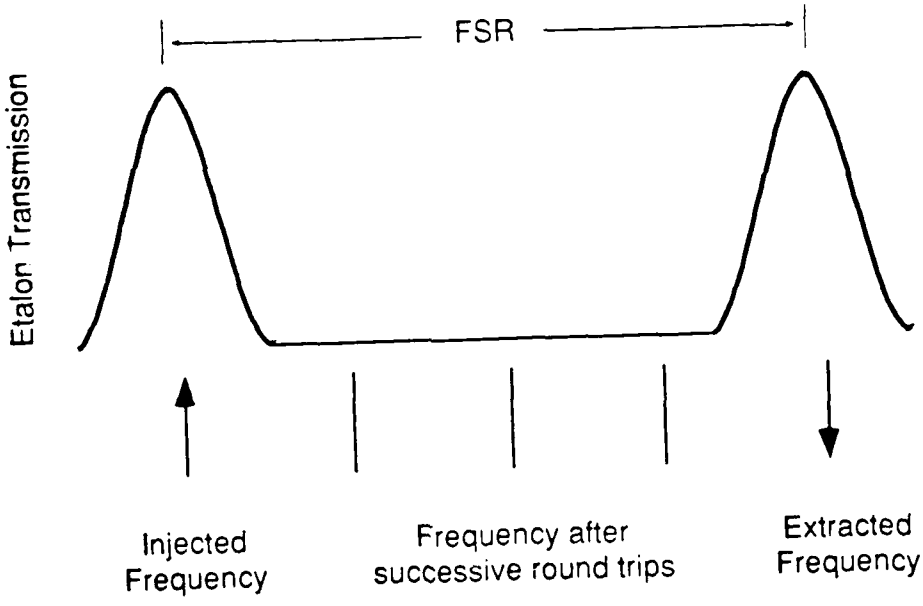

FREQUENCY EVOLUTION

Figure 1.2 Multipass etalon-coupled conjugated amplifier (MECCA) schematic layout and frequency evolution (conventional MECCA)

because the frequency shift introduced by the SBS medium places the beam outside the etalon transmission window as shown by the frequency evolution diagram in Figure 1.2. The beam oscillates between the etalon and SBS cell while marching in frequency space until it encounters another transmission window. By selecting the free spectral range (FSR) of the etalon to be an integral number of SBS shifts, the beam can exit the cavity after a predetermined number of round trips with virtually no loss. The advantages of this concept over LLNL ring regenerative amplifier are as follows:

- The coupling in and out of the cavity is done passively without using EO switches in the high power beam train
- The beam pulse length is not limited to the cavity length, this becomes important if long coherence length beams are desired
- There are no critical timing issues such as those associated with active switches
- Phase conjugation on each round trip prevents the accumulation of aberrations introduced by the amplifier

Because of the less than perfect wavefront fidelity of the SBS process, the amount of amplification possible by such a device is limited by the accumulated wavefront error. Furthermore, as discussed later, the advantage listed in the last bullet above was discovered to be a liability when short pulses are used in the configuration tested because of the thermalization of the SBS grating between each round trip. The thermalization or randomization of the SBS grating between pulses over time scales on the order of a phonon lifetime (which is comparable to the cavity round trip times), resulted in rapid degradation of the SBS reflectivity and fidelity (within 2 to 3 round trips). The reflectivity and fidelity were improved in short cavities where there was partial beam overlap and a sustained SBS driving field. This resulted in overall amplification of a factor of 30 and a beam quality of 1.8 x D. L. compared to predicted values of a factor of 125 and 1.2 x D. L. respectively in a cavity with ~ 25% overlap. This performance is expected to further improve when the pulse overlap is increased and the pulse length becomes long compared to the cavity round trip time.

The second configuration shown in Figure 1.3 is called the "alternate configuration MECCA or AC MECCA". Although it is less elegant than the conventional MECCA, it provides virtually all the advantages of the conventional MECCA but is configured to phase conjugate only once, thereby eliminating the deleterious effects of multiple SBS in a common volume.

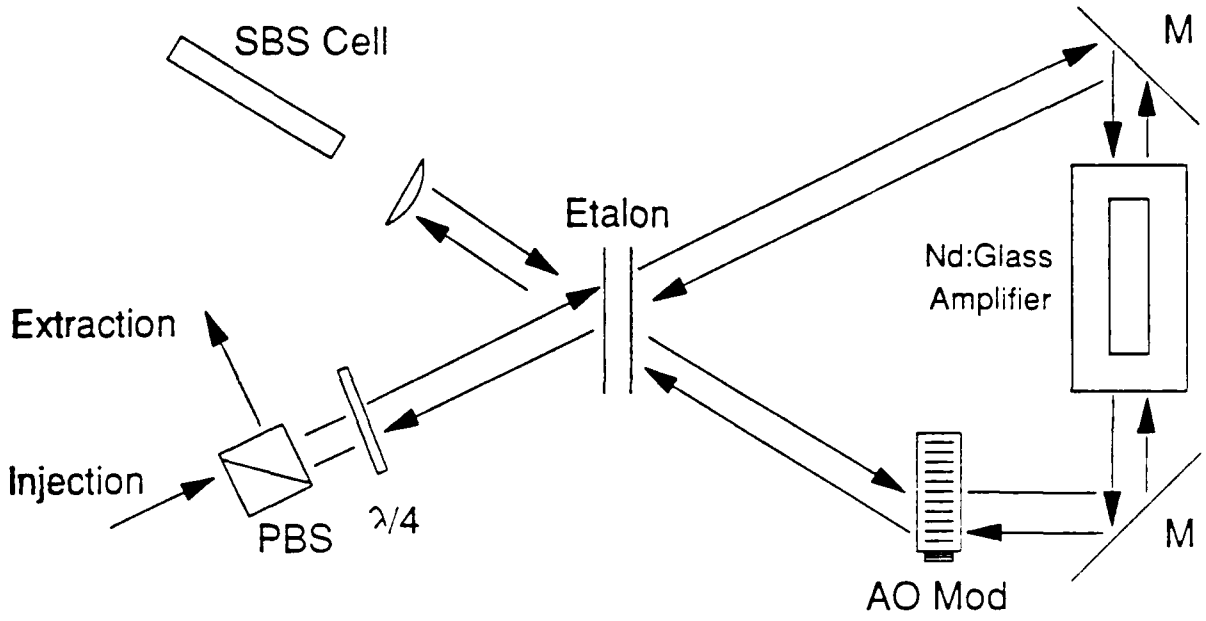

OPTICAL LAYOUT

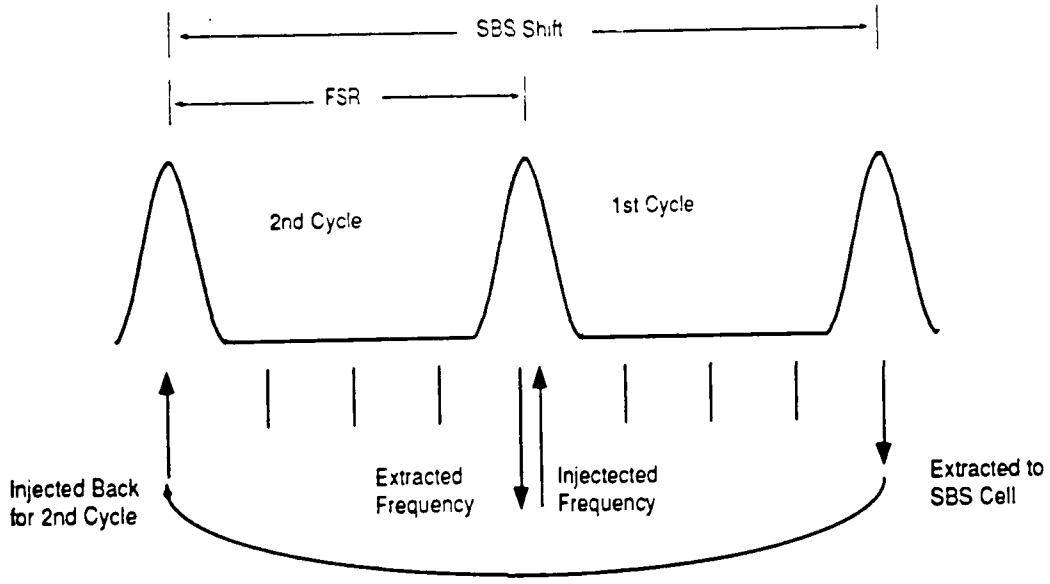

FREQUENCY EVOLUTION

Figure 1.3 Alternate configuration MECCA (AC MECCA) schematic layout

In AC MECCA, the master oscillator pulse is coupled into a ring cavity formed by an etalon and an acousto-optic (AO) modulator where the AO modulator provides the frequency shift that traps the beam inside the cavity. The etalon is arranged to be transmissive on an off axis resonance so that a ring cavity can be formed. As with conventional MECCA, the injected pulse oscillates inside the cavity while marching in frequency space until it encounters another transmission window. If the etalon FSR is adjusted to match an integral number of AO modulator shifts, the beam is again extracted after a predetermined number of round trips without significant loss but this time into a SBS cell. Upon reflection, the phase conjugated beam is polarization rotated and reenters the cavity provided the phase conjugation medium is selected to have a frequency shift equal to an integral number of etalon FSRs. The beam than retraces its path through the cavity for an equal number of round trips and is extracted by a polarizer. By phase conjugating only once, this concept eliminated the deleterious effects of the common focus multiple SBS inherent in the conventional MECCA resulting in moderate amplification and good beam quality.

The AO modulator, which is key to the operation of AC MECCA, operates in a CW or quasi-CW mode and therefore requires neither high voltage nor the critical timing of an EO switch; it is therefore much simpler to operate. In addition, AO modulators scale in a manner similar to high average power slabs (primarily in one dimension) and thus should not limit energy scaling of the system.

TRW tested the two MECCA configurations described above and made significant progress in establishing the potential and limitations of the two concepts. Work was also performed on fundamental SBS processes and a significant SBS database was generated as a result. The following are some of the highlights of the work performed under this contract:

- Demonstrated oscillation in an etalon coupled cavity and established requirements for efficient injection and extraction
- Demonstrated and characterized the conventional MECCA with moderate gains ($\geq$ 30) and beam quality (1.8 x D.L.)
- Developed two models, METALON and BRIWON to simulate MECCA extraction and beam quality respectively
- Characterized several SBS materials and established their dynamic range for fidelity and reflectivity. Identified freon as an excellent candidate for MECCA and other solid state laser applications

- Identified thermalization of the SBS grating as the main source of beam quality and reflectivity degradation in a short pulse, common focus, multiple reflection SBS cavity.
- The thermalization was demonstrated to decrease in short cavities with partial beam overlap and a sustained SBS driving field, suggesting further improvements in performance when the pulse length is much longer than the cavity round trip time.
- Designed the AC MECCA, which circumvents the common focus SBS issue while maintaining all the key advantages of the conventional MECCA
- Demonstrated oscillation in the AC MECCA cavity in a folded (nonring) configuration.
- Demonstrated moderate amplification (≥ 40) with good beam quality (1.3 x D.L.) in a 6 round trip AC MECCA.

These highlights and related efforts are described in detail in following chapters.

2. MECCA CONCEPT DESCRIPTION AND REQUIREMENTS

2.1 Concept Description

A schematic layout of the MECCA concept was shown earlier in Figure 1.2 along with the frequency space evolution of the beam oscillating in the MECCA cavity. A beam from a master oscillator is tuned to a transmission window of the etalon, propagates through the amplifying medium and into a SBS cell which serves as a phase conjugating medium. Phase conjugation through stimulated Brillouin scattering is discussed in some detail in Section 4.3 but for now we will assume that it provides a technique of reversing the wavefront of the incident beam while introducing a small Stokes shift on the beam frequency. The phase conjugated beam propagates back through the amplifier, where the aberrations are corrected, and back to the etalon. Because of the frequency shift introduced by the SBS process, the beam is no longer within the transmission window of the etalon and is reflected. The beam thus oscillates between the etalon and the SBS cell while marching in frequency space until it matches another transmission window of the etalon, at which point it exits the cavity. To optimize the extraction efficiency, the etalon free spectral range (FSR) must be an integral number of SBS shifts so that the amplified beam is transmitted with minimal loss and the number of round trips is controlled by varying the etalon FSR. Coupling into and out of the cavity is therefore achieved passively once the desired parameters are established and the etalon is tuned to resonance for the master oscillator frequency.

2.2 Requirements

Efficient extraction from MECCA places requirements on each of the system components which include the master oscillator, the etalon, the gain medium and the SBS medium as follows:

Master Oscillator: The two key requirements for the master oscillator are frequency stability and bandwidth. The frequency must be stable from shot to shot to insure that the MO pulse matches the transmission window of the etalon. This is achieved by using an

injection seeded MO such as the Quantel Y660 laser used in our experiments. The relative frequency stability of the Quantel/etalon pair was typically 10 to 15 minutes after which a minor adjustment was typically required to bring the two back into resonance. Another technique to provide good coupling between the MO and the etalon is to use a system where the MECCA etalon is also included in the MO cavity such that MO pulses automatically fall within the transmission window of the etalon. This technique would be most practical when designing an integrated MECCA system.

The second requirement for the master oscillator is the bandwidth. If the beam bandwidth is much smaller than the etalon transmission bandwidth, then small errors in the etalon FSR are better tolerated and do not seriously impact the extraction efficiency. If the MO pulse bandwidth is broader than that of the MECCA etalon, the etalon acts as a filter on the input pass, resulting in some loss. This typically is not an issue because the MO energy is a small fraction of the outcoupled energy, and losses on the MO pulse energy do not significantly impact the overall efficiency. However, under such conditions, the required precision to which the FSR must be set becomes much higher. The SBS process also causes some spectral broadening and this results in additional losses on the exit pass, where the overall efficiency is critically affected. The Quantel laser produces pulses that are 6 ns long and nearly transform limited with a bandwidth on the order of 200 MHz. This is perfectly adequate for liquid SBS media where the SBS shift is a few GHz and the etalon transmission bandwidth is typically $\geq$1 GHz. In gaseous media where the SBS shift is a few hundred MHz (see the discussion of SBS media below), the etalon FSR must be correspondingly smaller. Under these circumstances, the requirement for an adequate transmission bandwidth while minimizing losses during oscillation, makes the selection of the etalon finesse a critical issue (see below). On the other hand, gases introduce a much smaller SBS spectral broadening than Liquids and thus the losses upon extraction depend primarily on how precisely the etalon FSR matches an integral number of SBS frequency shifts.

Etalon: The etalon is a critical part of MECCA because it, along with the SBS cell, is the principal component which controls the extraction efficiency of the system. The design of the etalon has to include several key features: It must provide efficient input and output coupling, it has to be a good reflector for the frequency shifted pulses (minimize leakage prior to extraction) and the mirror separation has to be adjustable over distances of $\lambda/2$ to match the frequency of the MO, and over several cm to provide a FSR which is a precise integral number of SBS frequency shifts. Typical separations ranged from 2 to 10 cm.

These characteristics are best achieved by an air gap etalon equipped with piezo-electric transducer (pzt) controls for fine tuning. The finesse of the etalon has to be selected to strike an adequate balance between efficient input/output coupling and minimizing leakage. The higher the finesse, the lower the amount of the leakage but this comes at the expense of narrower transmission bandwidth which reduces the tolerances for efficient extraction. The optimum finesse was determined analytically by using the etalon model described in Section 3. A finesse of approximately twice the number of round trips desired was found to provide the necessary balance. By selecting a finesse that is twice the number of round trips desired, the first (and the next to the last) reflection from the SBS cell falls two etalon FWHM transmission bandwidths away from the injected (and extracted) frequency insuring good reflectivity for all nontransmitting pulses. The etalon used was a Burleigh RC-140 with mirrors coated to provide several finesses ranging from 6 to 20. The FSR could be varied from 0.5 GHz (L = 30 cm) to 15 GHz (L = 1 cm), providing a wide parameter range. A fine tuning range of a few microns was available via pzt drivers, which was ample for matching the transmission resonance to that of the master oscillator.

Gain medium: Two different gain media were used throughout MECCA testing. The first was a TRW built Nd:glass zig-zag slab amplifier, the second was a rod amplifier fabricated by Kigre Inc.. Both amplifiers were flashlamp pumped and had peak single pass gains in the range of 2.5 to 3. The slab had a rectangular cross-sectional area of 0.6 x 3 cm of which a subaperture of .6 x 1 cm was used; the rod diameter was 1 cm. Figure 2.1 shows the gain profile of the slab in the vertical dimension showing good uniformity over the central 1 cm area sampled. Initial experiments were performed with the slab amplifier because it has no birefringence and is capable of operating at rep-rates up to 10 Hz. It was later replaced by the rod amplifier because, at low rep-rates the wavefront aberrations in the rod are minimal, whereas the slab has approximately 0.5 wave of aberration due to multiple reflections from the total internal reflection (TIR) surfaces. Minimizing the aberrations in the gain medium was crucial to isolating the inherent beam quality issues associated with the MECCA geometry; the rod amplifier, operating at a rep-rate on the order of 0.1 Hz, was found to be the preferred gain medium.

The single pass gain of the amplifier was controlled by varying the delay between the flashlamp pulse and the arrival time of the injected MO pulse. This allowed continuous variation of the gain between 1 and 3. Figures 2.2 and 2.3 show the gain tuning curve of slab and rod amplifiers, respectively.

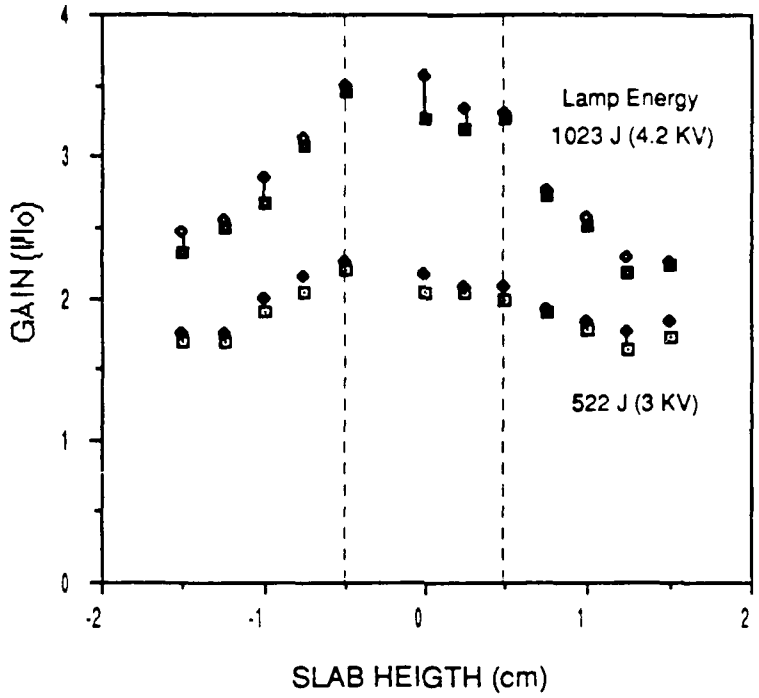

Figure 2.1 Slab amplifier gain profile. The master oscillator beam samples the central 1 cm region of the slab

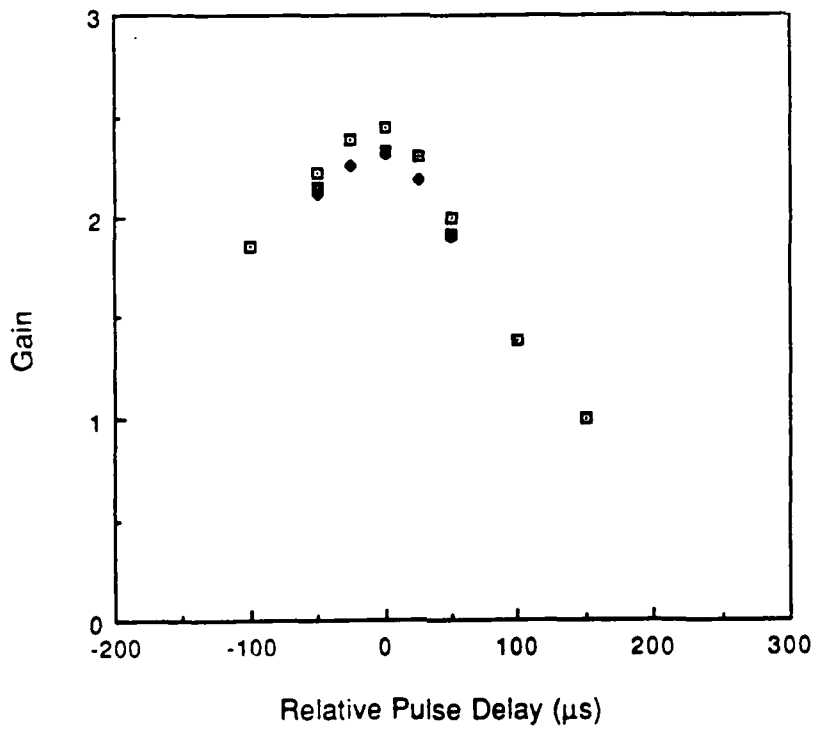

Figure 2.2 Slab amplifier gain as a function of master oscillator pulse delay time

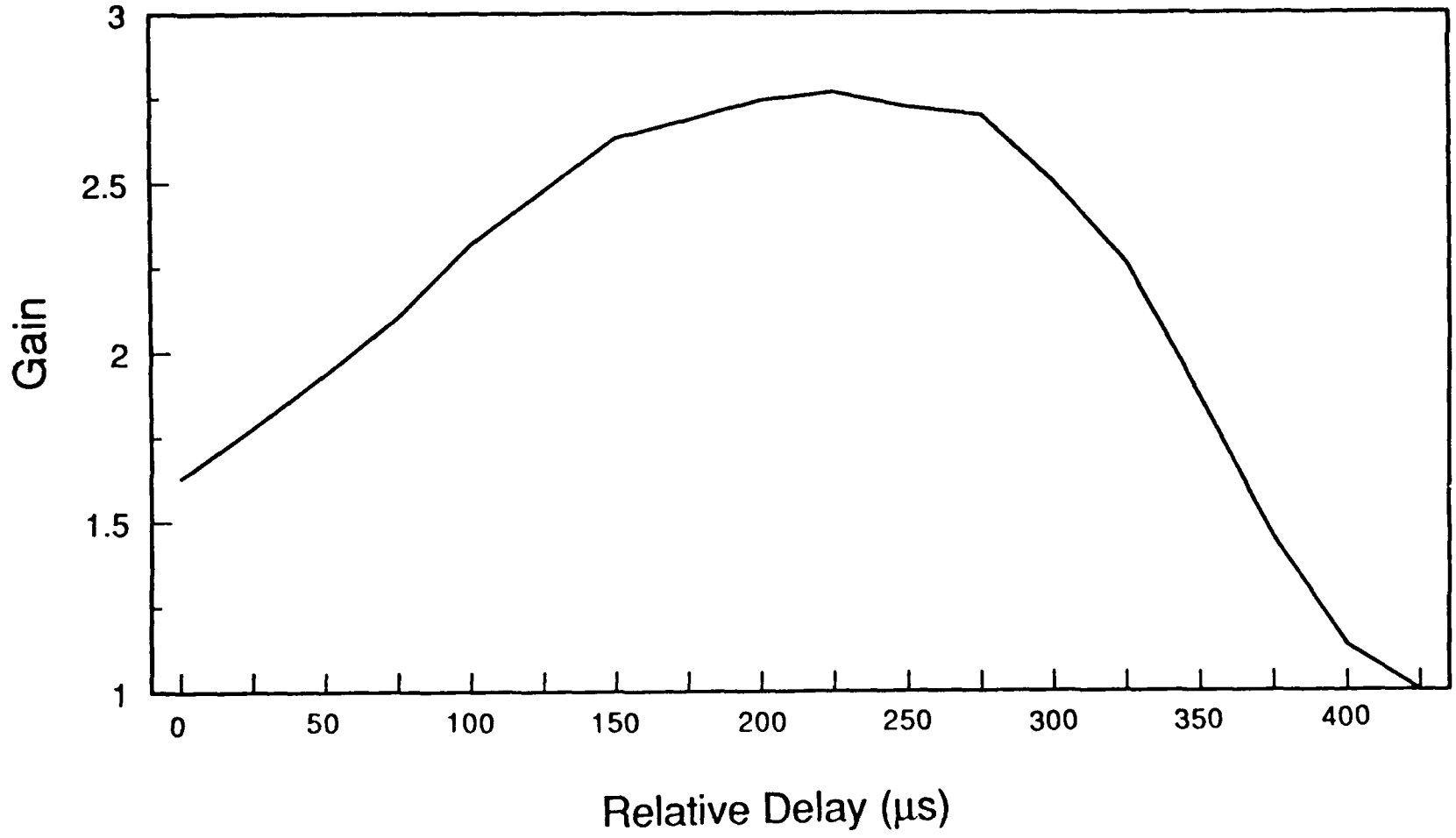

Figure 2.3 Rod amplifier gain as a function of master oscillator pulse delay time

SBS medium: The requirements for the SBS medium relate to three general issues. The first issue is that of inherent conjugation fidelity, which determines the ultimate beam quality of the amplified pulse; the second involves efficient extraction from the MECCA cavity; and the third is the lack of competing processes. It will be shown later in Section 3 that the reflectivity is not a crucial factor for the extraction efficiency provided that the slope efficiency is reasonably high ($\geq 60\%$).

To insure that the outcoupled pulse has good beam quality, the conjugation fidelity must be near unity for each round trip because even small amounts of residual aberrations accumulate, thereby limiting the range over which the system can be used. The conjugation fidelity determines the degree to which the SBS process is able to produce a conjugate wavefront, and is measured by either comparing interferograms or energy in a bucked measurements of the input to and return from the SBS medium. In our experiments the single pass fidelity is defined as the ratio of the energies in the bucket of the output beam to the input beam. Since our beam is typically a diffraction limited gaussian beam, the reference bucket diameter corresponds to the $1/e^2$ intensity point of the gaussian beam (86% of the energy). Using the simple minded assumption where the overall fidelity is given by $\mathcal{F} = F^n$ where F is the single pass fidelity and n is the number of round trips, the overall beam quality can be approximated by:

$$\text{Beam Quality} = \sqrt{1/\mathcal{F}} = (1/F)^{n/2}$$

where the beam quality is the number of times diffraction limited. If we now establish a beam quality requirement of 1.5 x D. L., the minimum single pass fidelity that can be allowed is:

$$F_{min} = (1/1.5)^{2/n}$$

For a four round trip MECCA this would correspond to an F_{min} of 0.82.

This requirement also implies that the conjugation fidelity must remain near unity throughout the energy range addressed by the system. Thus, as an example, in a cavity where the average net gain per round trip, $g_{ave} = 3$, and the overall amplification desired is $(g_{ave})^n = 81$, where n = 4 is the number of round trips, the maximum energy injected in the SBS cell (not counting saturation effects) corresponds to $(g_{ave})^{n-1} = 27$ times the energy injected on the first pass. This because the first SBS pulse has already experienced one pass through the amplifier (1/2 a round trip), and the last pulse has one more pass left (another 1/2 a round trip). Thus, in general, the dynamic range required by the SBS

medium is $(g_{ave})^{n-1}$. If in addition, the input pulse is 2 x threshold, the fidelity must be near unity at energy levels $2(g_{ave})^{n-1}$ x threshold, or for this example 54 x threshold.

The requirement for efficient extraction implies that the SBS shift is large enough that an etalon/SBS pair with practical parameters can be assembled. If we assume that a practical length for the etalon is on the order of 15 cm or less (FSR of 1 GHz or larger), and the minimum number of round trips to be used is 3, the frequency shift from the SBS cell must be on the order of 0.33 GHz or larger. As mentioned earlier, this is easily satisfied for liquids but not for gases. The most desirable gases, therefore, are those with low molecular weight (high speed of sound), such as methane, so that the SBS shift is large. Efficient extraction also requires the knowledge, to good precision, of the SBS frequency shift. Figure 2.4 shows a simple technique used to measure the frequency shift to an accuracy on the order of 10%. This is typically used as a starting value and a more precise measurement is obtained in the MECCA configuration itself by varying the FSR of the etalon and optimizing the outcoupled energy. By setting up a MECCA cavity tuned to, for example, 5 round trips, the measurement accuracy of the SBS frequency shift is improved by a factor of 5.

Competing processes are discussed in Section 4. An important issue to be mentioned here is the fact that competing processes may manifest themselves differently in a MECCA configuration than that for a single pulse SBS. As an example, when using temporally gaussian pulses we see no SRS in high pressure methane or nitrogen at energies 50 times threshold or higher. This because the slow rise time of the pulse allows the creation of the SBS grating and suppresses the lower gain SRS. In a MECCA configuration, the rise time of the pulse becomes shorter with each successive SBS reflection, and SRS can occur at the beginning of the pulse during the time when the SBS grating is not yet established and SRS (which is virtually instantaneous) can dominate.

2.3 Parameter Space

A wide parameter range was tested as part of the MECCA characterization. Figure 2.5 summarizes the key parameters and the range tested. Because of the magnitude of the test matrix available, MECCA performance for some of the parameter ranges was evaluated only qualitatively and detailed characterization was limited to areas which showed promise. In addition, off-line experiments were performed to evaluate several SBS media in terms of threshold, reflectivity and fidelity. The results are described in sections 4 and 5.

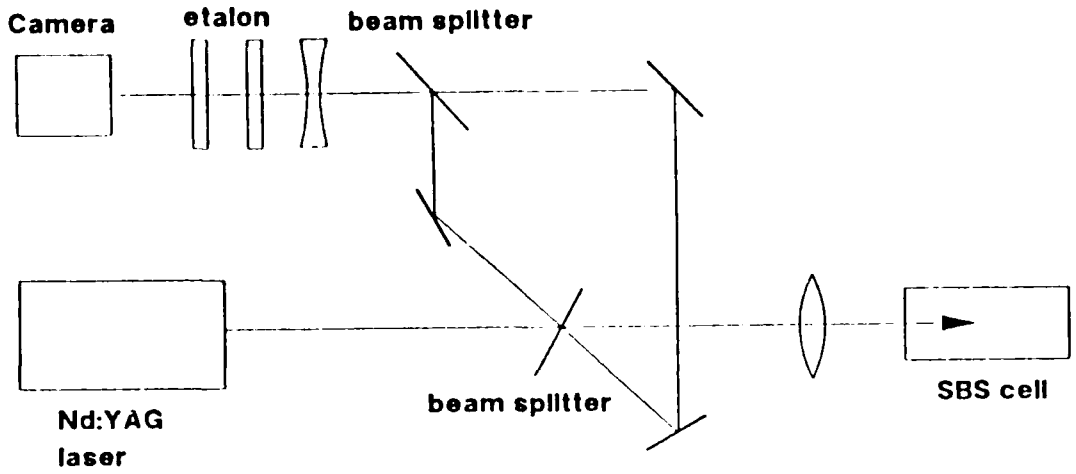

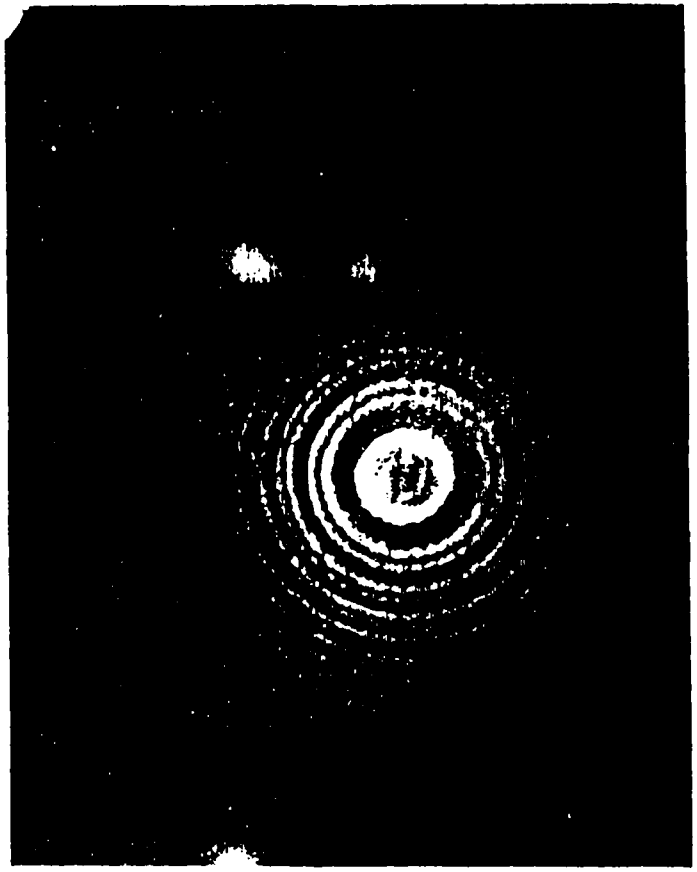

Figure 2.4 SBS frequency shift measurement optical layout

Master Ocillator Energy (mJ)	**5 to 100**
Etalon FSR (GHz)	**1 to 10**
Etalon Finesse	**6 to 20**
Amplifier Gain	**1 to 3**
SBS Media	
Gases	**Methane, Ethane, Nitrogen, Xenon**
Liquids	**Acetone, CCl4, Freon, n-Hexane**
Cavity Lengths (m)	**1 to 3.5**

Figure 2.5 MECCA characterization parameter space

3. MODELING AND PROJECTED PERFORMANCE

MECCA was modeled using two discrete models, METALON and BRIWON. METALON was a comprehensive 1-dimensional (propagation direction) model with portions that describe each of the key MECCA components and was primarily used to calculate extraction efficiency. The BRIWON model is a 2-dimensional (propagation and 1 transverse dimension) SBS model which was modified to include free propagation and diffraction from apertures. BRIWON was primarily used to model beam quality.

3.1 METALON Extraction Model

The METALON model components and their features are summarized in Figure 3.1. Also shown are the input parameters for each components and the calculated parameters. There are three major components as follows:

Etalon Model: This part of the model uses the input pulse characteristics, mirror reflectivities and separation as parameters to calculate the transmitted and reflected pulses. It does so by temporally dividing the input pulse in multiple segments and summing the electric fields inside and outside the etalon. This method allows the use of input pulses of arbitrary shape and the effect of pulse shape on the transient response of the etalon can be modeled. The model also has the capability of incorporating an absorbing medium inside the etalon in cases where a solid etalon is used. Since this is a one-dimensional model it assumes a diffraction limited, flat top beam (uniform intensity in the transverse dimensions). For on axis injection, the transverse intensity distribution is not relevant to the transmission characteristics of the etalon; the phase distribution however is, and the injected beam is spatially filtered to carefully collimated to provide a flat wavefront.

Gain Medium: The gain medium is modeled by solving the coupled rate equations for the excited state population and the photon flux to account for saturation effects. The initial excited state ion density is calculated from the specified stored energy and the dimensions of the medium. The photon flux is calculated using the emission cross-section of the medium selected. The gain medium is also segmented to accommodate the temporal shape of the incident field and to account for bidirectional propagation and pulse overlap in short

Model Feature	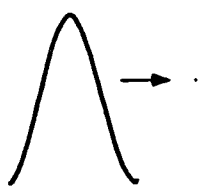 Input Pulae	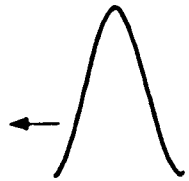 Output Pulse	 Etalon	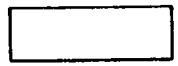 Gain Medium	 SBS Cell
Input Parameters	• Pulse Shape • Pulse Length • Pulse energy • Beam diameter • Center Frequency		• Mirror separation • Mirror Reflectance • Absorption (if any)	• Energy per unit Volume or small signal Gian • Gain length • emission cross-section	• threshold Energy • Slope efficiency • Frquency shift
Calculated Parameters		• Pulse Shape • Pulse Energy • Extraction Efficiency	• FSR • Finesse • Reflectivity of incident pulse (in either direction)	• saturated gain • energy extrated	• Reflectivity • Energy transmitted

Figure 3.1 Summary of METALON model components and capabilities

cavities. This is done by calculating the total field in each "bin" as the beam circulated in the cavity. The gain is assumed to be uniform in the transverse dimensions.

SBS Medium: The SBS process is modeled based on the experimentally measured performance of a particular medium. The threshold energy and the reflectance slope efficiency are used as input parameters to determine the reflectivity and temporal shape of individual pulses. As individual pulse segments are incident on the SBS medium, an amount of energy equal to the SBS threshold is subtracted from one or more segments and the rest reflected in an amount equal to the slope efficiency of the medium. The model does not assume any residual effects from previous pulses, and does not take into account competing processes beyond those implicit in the data used in the model. Thus dynamic effects such as SRS, which are pulse shape dependent or are unique to the multiple reflection nature of MECCA, are not modeled. Fidelity is not an issue with METALON because it is only a tool to estimate potential extraction efficiency.

3.2 METALON Performance Predictions

METALON was used to optimize the cavity design and to predict the potential extraction efficiency of MECCA. The first Task was the determination of the optimum finesse for the etalon. Figure 3.2 shows the reflection losses suffered by a 7 ns FWHM, temporally gaussian MO pulse as a function of the finesse for several round trips in a lossless cavity. The criterion for optimum finesse was established to be the lowest finesse that will result in reflection losses of no more than 20%. This is based on the assertion that the lower finesses provide the higher transmission bandwidths and thus are more tolerant to slight mismatches in frequency or broadening of the final extraction pulse due to the SBS bandwidth. Figure 3.2 illustrates that a finesse corresponding to approximately twice the number of round trips is required to meet this criterion.

Figure 3.3a and 3.3b show the model calculated intracavity and outcoupled pulses, respectively, as the beam oscillates in the MECCA cavity without amplification. It shows the transient response of the etalon on the input pulse representing a 6% loss, a very small amount of leakage during oscillation (~ 3%) and high efficiency pulse extraction (98%). Figure 3.4 summarizes the extracted energy predicted by METALON under a variety conditions with amplification. Figure 3.4a shows that there is an optimum number of round trips for each set of conditions beyond which the extracted energy decreases. This is understandable because once the medium is saturated, further reflections suffer the losses associated with the SBS medium and other optical elements without benefit of gain.

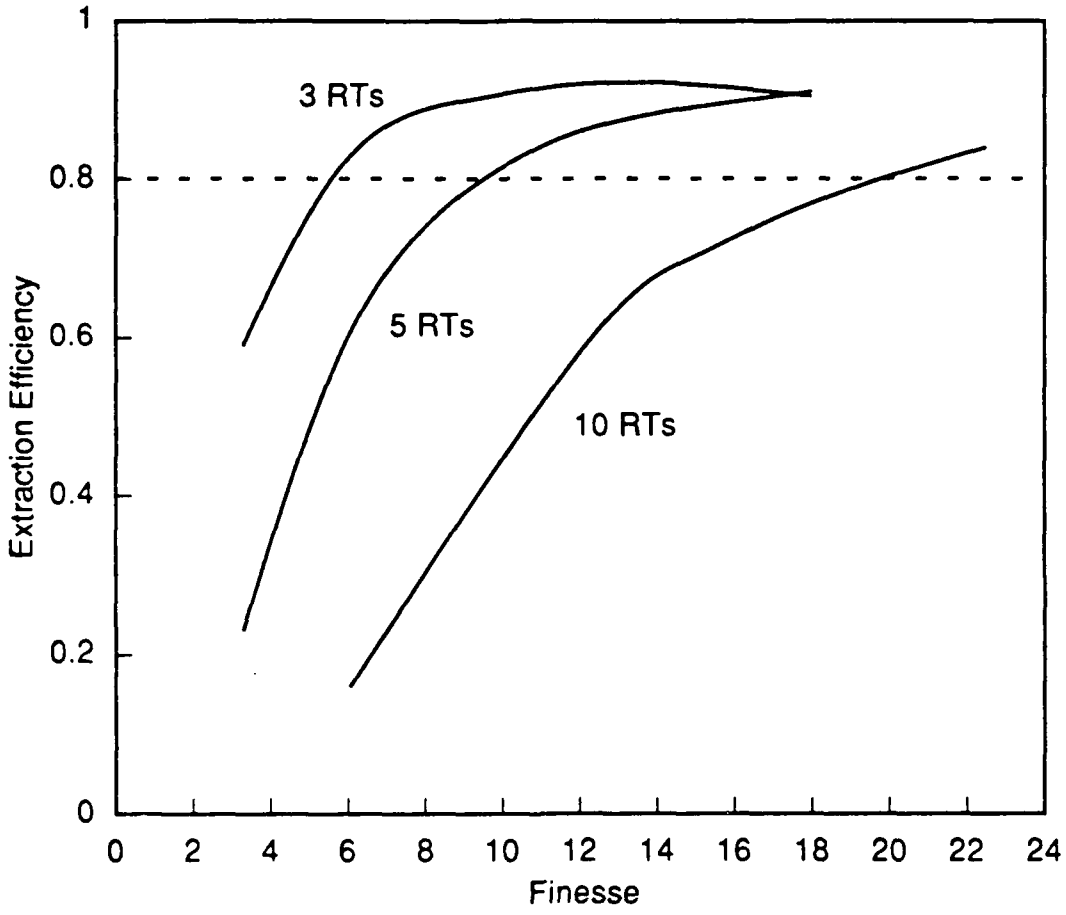

Figure 3.2 Extraction efficiency of a 7 ns FWHM, temporally gaussian MO pulse as a function of the finesse in a lossless MECCA cavity (SBS reflectivity of 1)

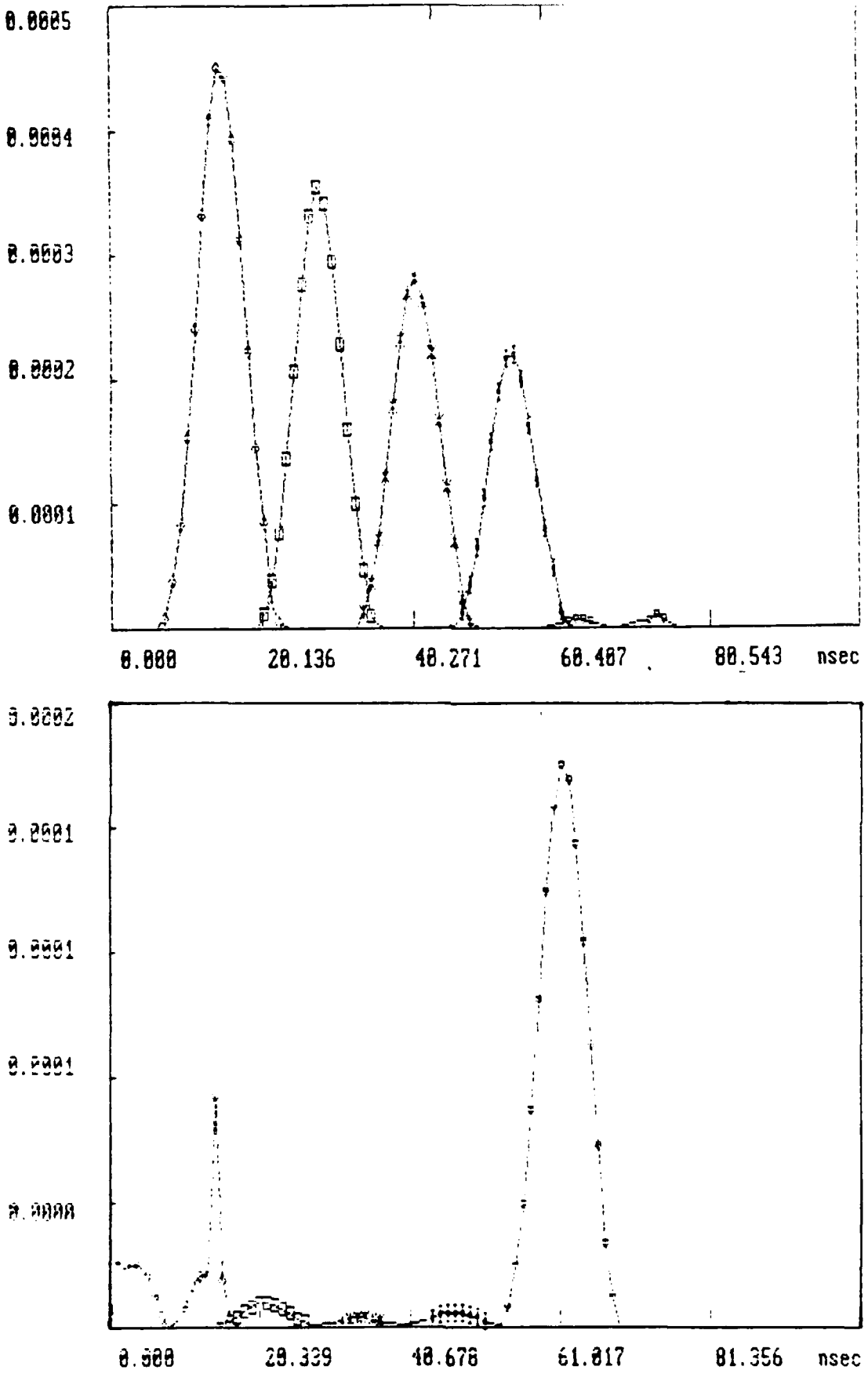

Figure 3.3 METALON prediction of MECCA pulse evolution. a) intracavity pulse train immediately downstream of the etalon, b) extracted pulse train immediately upstream of the etalon

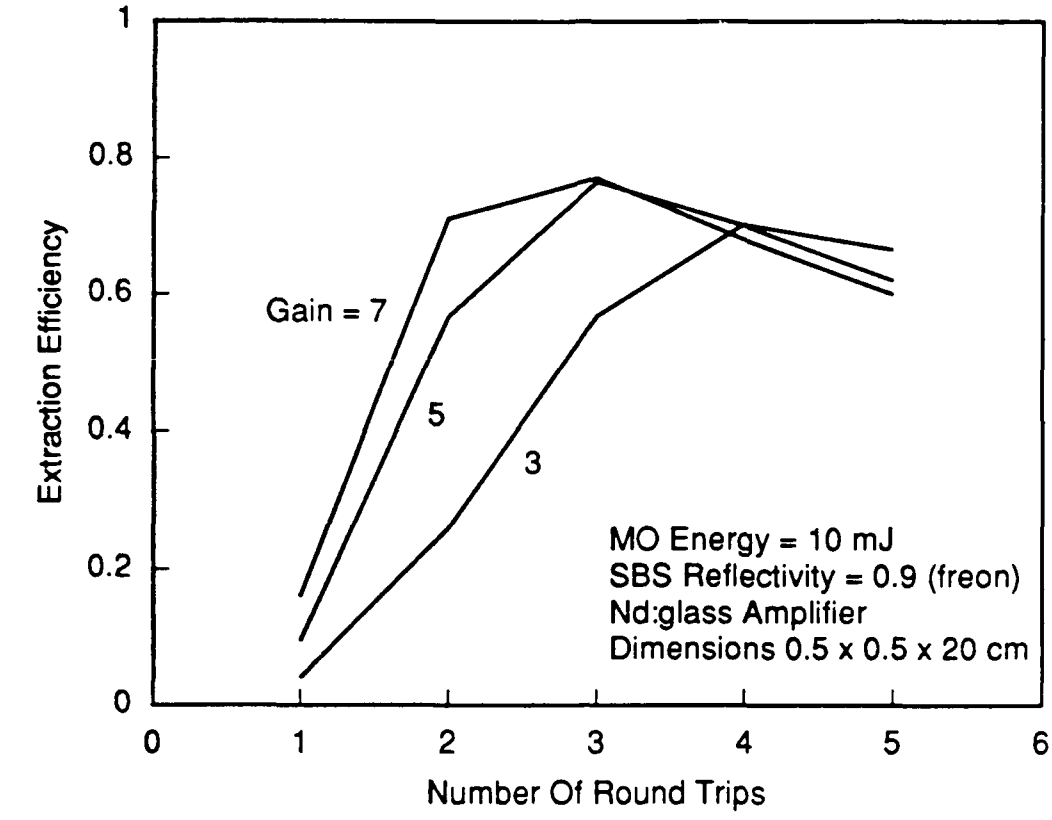

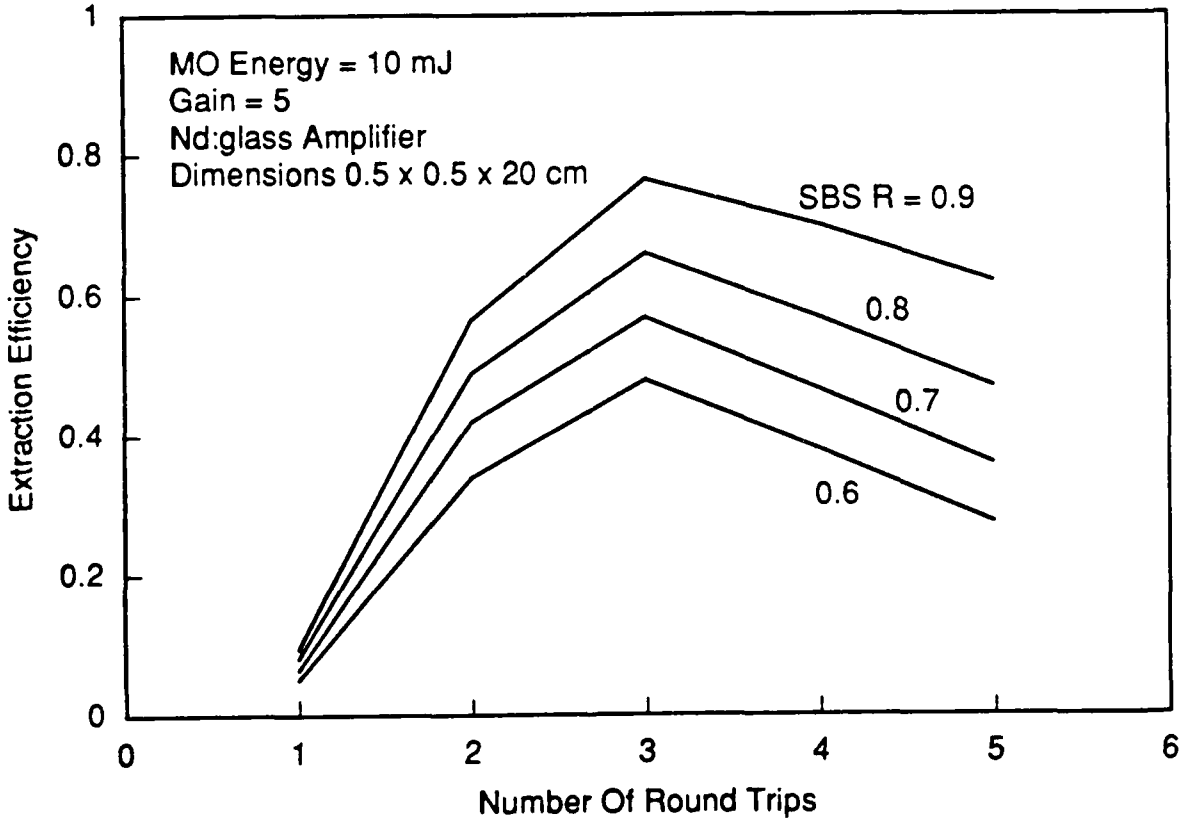

Figure 3.4 Summary of METALON predicted MECCA extraction efficiency. a) as a function of round trips for several single pass amplifier gains, b) as a function of round trips for several SBS reflectivities.

Figure 3.4b shows that varying the SBS reflectivity from 60% to 90% changes the extraction efficiency from 48% to 77%. That extraction efficiencies of nearly 50% are possible, with SBS reflectivities as low as 60%, is attributed to the fact that most of the energy is extracted on the last pass which ameliorates the impact of the SBS reflectivity on efficiency. The calculations also showed that the extraction efficiency is relatively insensitive to MO energy as long as the first pass is at least a factor of two above threshold. Varying the master oscillator energy has the effect of changing the optimum number of round trips required.

As mentioned earlier these very encouraging results do not include residual effects from the SBS cell and the beam quality is assumed unaffected throughout the amplification process.

3.3 BRIWON Beam Quality Model

The original BRIWON code developed at TRW is a 2-dimensional SBS code designed to predict the wavefront and intensity characteristics of a SBS reflected beam based on its input characteristics and those of the SBS medium. It uses wave optics in one transverse dimension and geometrical optics in the other to provide a reasonable model of the beam intensity profile as it is focussed in the SBS medium. The model constructs the SBS grating in the focal region of the beam and generates the return by amplifying a Stokes beam from noise (spontaneous emission). This model was extended by including free propagation to and from the etalon, and a diffracting aperture similar to that of the slab. Figure 3.5 shows the main components of the model, typical input parameters and the calculated results. Aberrations were typically introduced at the location of the slab but they could also be introduced anywhere else in the optical train. The main drawback of this model was that it is a steady state model and therefore fails to account for transient effect as well as those related to the decay of the SBS grating. As a result, each pulse incident on the SBS cell saw a "fresh" cell similar to that of the single pulse case. Nevertheless, the model was very useful in indicating the role that aberrations and diffraction play in MECCA.

3.4 BRIWON Performance Prediction

The BRIWON model was exercised in several steps, each step adding a new feature (such as aberration or propagation) to evaluate its effect. The results are summarized in Figure 3.6. The first configuration modeled was a very short cavity consisting of the

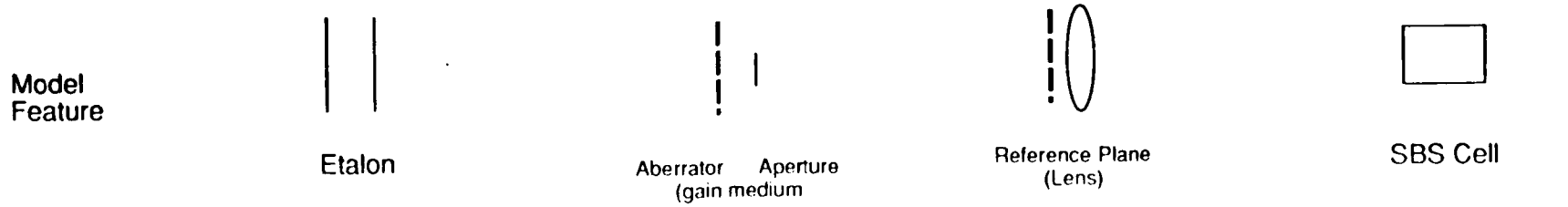

Figure 3.5 Summary of BRIWON model components and capabilities

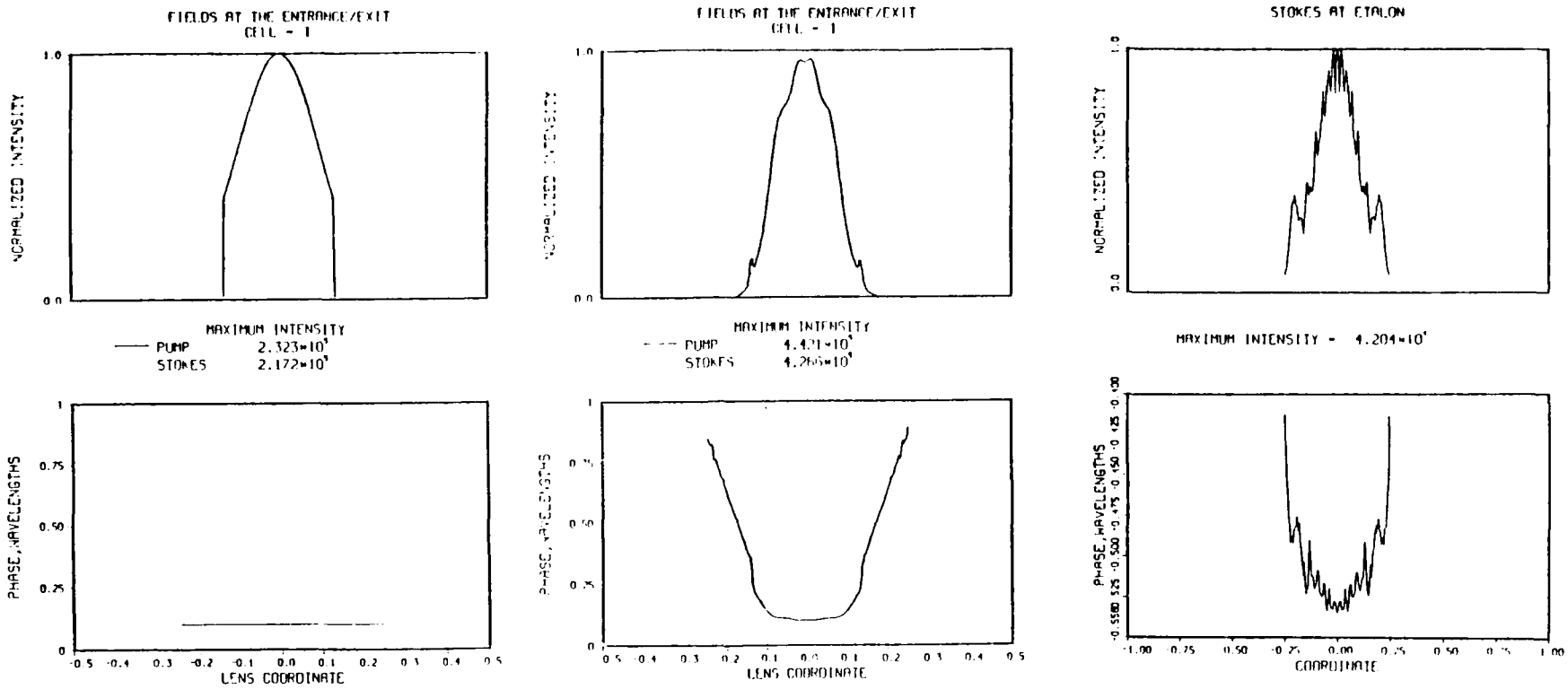

Figure 3.6 BRIWON predicted three round trip MECCA output beam cahracteristics under a variety of conditions. a) truncated, unaberrated gaussian beam propagating between the lens and SBS medium, b) same as a) but with three meters of propagation, c) short cavity with approximately one wave of wavefront aberrrations, d) one wave aberrations with 3 m propagation.

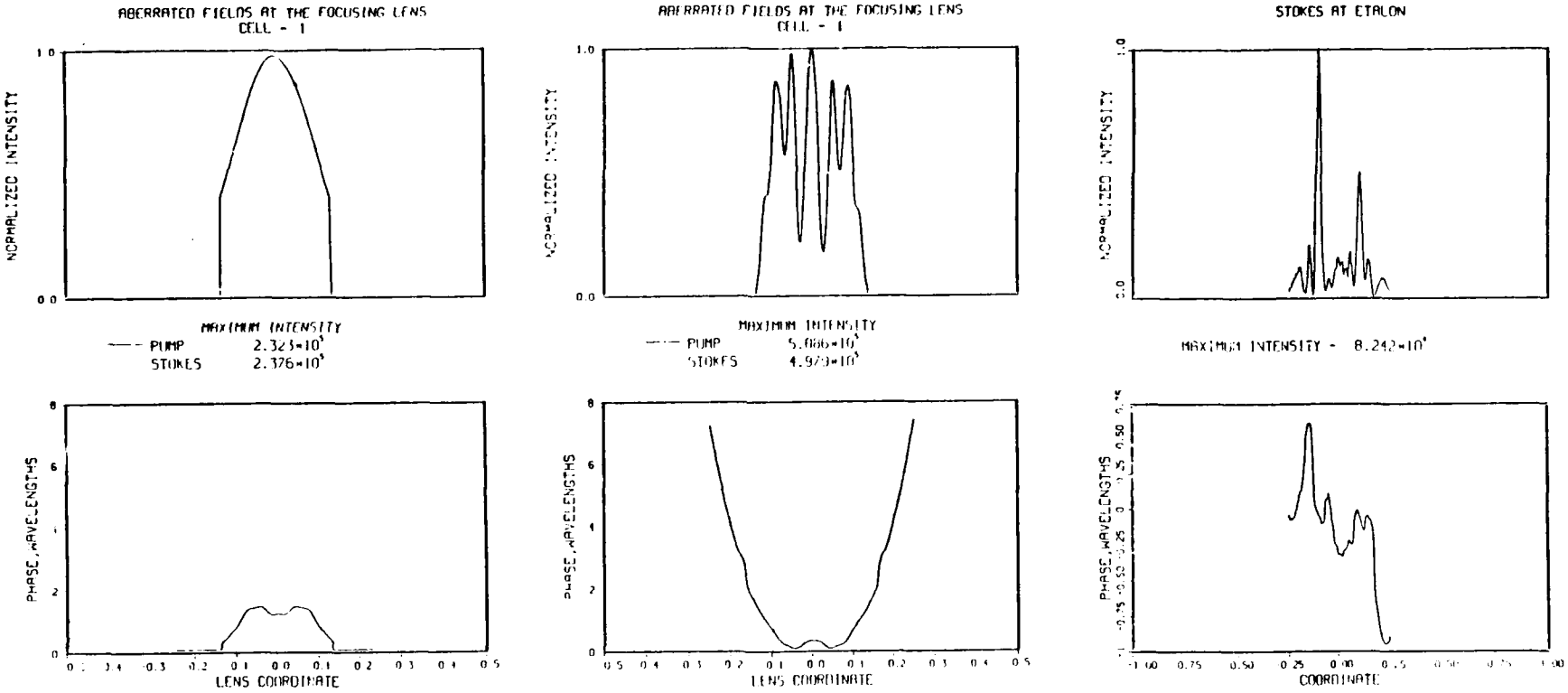
ABERRATED FIELDS AT THE FOCUSING LENS
CELL - 1
NORMALIZED INTENSITY
1.0
0.0
MAXIMUM INTENSITY
PUMP 2.323×10⁵
STOKES 2.376×10⁵
PHASE,WAVELENGTHS
LENS COORDINATE
ABERRATED FIELDS AT THE FOCUSING LENS
CELL - 1
NORMALIZED INTENSITY
MAXIMUM INTENSITY
PUMP 5.066×10⁵
STOKES 4.973×10⁵
PHASE,WAVELENGTHS
LENS COORDINATE
STOKES AT ETALON
NORMALIZED INTENSITY
MAXIMUM INTENSITY - 8.242×10⁴
PHASE,WAVELENGTHS
COORDINATE

etalon and the SBS medium (no propagation). An unaberrated beam with a truncated (apertured) gaussian intensity profile was allowed to propagate back and forth three times and the resulting intensity profile is shown in Figure 3.6a. It shows a small amount of intensity modulation but good overall fidelity. The next configuration was to add approximately 3 meters of propagation distance between the etalon and the SBS cell. Figure 3.6b shows that this results in an increase in the spatial frequency of the intensity modulation but the modulation depth remains small and the wavefront error is also very small. Figure 3.6c shows the result for a short cavity in which approximately 1 wave (pp) of aberration is added at the SBS lens. The aberration is described by the equation:

$$A = 0.4\lambda\cos\theta_1 - 0.3\lambda\cos\theta_2 + 0.04\lambda\cos\theta_7$$

where the subscript on the angle represents the number of cycles across the beam aperture (the spatial frequency of the wavefront aberration). The calculations show high intensity modulation ($\geq 80\%$), but with nearly perfect wavefront fidelity. This type of modulation is not very desirable in solid state laser amplifiers because it can lead to deleterious effects such as self focusing, but in and of itself represents only a small degradation in beam quality. This type of intensity modulation is also observed experimentally especially in cases where the SBS medium is restricted to only a few Rayleigh ranges (as is the case in BRIWON). The "intensity fidelity" can be improved by extending the SBS medium beyond what is conventionally known as the interaction region and Reference 1 has shown this in a SBS MOPA where part of the amplification of the Stokes beam occurs in the near field of the pump (amplifier). Finally, Figure 3.6d shows the results for the same aberrations combined with 3 m propagation to the etalon. The beam in this case has degraded to the point where the intensity modulation is nearly 100%, with very high spatial frequencies, and the wavefront fidelity is very poor. This result is probably due to intensity and phase mixing during propagation which results in phase information being lost when the beam is focused in the SBS medium (far-field).

These results underscore the need to minimize aberrations and in particular diffraction in the presence of aberrations. To accomplish this, the experimental layouts were modified to incorporate image relaying optics, eliminating diffraction from intracavity apertures. In addition, the slab amplifier was replaced with the low aberration rod amplifier and the MO beam size was reduced so that it can propagate through the rod without significant diffraction. These modifications resulted in an experimental arrangement similar to the first case described above (Figure 3.6a) which predicted excellent beam quality after three round trips.

4. MECCA EXPERIMENTS

The MECCA experimental effort went through four phases as described later in this chapter. The following is a summary of the evolution of the experimental effort to help follow the detailed discussion.

The first experimental phase was the demonstration of the MECCA cavity and identifying key requirements for efficient extraction. The experiments were performed without a gain medium. This phase of experiments was highly successful because we were quickly able to demonstrate oscillation in a cavity formed by an etalon and a methane SBS cell and were able to efficiently extract a pulse after four round trips.

In the second phase we introduced a gain medium and attempted to extract an amplified pulse using methane as the SBS medium. Here we encountered problems with a competing process SRS, which was not observed at the low energies, and we tested several SBS materials to find ones that avoid this problem. Acetone and ethane were found to eliminate SRS but we discovered severe beam quality degradation similar to the ones predicted by BRIWON. The layout was therefore modified to minimize aberrations and diffraction, but the problem persisted, indicating that another mechanism was causing the beam quality degradation.

Phase three was based on the speculation that SBS fidelity, and the accumulation of aberrations may be the cause of the poor beam quality. Experiments were performed to measure the wavefront fidelity of SBS under different conditions and using different materials. Freon was found to have excellent dynamic range and not susceptible to competing processes and was selected as the material of choice.

Phase four consisted of MECCA experiments with freon where the beam quality problem persisted. A careful investigation of common focus SBS was performed to identify the source of degradation. This resulted in significantly improved performance with moderate gain and beam quality and also led to the development of the alternate configuration MECCA (AC MECCA) which is described in Chapter 5.

4.1 MECCA Cavity Demonstration

The MECCA cavity concept was demonstrated using the optical layout schematically shown in Figure 4.1. The apparatus included the injection seeded Quantel master oscillator which was spatially filtered and expanded to minimize the probability of

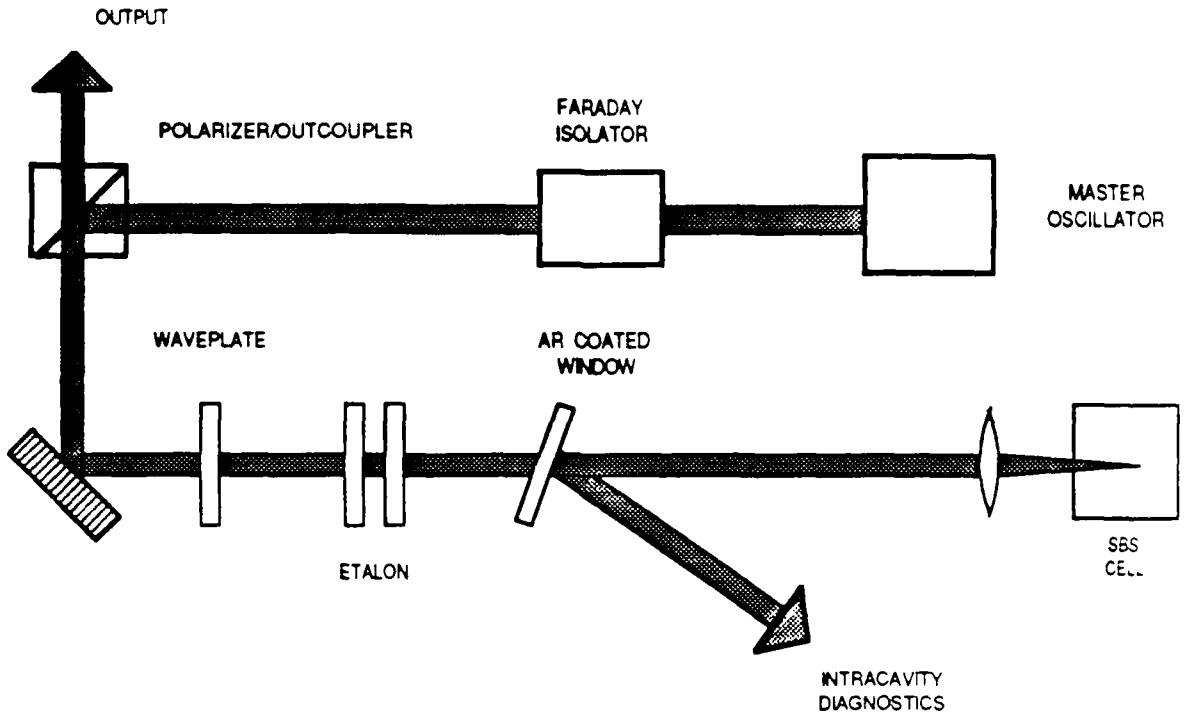

Figure 4.1 Optical layout for the MECCA cavity demonstration

damaging the etalon. Up to 120 mJ, with a pulse length of 6±1 ns could be injected into the cavity. A half wave plate/polarizer pair was used as an attenuator. The polarizer also served as the outcoupler for the extracted beam which was polarization rotated using a $\lambda/4$ plate further downstream. A four round trip MECCA cavity was formed with the Burleigh air gap etalon with a FSR of 3.4 GHz (4.4 cm mirror separation) and an SBS cell containing 60 amagat of methane with a characteristic SBS frequency shift of approximately 0.85 GHz. Methane was used because it has a relatively high SBS frequency shift, high breakdown threshold, low SBS threshold and high reflectivity. Methane is also easy to obtain in high purity, eliminating the need for purification. Figure 4.2 shows the curve for incident energy vs reflected energy for methane indicating a threshold energy of 4 mJ and a reflectance slope efficiency of 88%.

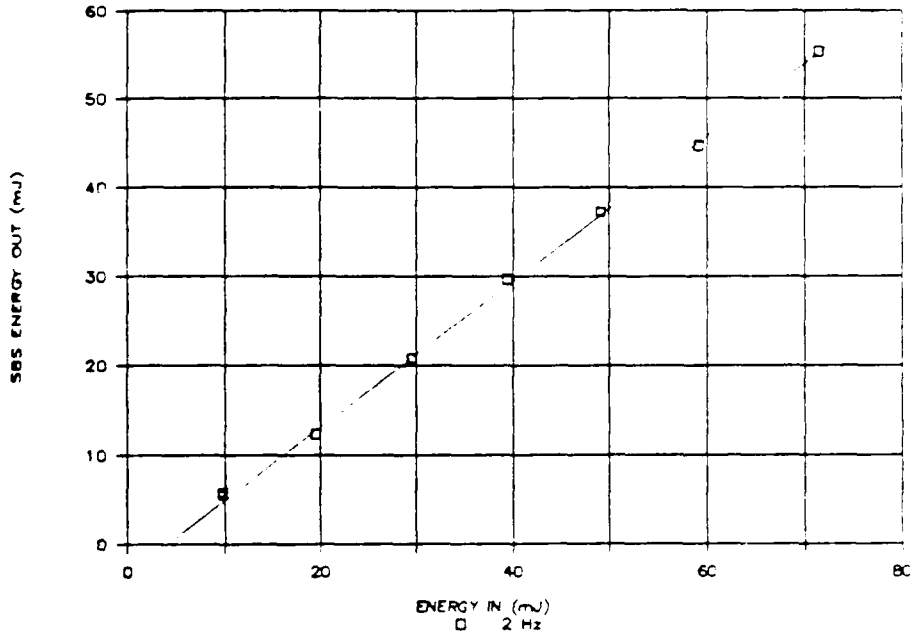

Figure 4.2 SBS reflectivity and threshold in methane

An intracavity wedge was used to diagnose the oscillating pulse and a wedge upstream of the etalon was used to monitor the reflection from the etalon and the extracted pulse from the cavity. Fast vacuum photodiodes were used to detect the pulses and the cavity round trip time was set to approximately 20 ns to eliminate pulse overlap and enable resolution of individual reflections inside the cavity. Figure 4.3a shows the oscillation pattern seen by the intracavity wedge when a 60 mJ pulse is injected into the cavity. The first pulse represents the beam transmitted through the etalon, the second pulse shows the beam after one complete round trip, and so on. The beam outcouples after 4 round trips and there is a very small residual beam reflected from the etalon probably due to the etalon transient response. Figure 4.3b shows the initial reflection from the etalon and the pulse extracted after four round trips. The reflected pulse from the etalon was created by slightly mistuning the etalon to provide a time reference for the extracted pulse. Two important features were immediately observed; the first was that the data in Figure 4.3b showed virtually no leakage of the oscillating pulses prior to extraction; the second was that the oscillation pattern in Figure 4.3a indeed terminates after the fourth reflection from the SBS cell indicating good extraction efficiency. These results were extremely encouraging; hence, at this point, no attempt was made to examine the beam quality of the extracted pulse.

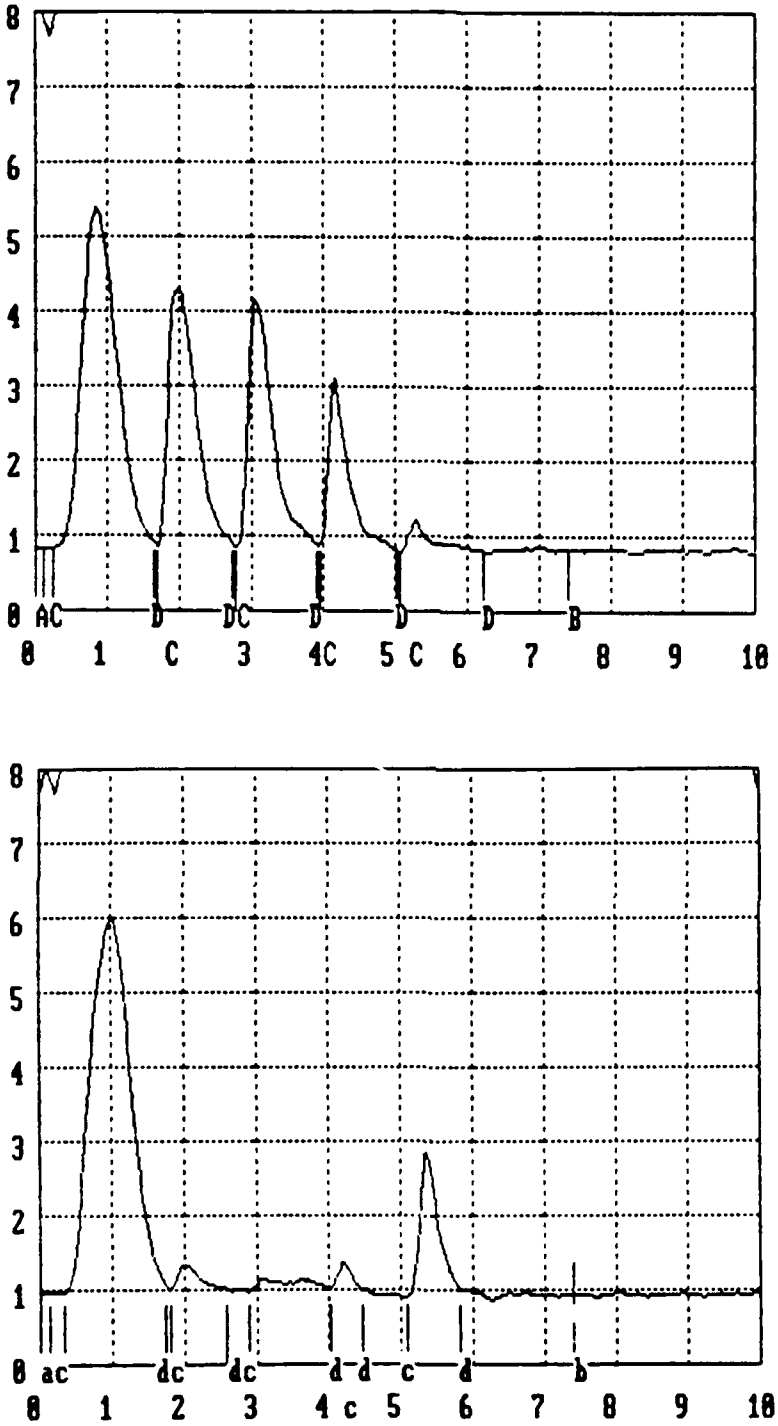

Figure 4.3 MECCA cavity demonstration. a) intracavity oscillation, b) reference pulse reflected from the etalon and extracted pulse after four round trips

4.2 MECCA Experiments With Gain

The experimental apparatus for MECCA with gain underwent many changes, the most notable of which were the introduction of image relaying optics and replacement of the slab amplifier with the rod amplifier. The bulk of the experiments were done with four SBS media: methane, acetone, ethane and freon. The experiments with freon were the last series performed and are described in Section 4.3. The other sets of experiments, the main results and conclusions are summarized in Figure 4.4. The following is a brief discussion of each set.

Test Series	1	2	3
Gain Medium	Nd:glass slab	Nd:glass slab	Nd:glass rod
Gain	1 to 2.5	1 to 2.5	1 to 2.8
Optical Layout	Free Diffraction	Free Diffraction	Image Relayed
SBS Medium	Methane	Acetone	Ethane
Freq. Shift (GHz)	0.9	3	0.6
Threshold (mJ)	4	3	3
Slope Efficiency	.77	0.90	0.88
Etalon FSR	3 to 9	3 to 9	2 to 6
Finesse	6 , 11, 20	6, 11	6, 11
Major Results	• SRS • Low Amplification	•Intensity Breakup • Absorption • Low Amplification	• Intensity Breakup • Low amplification

Figure 4.4 Summary of preliminary experiments and major results

Test Series 1: Slab Amplifier With Methane SBS Medium

These were the first series of tests with an amplifier, and other than the introduction of the amplifier, the experimental arrangement was very similar to that used for the MF CA cavity demonstration. An additional wedge was placed immediately in front of the SBS cell to sample the pulses entering and exiting the SBS cell. The key result from this set

of experiments was the fact that SBS in the MECCA configuration was qualitatively different than single pulse experiments, and SRS was observed on most SBS pulses which had already experienced one or more SBS reflections. Figure 4.5 shows the pulse train exiting the SBS cell. The onset of SRS exhibits itself as a spike at the front of the pulse and is never present on the input pulse (1st reflection). The presence of SRS was diagnosed by dispersing a sampled beam exiting the SBS cell using a grating. The reflection from the grating was calibrated and was found to contain 1.5 μm light corresponding to the first vibrational Stokes shift in methane. As explained earlier, SRS was not observed on single pulse experiments because the slow rise time of the temporally gaussian beam allows the SBS grating time to establish itself and the lower gain SRS is suppressed. However, a pulse already reflected once from the SBS cell has a much sharper rising edge because the front tail of the gaussian is used to establish the first SBS grating. Thus, during the early part of the pulse SRS, which is virtually instantaneous, can dominate. The SRS pulse not only represents a loss mechanism, but it also introduces significant heating in the focal volume by populating vibrational levels which deactivate and heat the medium.

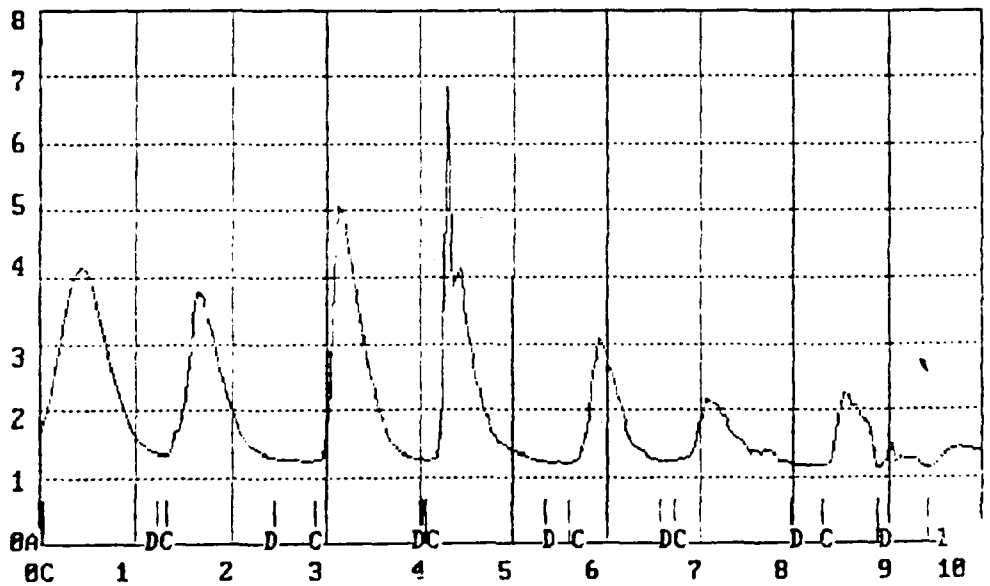

Figure 4.5 Intracavity MECCA pulse train with gain using methane as the SBS medium. The pulse trains are measured in front of the SBS cell, the reflections from the SBS cell are time delayed and added to the input train so that each input pulse has its reflection next to it.

There are two methods of avoiding SRS in the medium: the first is to use a liquid; liquids have much shorter phonon lifetimes (a few ns instead of tens of ns), and can respond much faster to the incident field. This led to Test series 2 described next. The second method is to find a gas which is a good SBS medium but has very low Raman cross-section. Two gases fell under this category: nitrogen and ethane. Nitrogen was tested but was also found to suffer from SRS, ethane did not, and was used in Test series 3 described further below.

Test Series 2: Slab Amplifier With Acetone SBS Medium

For many applications, acetone has been demonstrated to be an excellent SBS medium. Figure 4.6 shows an energy incident vs. energy reflected curve of acetone indicating a low threshold of 3 mJ and excellent reflectance slope efficiency of 90%. Its major drawback is that it is difficult to obtain (and maintain) high purity acetone because it is such a good solvent. The acetone we obtained was rated 99.8% and care was taken to avoid contamination. Another advantage of acetone is its very large SBS frequency shift of 3 GHz at 1.06 μm. This enabled us to perform experiments with the etalon tuned to any number of round trips, including one or two. By increasing the number of round trips one at a time, we were able to observe for the first time the catastrophic degradation of the beam quality. Figure 4.7 shows the intensity profile of the outcoupled beam after one two and three round trips. The breakup of the beam into high spatial frequency components is similar to that predicted by BRIWON when significant aberrations are present and no image relaying is used.

Test Series 3: Rod Amplifier With Ethane as the SBS Medium

This series of tests was designed to address all potential issues predicted by the BRIWON model and a minor issue related to acetone as the SBS medium. It was observed during Test series 2 that there was a finite amount of absorption in acetone regardless of its purity. This manifested itself as higher SBS reflectivity when the SBS cell was positioned to minimize the penetration depth of the beam into the liquid. To avoid any potential deleterious effects caused by this absorption, a new SBS medium, ethane, was used. In addition, the slab was replaced with a rod amplifier with no significant aberrations, and the cavity was reconfigured to include two image relaying telescopes (Figure 4.8). The first telescope relayed the plane of the etalon to the middle of the amplifier and the second telescope relayed the midplane of the amplifier to the SBS lens. The second telescope was

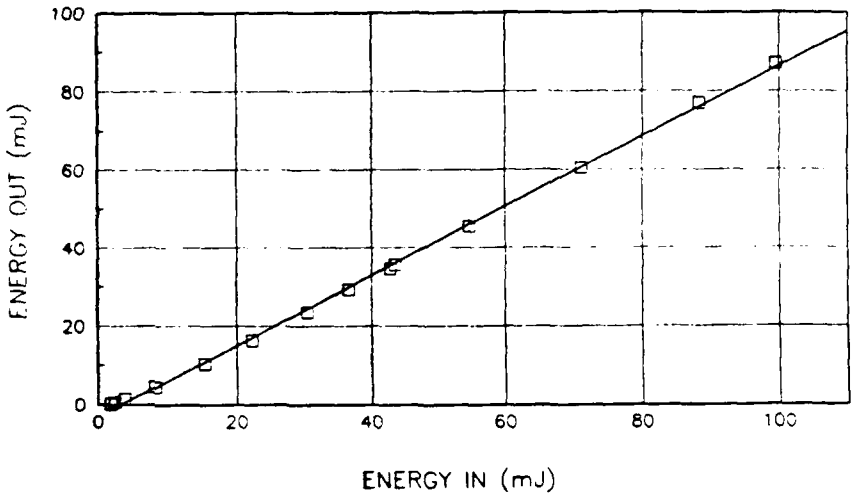

Figure 4.6 SBS reflectivity and threshold in acetone

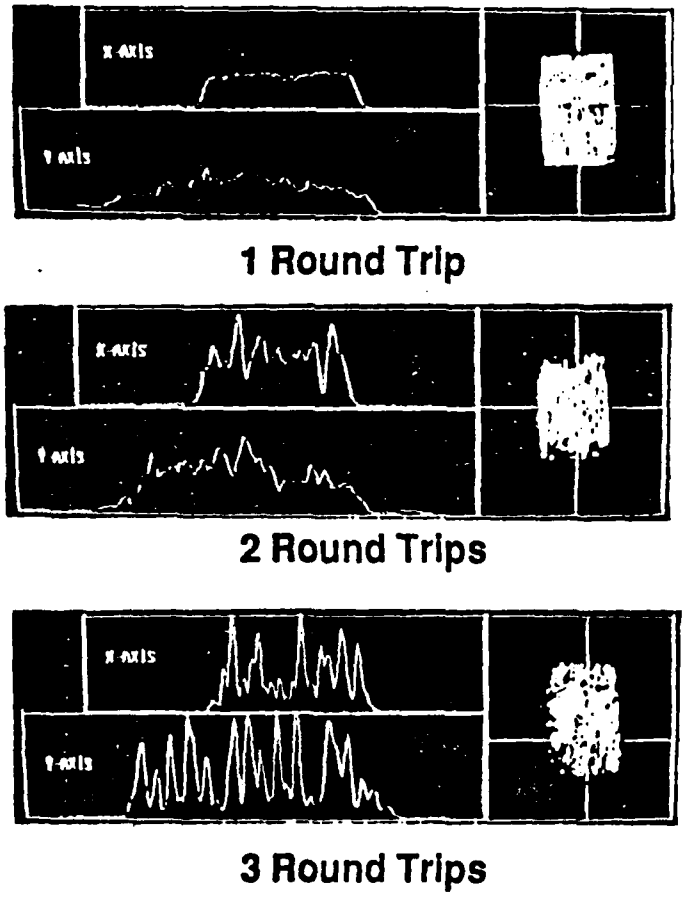

Figure 4.7 Nearfield intensity distribution of the extracted pulse as function of the number of round trips with acetone as the SBS medium

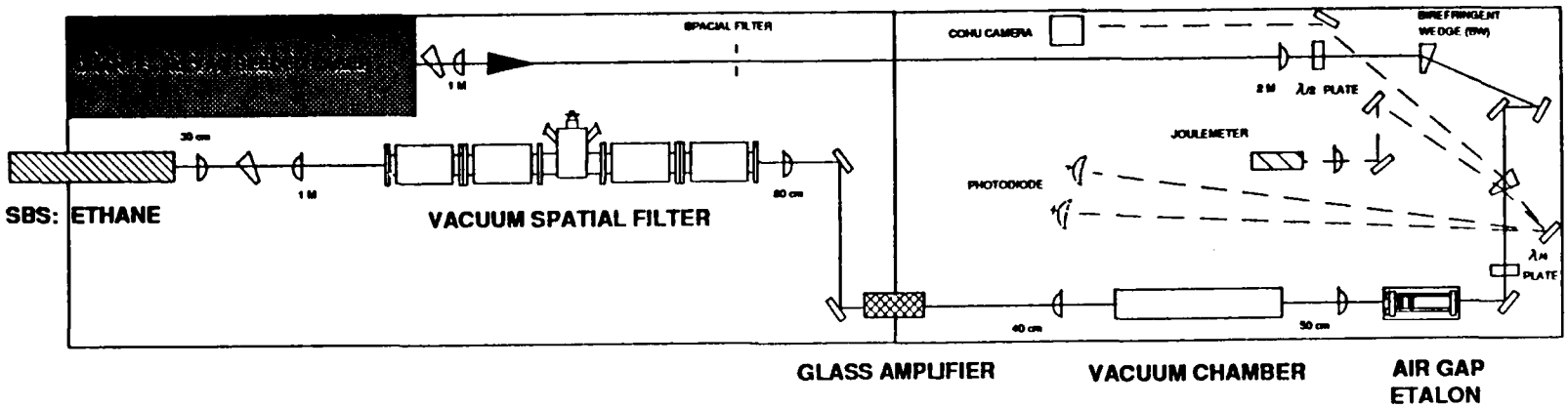

Figure 4.8 Optical layout of MECCA cavity with the rod amplifier and modified to include image relaying telescopes

also equipped with a vacuum spatial filter. The purpose of this was to assess the benefits of using an oversized filter to eliminate some of the high spatial frequency components on the return beam from the SBS cell. To further minimize diffraction effects, the spatially gaussian master oscillator beam was demagnified to be less than the rod diameter, so that there were no diffracting apertures in the optical train.

The use of ethane as an SBS medium was first noted in Reference 2. The authors noted that at 60 to 70 amagats (800 to 1000 psi), ethane has good SBS gain and very low Raman cross-section. The only inconvenient feature of ethane is a vapor pressure of approximately 35 amagats (500 psi) at room temperature with a critical temperature of 32°C. To increase the pressure to 60 amagats, one must heat partially liquified ethane above the critical temperature. In order to achieve this an ethane distillation and transfer apparatus was assembled where ethane was distilled directly into a temperature controlled and thermally isolated SBS cell. Figure 4.9 shows a schematic of the distillation apparatus. The distillation apparatus consisted of a vertical section of tubing above the SBS cell which was surrounding by another tube carrying water at 5°C. The temperature gradient between the tube and the ethane cylinder caused the gas to condense inside the tube and drop into the SBS cell. The cell volume was 75 cm^3, and 30 to 40 cm^3 of liquid ethane could be

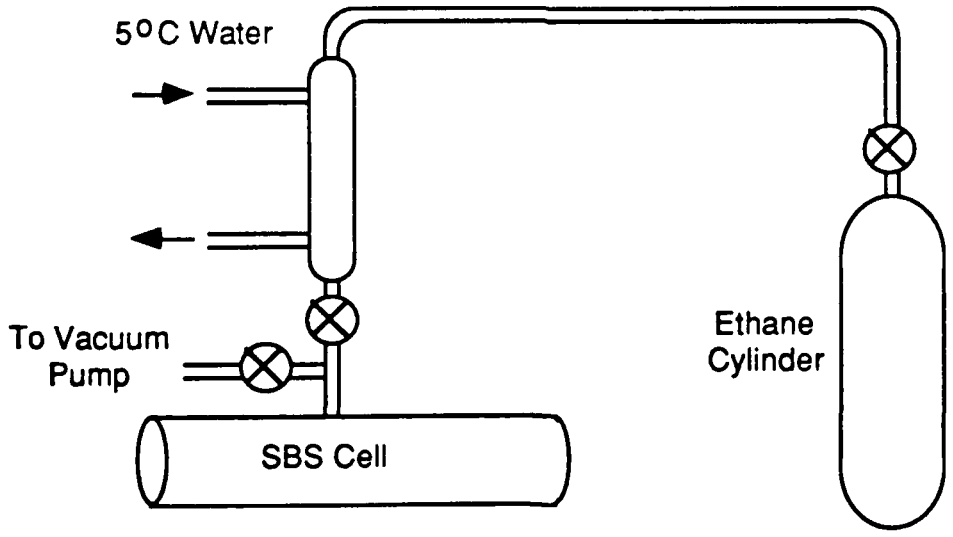

Figure 4.9 Schematic diagram of the ethane distillation apparatus

transfered in a few minutes. After distillation, the cell temperature was raised to the operating temperature of 38±1°C. A high degree of temperature stability was required because at these temperatures ethane exists in a highly compressible phase such that any temperature gradients in the cell result in significant density fluctuations in the medium. This could act as a severe aberrator to the input beam and may not be corrected if it is close to the focal volume.

At 60 Amagats ethane was a fairly good SBS medium but temperature control remained a problem, and coupled with this, was the SBS frequency shift which varies rapidly near the critical temperature. An on-line etalon was necessary to measure the SBS shift throughout an experiment to insure that conditions had not changed. A fortuitous breakthrough occurred when helium was mixed with the ethane. The original purpose for this was to increase the SBS shift by increasing the speed of sound in the medium. The SBS shift was indeed increased from approximately 0.6 GHz to 0.8 GHz; however, at the same time, the large thermal conductivity of He made the entire slug of gas isothermal and significantly less susceptible to temperature fluctuations. Thus, the standard SBS medium became a 60:90 amagat mixture of ethane and helium operating at approximately 38°C. With this mixture the only concern was He diffusion out of the cell which was easily replenished every morning.

Figure 4.10 shows the reflected vs incident energy curve for ethane. It shows a threshold of 3 mJ and a slope efficiency of 89%, nearly identical to those observed for acetone. MECCA extraction experiments were performed with a three round trip configuration. Figure 4.11a shows the intracavity SBS input and reflected pulses and Figure 4.11b shows a photodiode trace of the extracted pulse with a reference pulse which is calibrated to match the input pulse in energy. No evidence of SRS is observed, however, the overall amplification is only a factor of roughly 2 which is attributed to the degradation of the SBS reflectivity. Figure 4.12 shows the intensity distribution of the extracted pulse indicating the catastrophic beam breakup typical of earlier experiments. Using spatial filters of any size resulted in increased loss and did not improve performance. The main conclusion from these experiments was that the effects predicted by the BRIWON model alone are not enough to explain the severe degradation in the beam quality seen in the experiments. BRIWON had predicted that this type of degradation was due to a combination of diffraction and aberrations, and both phenomena were eliminated from the latest set of experimental arrangement.

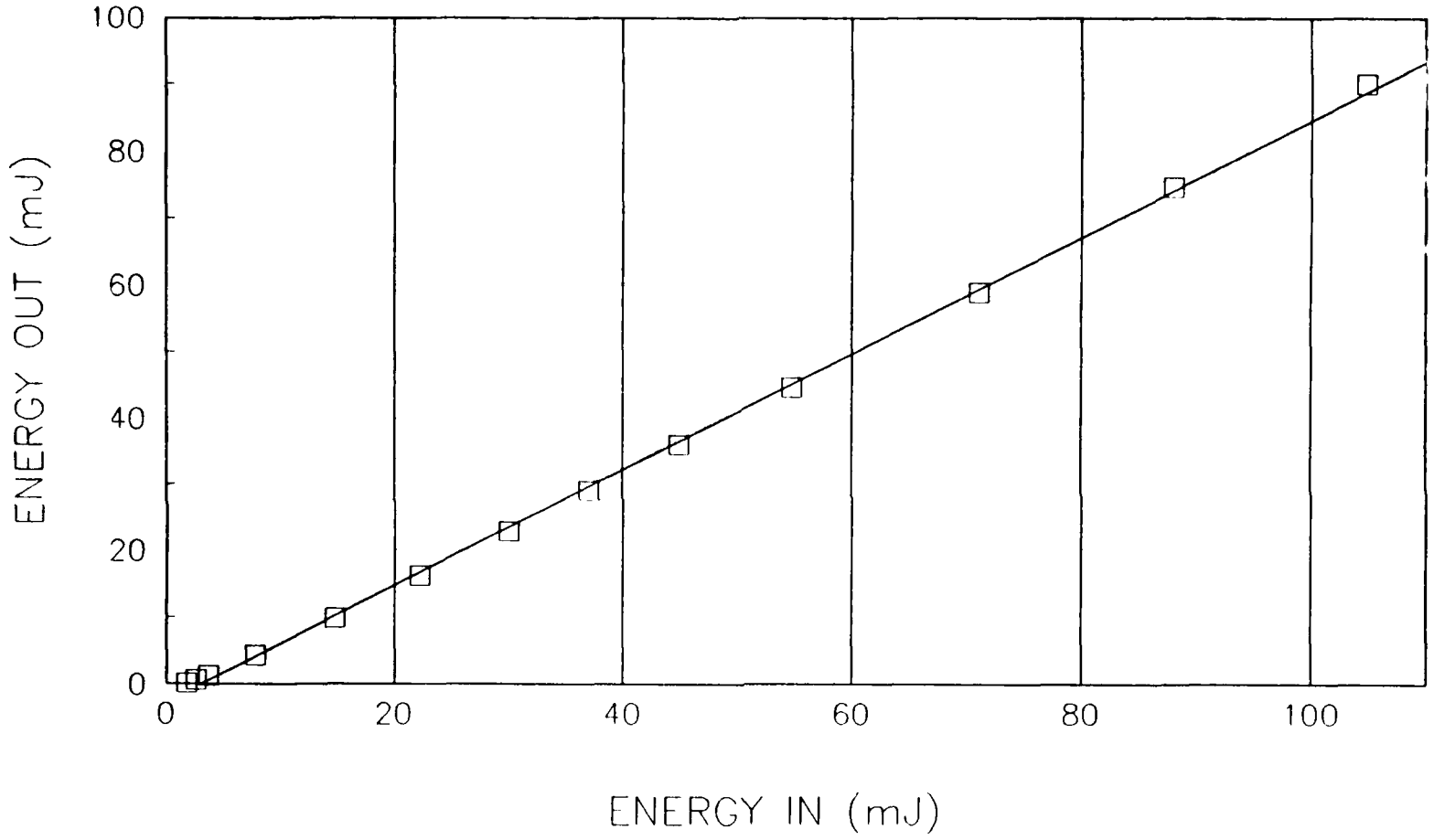

Figure 4.10 SBS reflectivity and threshold in ethane

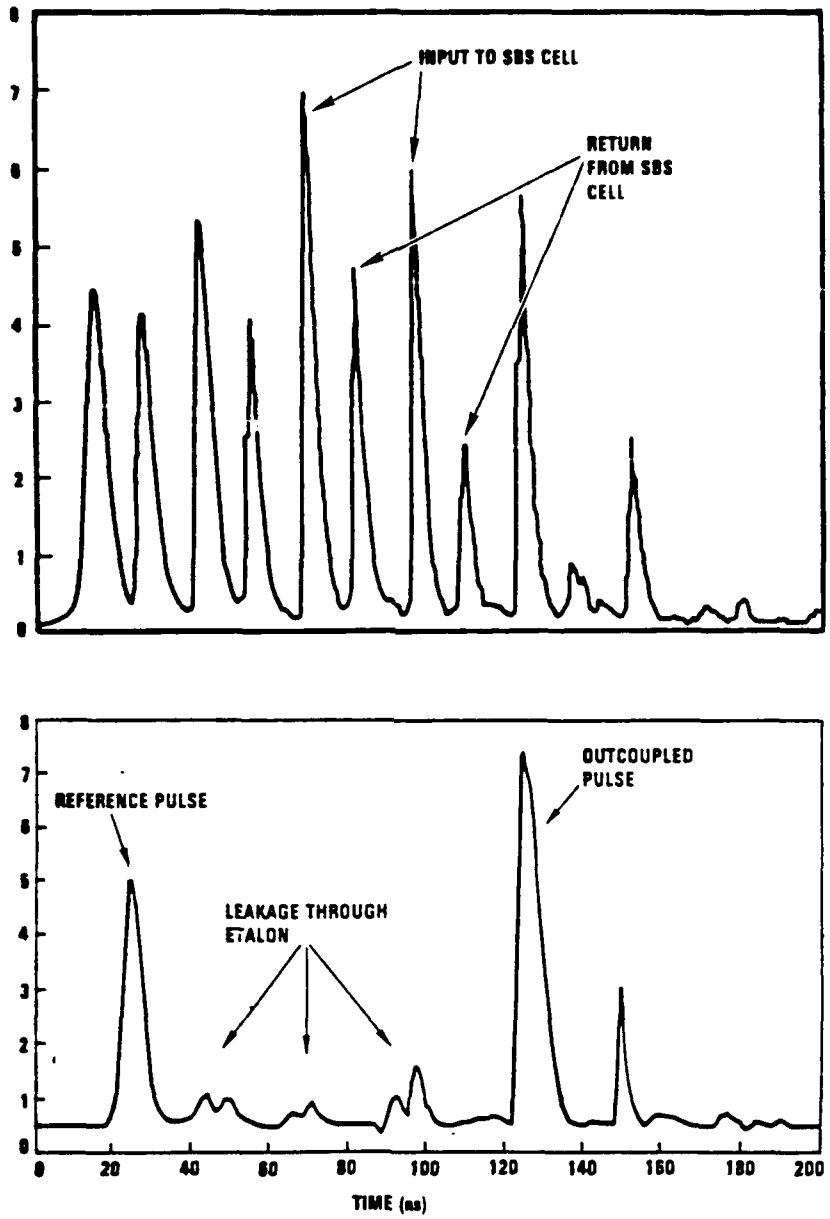

Figure 4.11 Overall amplification using the MECCA layout shown in Figure 4.8. a) Intracavity pulse train, b) extracted pulses; the first major pulse is calibrated to match the input pulse, the second pulse is the pulse extracted after three round trips.

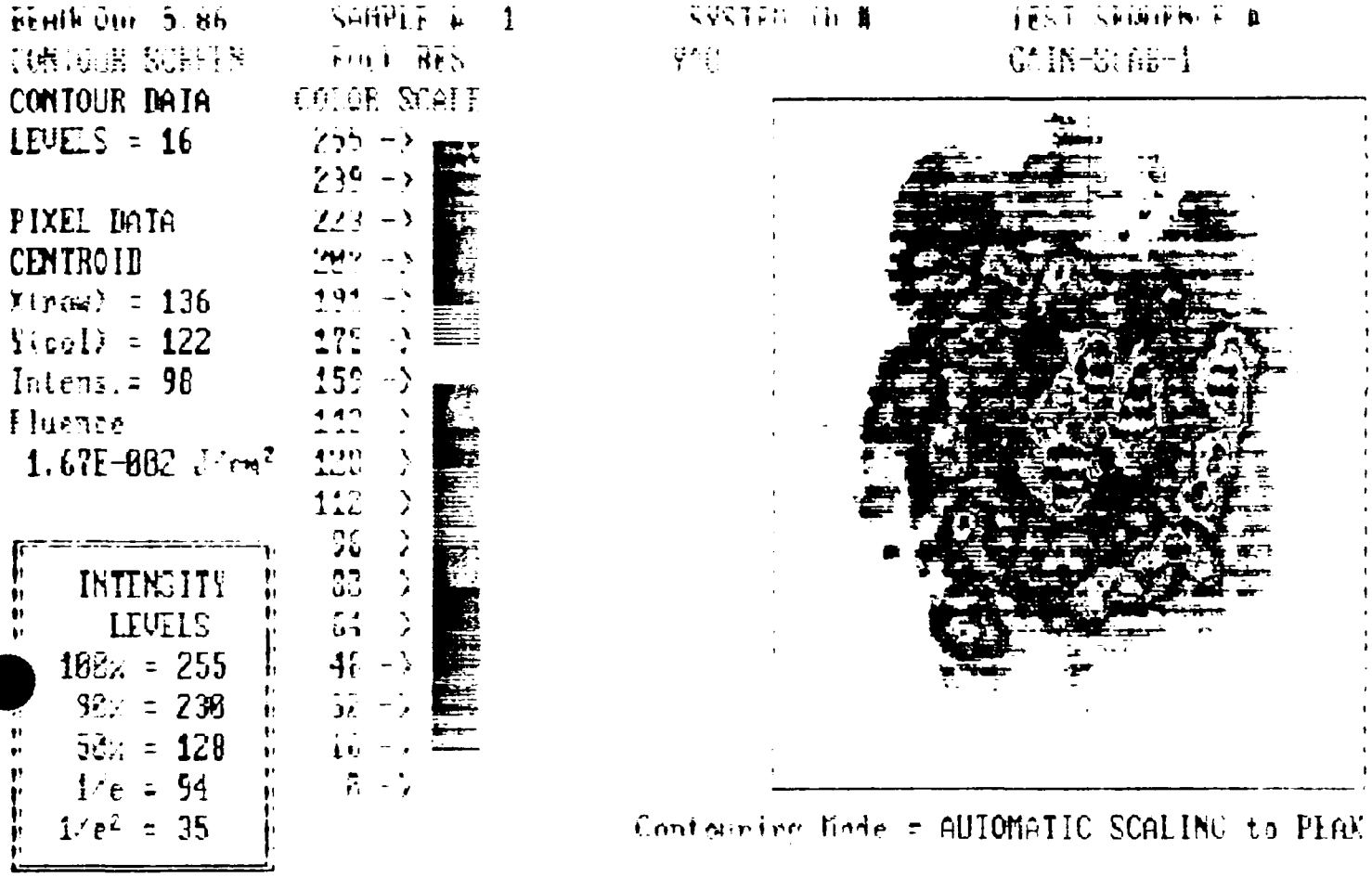

Figure 4.12 Nearfield intensity distribution of the pulse extracted after three round trips using the MECCA layout shown in Figure 4.8

4.3 SBS Physics and Material Considerations

The preliminary MECCA experiments described in the previous section indicate that the beam quality of the intracavity pulse degrades with successive round trips in a manner that the BRIWON model calculations cannot explain. In addition, the net intracavity gain degrades long before amplifier saturation effects should occur. These problems justify a more careful consideration of the demands that MECCA imposes upon the SBS process.

In particular, one requirement that the MECCA scenario places on the SBS medium is a wide dynamic range (over laser pulse energies 50 to 100 times threshold) for both the reflectivity and the phase conjugate fidelity of the SBS reflection. Possible factors limiting the dynamic range of SBS are various competing processes whose effect might be to suppress SBS efficiency or degrade the SBS phase conjugation fidelity. Another requirement that MECCA imposes is that the condition characterizing the SBS medium on any given round trip has not been adversely affected by the previous round trips. As it happens, this is a crucial issue and will be addressed in Section 4.3. This section presents the results of dynamic range measurements for various candidate SBS media. The effect of focussing geometry (f/#) and near-field phase aberration plates will be discussed.

4.3.1 Description of Stimulated Brillouin Scattering

Stimulated Brillouin scattering takes place through the electrostrictive interaction of electromagnetic radiation and acoustic phonons. An incident pulse of laser radiation is sent into a Brillouin active medium, causing the simultaneous buildup from thermal noise of a forward propagating acoustic wave and a backward propagating optical wave whose frequency is downshifted from that of the incident wave by the acoustic grating frequency, or Brillouin frequency.

An amount of energy termed the SBS threshold energy is required to establish an acoustic grating of intensity sufficient to amplify the thermal noise to the levels of the incoming pulse energies. Once established, the grating serves to reflect the remainder of the incoming pulse with an efficiency commonly known as the "slope efficiency." Together, the SBS threshold and slope efficiency determine the overall reflectivity of the incident laser pulse. By measuring the SBS return energy as the incident pulse is varied, one can establish experimentally the SBS threshold energy and slope efficiency for a particular medium.

Two particularly important properties characterizing the acoustic grating are the speed of sound in the SBS medium and the phonon lifetime. The speed of the acoustic grating determines the Brillouin shift as the Doppler shift of the incident wave reflected from a receding grating. The Brillouin shift, $\Delta\omega_B$, of the SBS return wave is thus given by the expression

$$\Delta\omega_B = 2\,\omega_O\,(v_S/c),$$

where v_S and c equal the speed of sound and light in the SBS medium, respectively, and ω_O is the frequency of the incident beam. This, of course, is equal to the frequency of the electrostrictive driving field and thus to the acoustic grating frequency.

The phonon lifetime of a material is the characteristic time scale for elastic scattering of an acoustic phonon. In so far as a macroscopic acoustic grating is an ordered collection of acoustic phonons whose k vectors are all approximately parallel, the phonon lifetime is the time that it would take for such a grating to decay, in the absence of a driving field, into disordered density fluctuations resembling turbulence. The scattering of the phonons has the effect of destroying their spatial coherence, although the total acoustic energy is not diminished. Borrowing the parlance of temporal coherence theory, we might say the phonon lifetime specifies a transverse relaxation time (T_2) for the SBS medium. The decay of the acoustic grating will appear as an especially important player in the multiple reflection conditions required of the MECCA concept.

One desires to find a medium that maintains high reflectivity over as wide an energy range as possible. In terms of the MECCA concept, the medium should have a high reflectivity at a pulse energy roughly equal to the energy the laser pulse has just prior to its final (single) pass through the amplifier, and a threshold low enough to support an SBS reflection for the laser pulse after a single amplifier pass. This means that for round trip amplifier gains of 10, a dynamic range of 100 in the SBS medium will allow overall gains of 1000.

The same wide dynamic range is desired for the wavefront fidelity of the SBS reflection. Phase conjugate fidelity is a measure of how well the SBS reflection reverses the wavefront of the incoming beam, and therefore how well the optical system aberrations will be corrected upon retraversal of the optical elements that created those aberrations. Various experimental methods are employed to measure this ability quantitatively. Most of them seek to measure the fraction of reflected energy that resides in the conjugate portion of the SBS return beam. Essentially, the wavefronts of the incident and return beams are compared to see how well they are matched. Our method as described below in the

experimental description of the dynamic range experiments consists of energy in a bucket measurements.

Unlike the nonlinear interactions responsible for phase conjugate reflection by degenerate four wave mixing (DFWM), the nonlinear polarization generated during stimulated Brillouin scattering is not manifestly phase conjugate to the incident beam. The SBS reflection is said to consist of a conjugate and a non conjugate fraction. As shown first by Zeldovich, under favorable conditions, the conjugate fraction SBS dominates the return beam.

4.3.2 Competing Processes

In general, the nonlinear processes occurring simultaneously with SBS can result in the aberration of the incident wavefront, the generation of frequencies not present in the incident beam, or both. SBS can correct most aberrations provided they are produced in the near-field of the beam. Aberrations produced by most competing processes, however, occur in the focal volume where the intensities are the highest. These type of aberrations are not corrected by SBS because they do not contribute to the formation of the acoustic grating which is driven by the far-field intensity distribution of the incident beam.

Stimulated Raman Scattering (SRS): SRS as a competing process in methane was already mentioned earlier in section 4.1. The lifetimes of the optical phonons that accompany SRS are generally much smaller than those of the acoustic phonons that accompany SBS. As a result, it is still possible under certain conditions to generate a significant SRS return even if the gain-length product for SBS exceeds that for SRS. These conditions typically arise when the pulse energy is above threshold for both processes and the leading edge of the pulse has a rise time that is much faster than the acoustic phonon lifetime. If such circumstances prevail, then the Raman return generated during the early portion of the input pulse will diminish as the Brillouin return starts to dominate.

While SRS is capable of generating phase conjugate wavefronts, the large wavelength shifts render it unacceptable for use in MECCA. In addition, the generation of the Raman pulse is accompanied by the deposition of energy, in the form of vibrational energy, into the Brillouin medium. This energy deposition results in density fluctuations that could cause problems for the conjugation of subsequent pulses. The presence of even small Raman return energies is therefore to be avoided. This means avoiding media with large Raman cross-sections such as methane and n-hexane which are well established as a

good SBS media for most single shot applications, but too efficient a Raman generator for use with MECCA.

Thermal Blooming: Thermal blooming is a process whereby a medium is heated by absorption of incident radiation, resulting in a modification of the beam focus. Because of the thermal nature of this process, it should not affect the propagation of optical radiation on a single shot basis, but absorption and subsequent heat generation will affect subsequent pulses. In our studies, blooming has been observed under certain circumstances and is accompanied by reduced conjugation fidelity and reflectivity. Evidence of thermal blooming is manifest both in the patterns of the beam transmitted through the SBS cell and in the increasing degeneration of conditions with increased laser repetition rate. We have found that acetone and ethanol are media susceptible to thermal blooming specially if their purity is compromised.

Self Focussing: Self focussing would degrade the conjugation fidelity by compromising the far-field intensity distribution critical to forming a faithful acoustic grating. Self focussing may also enhance the probability of another deleterious effect, namely that of optical breakdown. In our studies, we have no definitive observations of self focussing, but its presence was speculated in CCl_4. Breakdown in CCl_4 was observed at very low energies ($\leq$ 20 mJ) regardless of material purity.

Optical Breakdown (OBD): Shen (Ref. 3) has given a theoretical treatment of optical breakdown and discussed experimental studies in its context. Typically OBD occurs because of the generation of free electrons through multiphoton ionization in the focal volume. In some instances, free charges may already be present through ionic contamination or generation from previous pulses. Once free electrons are produced, they are driven by the remainder of the optical pulse to create more electrons in a process of avalanche ionization. This takes place while charges diffuse from the focal volume. Thus, the evolution of optical breakdown is determined through the competition of avalanche multiplication and diffusion.

Recent experiments by Mullen et.al. (Ref. 4) have increased the thresholds for optical breakdown by using artificial means to clear free electrons from the focal volume. In these studies, a strong electric field was applied to the focal volume by a pair of electrodes immersed in the SBS medium. This technique has been demonstrated successful in increasing optical breakdown threshold by purging the focal volume, on nanosecond time scales, under multiple pulse conditions not too different from that in MECCA.

4.3.3 Candidate Media

At sufficiently high pulse energies, the aforementioned nonlinear parasitic processes would occur in any medium. They would thereby limit the upper energy range of the conjugator. The lower practical energy range of the SBS medium is determined by the threshold energy required to establish an acoustic grating, as discussed earlier in Section 4.3.1. This energy, in turn, is determined by material properties such as the acoustic phonon lifetime and the photoelastic constant of the material. Several media were tested as potential phase conjugators for MECCA and the performance of some was shown earlier in Section 4.1. Figure 4.13 summarized the characteristics of some of the SBS media tested.

The two media with the best dynamic range for SBS are nitrogen gas and trichloro-trifluoro ethane (hereafter freon-113 or simply "freon"), which is a liquid at room temperature. These are found to have low threshold energies (25 mJ and 4 mJ, respectively) and are relatively immune to the effects of thermal blooming, Raman generation, and optical breakdown (Nitrogen produced small amounts of SRS in a MECCA configuration). Results for these media will be presented in more detail in the following sections.

Medium	Threshold (mJ)	Reflectivity Slope Efficiency	SBS Frequency Shift (GHz)	Phonon Lifetime (ns)	Parasitic Processes
Acetone	3	0.9	3	1.7	Absorption
CCl_4	5	0.9	2.8	0.7	Self Focussing
Ethane (800 psi)	3	0.88	0.6	20*	Absorption
Freon	5	0.92	1.8	4	None
Methane (1500 psi)	4	0.78	0.9	17	SRS
Nitrogen (1000 psi)	45	0.82	0.7	20	SRS
Xenon	10	0.95	0.3	37	OBD

* Estimated

Figure 4.13 Table of SBS media tested for MECCA and their characteristics

4.3.4 Dynamic Range Measurements

Experiments were performed to measure the dynamic range of SBS conjugation fidelity using two media: nitrogen and freon. The experiments with nitrogen were performed because data generated on TRW IR&D had shown that high purity nitrogen showed good but declining fidelity over a large dynamic range, and was not susceptible to competing processes in a single shot configuration. The experiments in nitrogen were performed to evaluate the effect of phase plates on fidelity. The experiments with freon were performed because Soviet literature indicated that it has excellent reflectivity and is not susceptible to competing processes over a large range of energies. the absence of competing processes made it a good candidate to consider for MECCA, however, no data was available on the fidelity dynamic range.

SBS in Nitrogen using Phase Plate Aberrators: Phase plates and lens arrays have been suggested as a method for improving the SBS fidelity dynamic range by smoothing the far field intensity distribution. Experiments were performed in nitrogen using the optical layout shown in Fig. 4.14. The master oscillator beam is provided by the Quantel injection seeded Nd:YAG laser which was described earlier. An external spatial filter was employed for beam cleanup; the beam subsequently traversed a rotatable half wave plate and birefringent wedge polarizer combination, which allowed for intensity adjustment. An anamorphic prism pair and hard aperture shaped the beam into a rectangle measuring 15 mm by 5 mm; this was matched to the acceptance aperture of a Nd:YAG slab amplifier, which was flashlamp pumped synchronously with the Quantel oscillator. The system can operate at a repetition rate of 2, 5, or 10 Hz.

Upon emerging from the amplifier, the beam was focussed by a spherical lens into a stainless steel cell pressurized with nitrogen gas to 1900 psi. Lens focal lengths of 30, 50, and 80 cm are used to achieve f/#'s of 35, 58, and 92, respectively. The SBS input and return beam energies are sampled by an AR wedge and directed to the energy probes E2 and E3, respectively; the ratio of these energies gives the SBS reflectivity.

The phase conjugate fidelity of the SBS process is characterized by the "power-in-the-bucket" method. The return beam is focussed with a 1 m focal length lens through a slit positioned in the focal plane; the slit is constructed to transmit 93% of the far-field beam energy of a diffraction limited beam. The energy probe E4 measures a sample of the total return beam energy, and probe E5 measures the energy transmitted through the rectangular slit. The ratio of these two energies, as measured for the SBS reflection, indicates the absolute quality of the return beam.

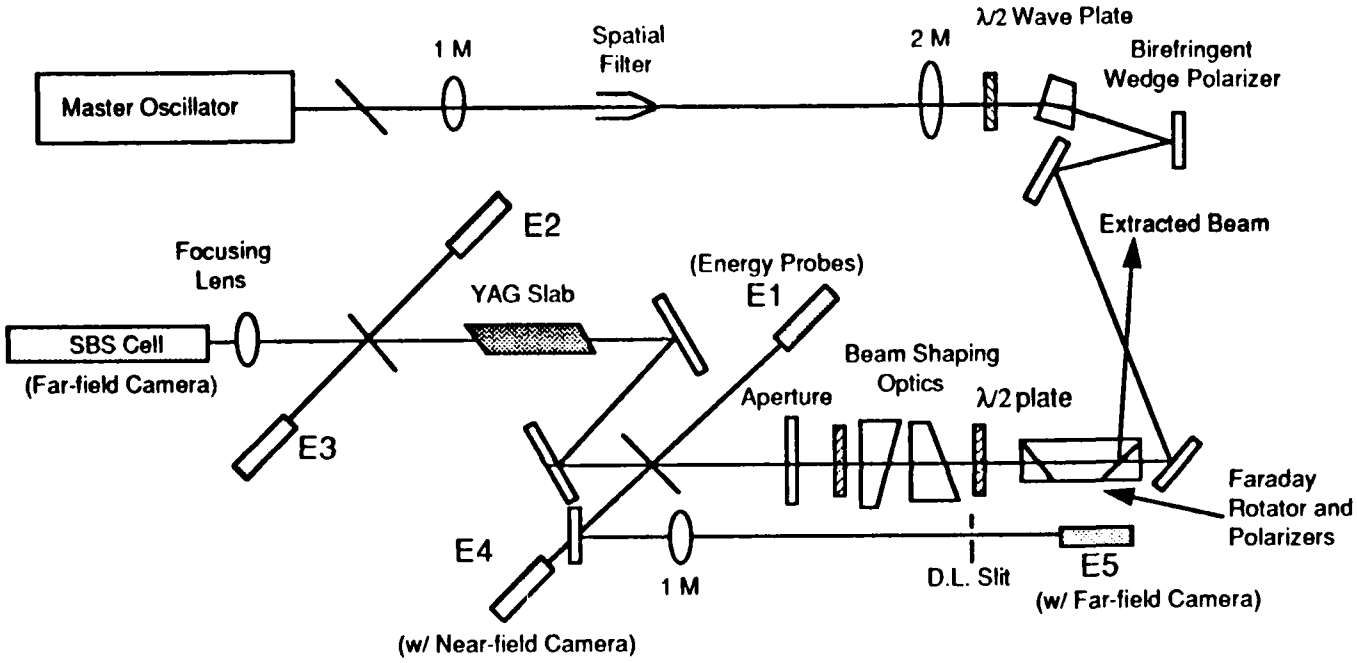

Figure 4.14 Optical layout for measuring the SBS reflectivity and fidelity dynamic range in nitrogen

In general, the return beam quality is determined both by the quality of the original input beam and by the phase conjugate fidelity of the SBS reflection. With this particular amplifier, the major source of optical aberrations is the slab itself. These aberrations however are not very severe at repetition rates below 10 Hz and are well corrected by SBS. The fidelity of the SBS return therefore includes correction of these aberrations and is defined by:

$$F = E5/E4 * 1/0.93,$$

that is, as the power-in-the-bucket ratio of the SBS return relative to the power-in-the-bucket ratio of a diffraction limited beam.

Figure 4.15 to 4.17 show the SBS characteristics of nitrogen obtained on TRW IR&D. They serve as a background to compare with the phase plate data. Figure 4.15 displays the SBS return energy versus the SBS input energy (or the energy probe readings E3 vrs E4 in Fig 4.14) for nitrogen using an f/# equal to 35. In accordance with the introductory discussion of this section, the extrapolated abscissa intercept of the asymptotic portion of this curve is the SBS threshold energy. The asymptotic slope is known as the slope efficiency, which is the limiting SBS reflectivity, realized in the limit of large injection energies. For this particular f/#, the threshold energy equals 25 mJ, and the slope efficiency equals 91%. Figure 4.16 plots the reflectivity vs input energy directly for three different f/# 's: 35, 58, and 92. From these plots it can be more readily seen that the reflectivity is better than 75% for input energies greater than 200 mJ.

Theory indicates that the gain-length product for SBS should be independent of the f/# for a bulk focus geometry. The slope efficiency is indeed independent of the lens focal length; however, the SBS threshold energies are found to decrease with shorter focal length lenses. Such a discrepancy with theory suggests the influence of some parasitic process; this discrepancy appears also in the fidelity data.

Figure 4.17 is a plot of fidelity as defined above vs input energy using nitrogen as the SBS medium. Fidelities of better than 80% are obtained over a tenfold dynamic range when the shorter focal length lenses are employed. In general, the fidelity degrades at the higher input energies and the effect is more pronounced for larger f/#s. Similar results have been reported by other workers using using both CS_2 and n-hexane as phase conjugating media (Ref. 5).

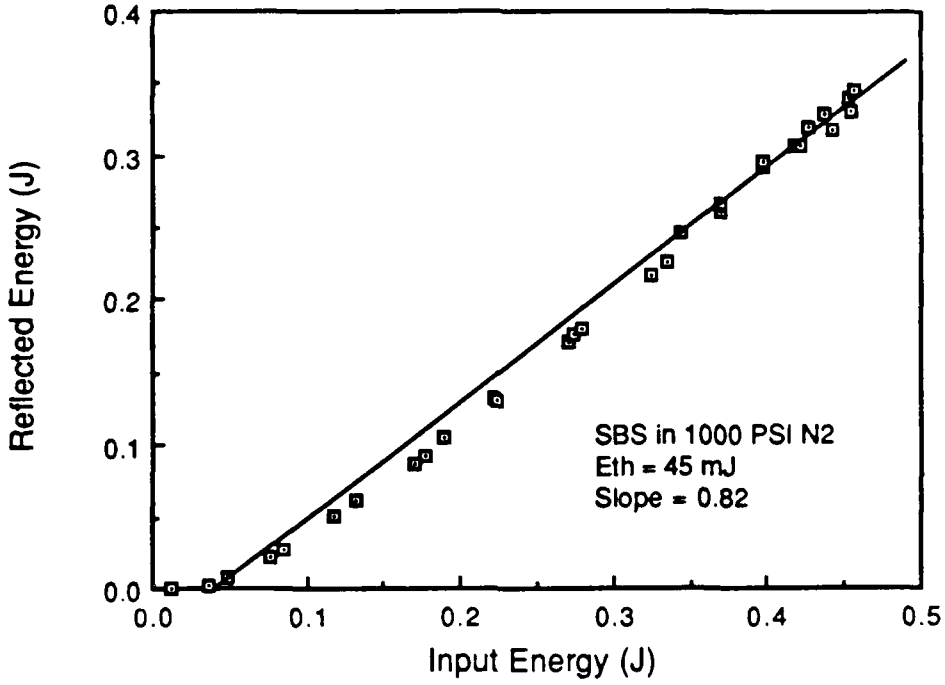

Figure 4.15 SBS reflectivity and threshold in nitrogen

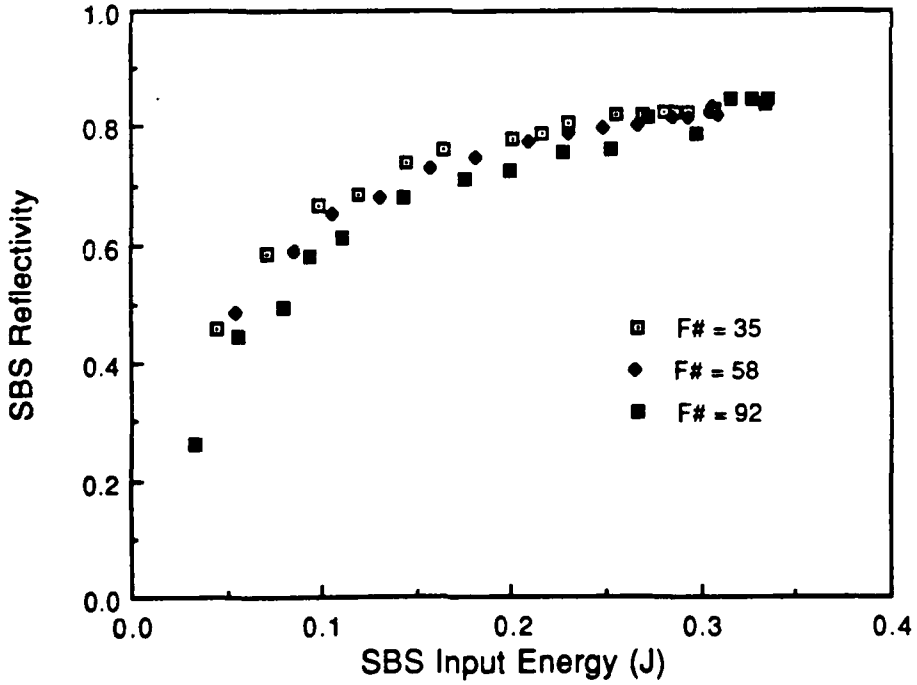

Figure 4.16 SBS reflectivity in nitrogen for several f/#s

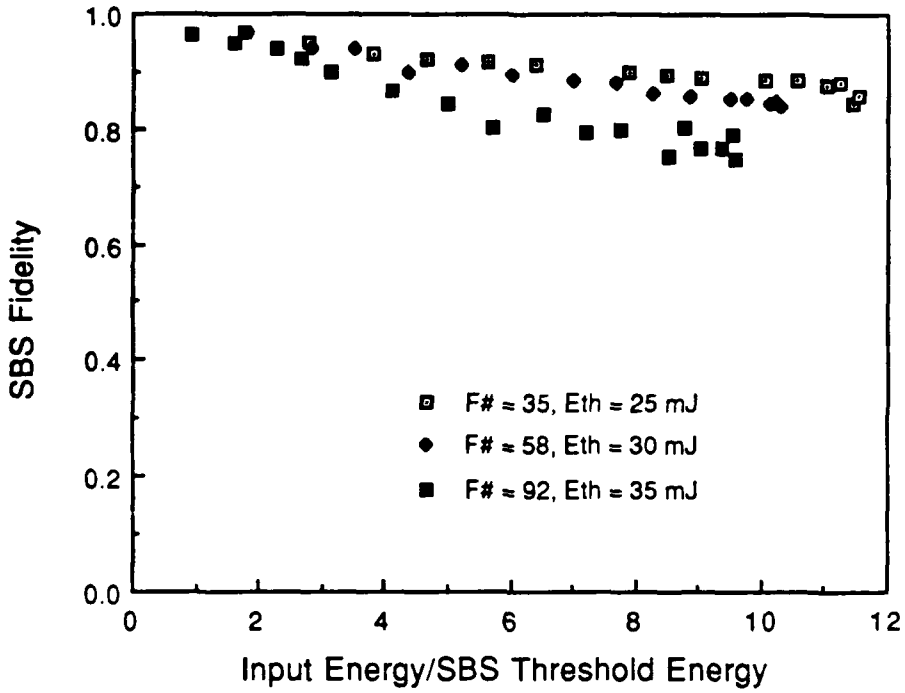

Figure 4.17 SBS fidelity in nitrogen for several f/#s

A phase plate consisting of a random distribution of 2 mm hexagonal half wave piston error was used to improve the dynamic range. This phase plate is similar to ones used at the University of Rochester Laser Energetics Lab. to improve the far field uniformity of the their fusion laser. This element was inserted into the beam immediately before the SBS focussing lens. Figure 4.18 is a plot of fidelity versus input energy for flashlamp repetition rates of 5, 10, 20, and 40 Hz. The intriguing aspect of this result is that the fidelity is now, to within the experimental precision, independent of input energy and rather insensitive to flashlamp repetition rate (slab aberrations). The introduction of the phase plate also results in fidelity (F = 0.5) that is poorer than that without using the phase plate (F = 0.8); however, the relative trends evident in Figure 4.17 suggest that at higher energies, the use of this optical element may result in fidelity improvements. The lower fidelity makes the use of this device impractical for MECCA because it would result in the accumulation of significant aberrations within a few round trips.

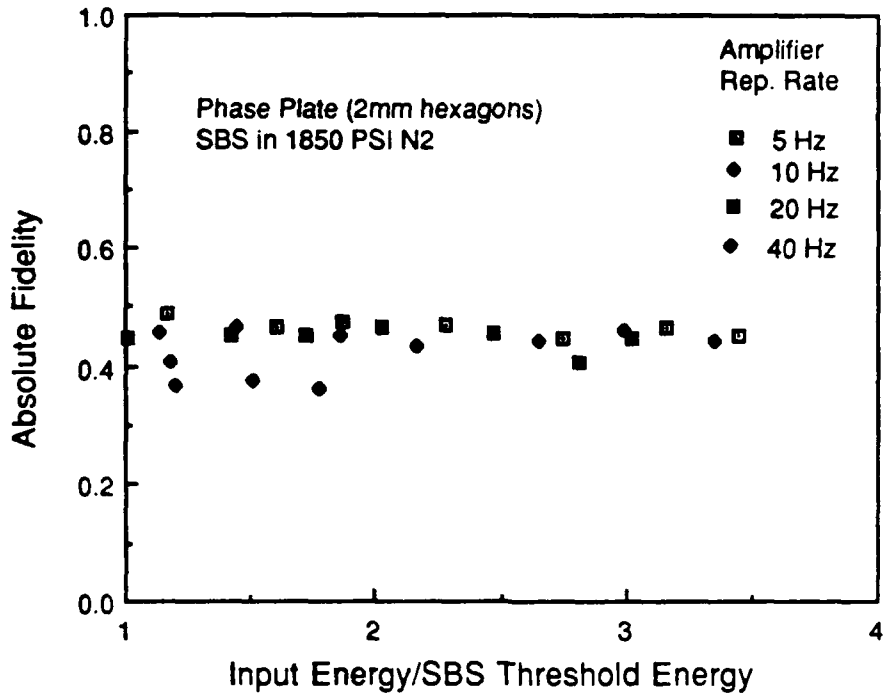

Figure 4.18 SBS fidelity in nitrogen using a distributed phase plate for several amplifier rep-rates (different levels of induced aberrations)

SBS in Freon: The experimental setup used to measure the SBS dynamic range in freon 113, is depicted in Fig. 4.19. This arrangement was designed to provide the maximum amount of amplification with the minimum amount of aberrations into the SBS cell. The amplifier used the Nd:glass rod built by Kigre and described earlier in section 2. In order to eliminate birefringence, it was found necessary to run the amplifier at a 0.05-0.1 Hz repetition rate. The master oscillator arrangement remained the same as that described above. Upon emerging from the waveplate polarizer intensity filter, the laser beam passed through a vacuum telescope in order to better match the beam diameter to the size of the rod. The beam double passed the amplifier rod, and was polarization coupled with a quarter wave plate and polarizing beam splitter to the SBS cell. As in the previously described setup, AR wedges and pyroelectric energy probes were used to monitor the energy of the beam at various points. Probes E1 and E2 monitored the energy injected into and extracted from the amplifier rod, giving a measure of the double pass gain. Probe E3 monitored the energy injected into the SBS cell. A sample of the SBS return beam was directed through a 50/50 beamsplitter to meter E4, while the rest of this sample was focussed with a 1 m lens through a 300 μm pinhole and the transmitted energy measured

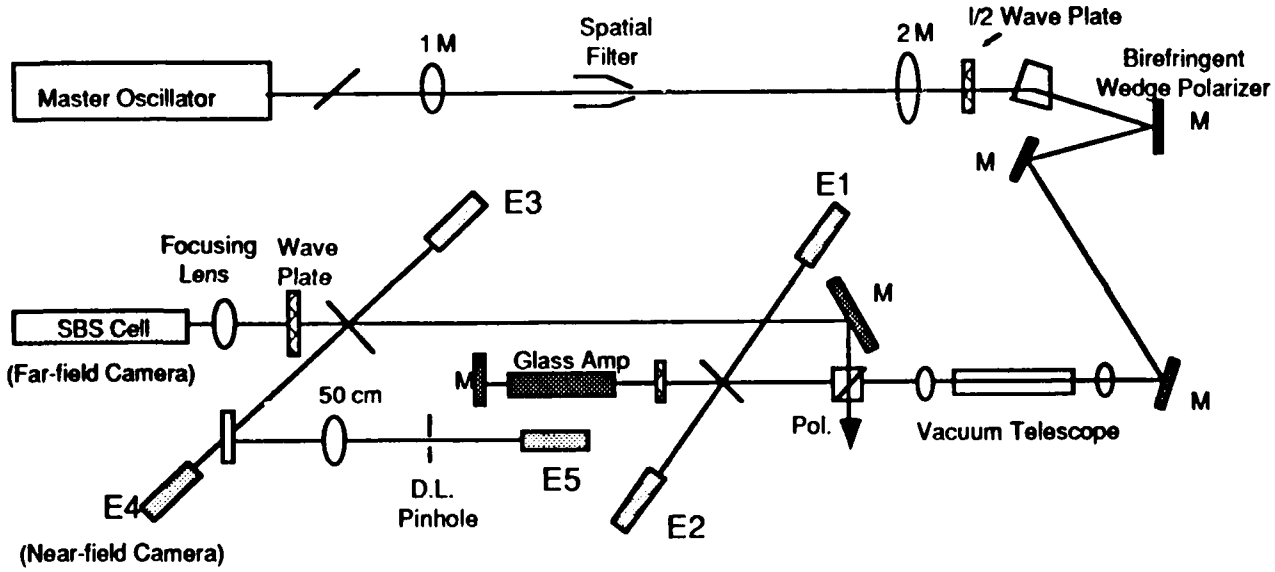

Figure 4.19 Optical layout for measuring the SBS reflectivity and fidelity dynamic range in freon 113

with probe E5. The ratio E4/E3 constituted a measurement of the SBS reflectivity. With the beam size used in this experiment, 92% of a diffraction limited beam was expected to pass through the pinhole. The SBS fidelity is thus defined as:

$$F = E5/E4 * 1/0.92$$

By far, the best dynamic range results for stimulated Brillouin scattering reflectivity and fidelity were obtained using freon-113 as a medium. Figure 4.20 is a plot of reflectivity vs input energy for f numbers of 10 and 50. Here, f/50 resulted from focussing a 1 cm diameter beam into the cell with a 50 cm focal length lens; f/10 was arranged by expansion with a 5:1 Galilean telescope. The threshold energy is 4.8 mJ for both focal conditions; the reflectivity exceeds 80% from input energies of 50 mJ to the maximum energy of 680 mJ. The reflectivity maintains a constant value of 90% from 200 mJ to the maximum energy, and shows no evidence of falloff.

Figure 4.21 shows the plots of SBS fidelity that correspond to the reflectivity data shown in Fig. 4.20. Excellent fidelity (better than 80%) is obtained over the entire investigated dynamic range for the f/10 focal system; as was the case with nitrogen, we find that fidelity is degraded when increasing the f/number of the system.

It is interesting to note that as the above noted fidelity degradation takes place, the reflectivity data gives no clue that anything is awry (compare Figs. 4.20 and 4.21). The fact that reflectivity is maintained at the 90% level with the f/50 optical system belies the degradation in fidelity. In general, we have found for all the SBS experiments, be they single reflection or multiple reflection, that SBS fidelity is far more sensitive to adverse conditions than is the reflectivity. A Soviet group has reported excellent results for the reflectivity of freon-113 for pulse energies up to 0.5 J and a repetition rate of 17 Hz. To our knowledge, ours are the first studies establishing faithful wavefront reconstruction.

One parasitic process that was sometimes in evidence for this medium was stimulated Raman scattering. It was discovered that Raman processes were most likely to occur when the beam penetration depth into the SBS cell was long. Under these conditions, visible antistokes lines could be seen radiating in both the forward and backward directions. Raman generation could be suppressed simply by limiting the interaction length within the medium; for example, a 50 cm focal length lens placed 30 cm or more away from the entrance window of the cell (penetration depth of 20 cm) was sufficient to eliminate Raman generation and resulted in excellent SBS behavior, as detailed below.

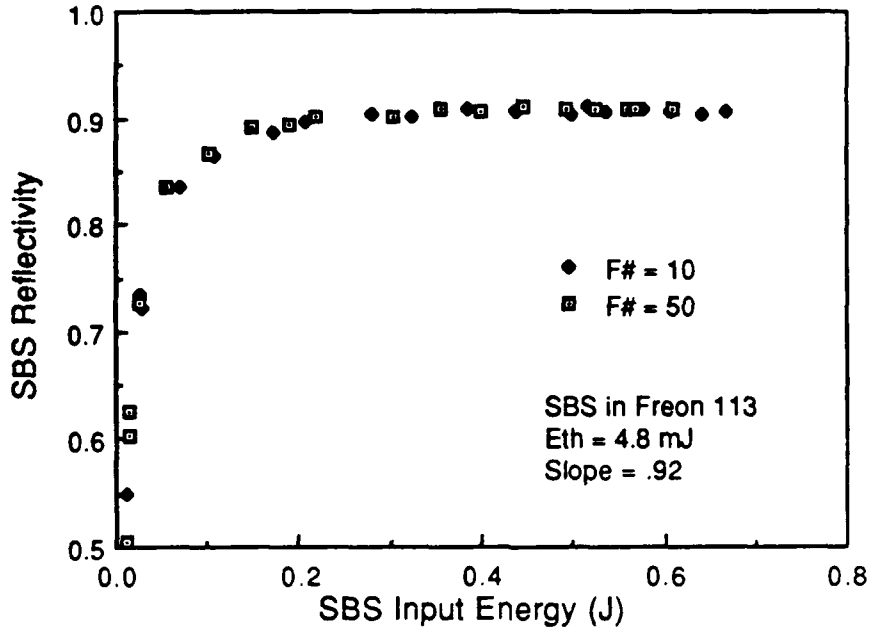

Figure 4.20 SBS reflectivity in freon for two f/#s

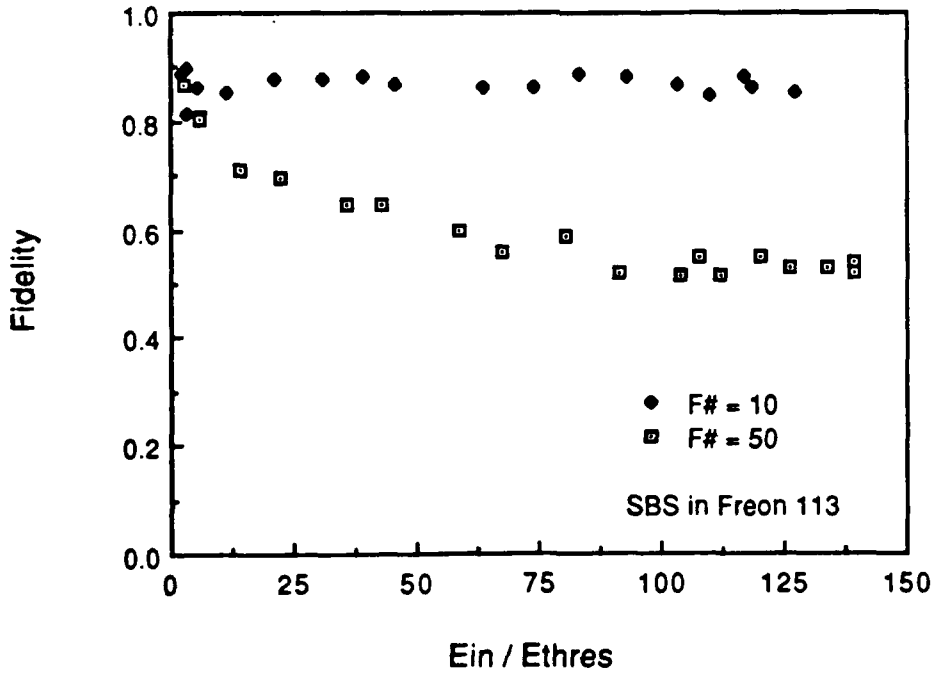

Figure 4.21 SBS fidelity in freon for two f/#s

Finally, we note that at the upper end of the energy range, optical breakdown could be seen (and heard) in the focal volume. This breakdown has no apparent adverse effect on the SBS fidelity or reflectivity. One expects that the influence of OBD will depend upon the time scale for conversion of the OBD disturbance into random density fluctuations and thus the destruction of the acoustic grating. Apparently, this conversion is not occuring early enough to have an effect on the SBS reflection of the 7 nsec pulse. And has disappeared prior to the next pulse 100 to 500 ms later. However, it could play an important role in MECCA where the pulse train may last 100 to 200 ns.

In conclusion, we have found that freon-113 shows excellent fidelity and reflectivity for bulk focus SBS over a wide dynamic range. Thermal blooming is absent, and Raman generation may be avoided by restricting the interaction length. Reflectivities in excess of 80% and fidelities of 90% were measured for energy ranges from 50 mJ to 680 mJ with the best fidelities resulting from the use of low f-number focal systems. This level of performance made freon the SBS medium of choice for MECCA.

4.4 MECCA characterization

This section describes the final set of conventional MECCA related experiments performed using freon as the SBS medium. The experiments investigated the fundamental processes that govern conventional MECCA, its limitations and the conditions which optimize extraction and beam quality.

4.4.1 Preliminary experiments with Freon as an SBS Medium.

As reported in the previous section, very good SBS fidelity and reflectivity was observed in freon from energies of 10 mJ to over 680 mJ. This suggested that freon is an ideal candidate for MECCA. The measured fidelity of F = 90% implies that it is theoretically possible to operate a MECCA with as many as 8 round trips and maintain a beam quality of 1.5 x D.L where:

$$\text{Beam Quality} = [\ 1/F^n\ ]^{1/2}$$

and n is the number of round trips. Thus, in a three round trip MECCA cavity with a net round trip gain of 5, the cavity should achieve an overall gain of over 100 with good beam quality for injected pulse energies on the order of 5 mJ. The round trip gain of 5 includes the SBS reflectivity, which we tentatively assume remains at a level of 80% or better,

Figure 4.22 depicts the first experimental attempt to deploy freon in a MECCA cavity. The net round trip is measured by temporarily removing the etalon from the setup and placing a mirror before the SBS cell; the return energy is then recorded with the amplifier rod off. This is then compared with the return energy obtained with the flashlamp off and the SBS cell reflecting the input pulse instead of the mirror. We find a net round trip gain of approximately 5. The Fabry-Perot etalon is adjusted for three round trips; for the SBS shift of freon (1780 MHz), this requires a mirror spacing of $3 \times 10^{10}/(3 \times 2 \times 1780 \times 10^{6}) = 2.8$ cm. The 5:1 Galilean expansion telescope and focussing lens combination result in an f/10 focal parameter. The vacuum spatial filter is equipped with a variable size aperture, and is meant to provide only loose spatial filtering to inhibit the buildup of parasitic oscillations and control the growth of high spatial frequencies that may result from nonideal SBS fidelity. The vacuum spatial filter also images the Fabry-Perot etalon onto the Nd:Glass amplifier rod. A 1.06 μm AR coated wedge picks off samples of the input and reflected pulse trains and directs them into vacuum photodiodes; the signals recorded by these two diodes are delayed relative to eachother, added and recorded by a transient digitizer.

Figure 4.23 shows the SBS input and output pulses with no pinhole present in the vacuum spatial filter. The pulse energy initially injected into the cavity is approximately 5 mJ. The sampled input and output pulses are labelled "I1, I2, I3," and "R1, R2, R3," respectively. It is immediately apparent from this trace that the multipass arrangement yields results that cannot be anticipated based on the single pass dynamic range data. Although the reflectivity of the first and second round trip pulses are high, the reflectivity of the third round trip is only 16%. The energy of this input pulse is approximately 120 mJ, which in the single pass case would give a reflectivity of 85 %. The energy of the final extracted pulse was not measured here, but we can estimate the net multipass gain to be 15 from the height of the pulses recorded on the digitizer trace.

The beam quality of the extracted pulse as measured using the power-in-the-bucket method is only 2.7 x D.L., which is much smaller than one would naively expect from three reflections each with a fidelity of 90%, i.e., $BQ = [1/(0.9)^3]^{1/2} = 1.17$. Another indication of the degradation in beam quality with successive round trips is indicated in Figure 4.24, which is the input/output trace recorded following the insertion of a 400 μm pinhole in the vacuum spatial filter. The energy of the third SBS input pulse has been reduced as a result from 120 mJ to 27 mJ; a pinhole of this size should transmit more than 95% of the energy of a diffraction limited beam. With the use of a 300 μm pinhole, this energy is further reduced to 6 mJ. This implies that the SBS reflections, and in particular the third reflection, are creating unexpectedly high spatial frequencies in the beam profile.

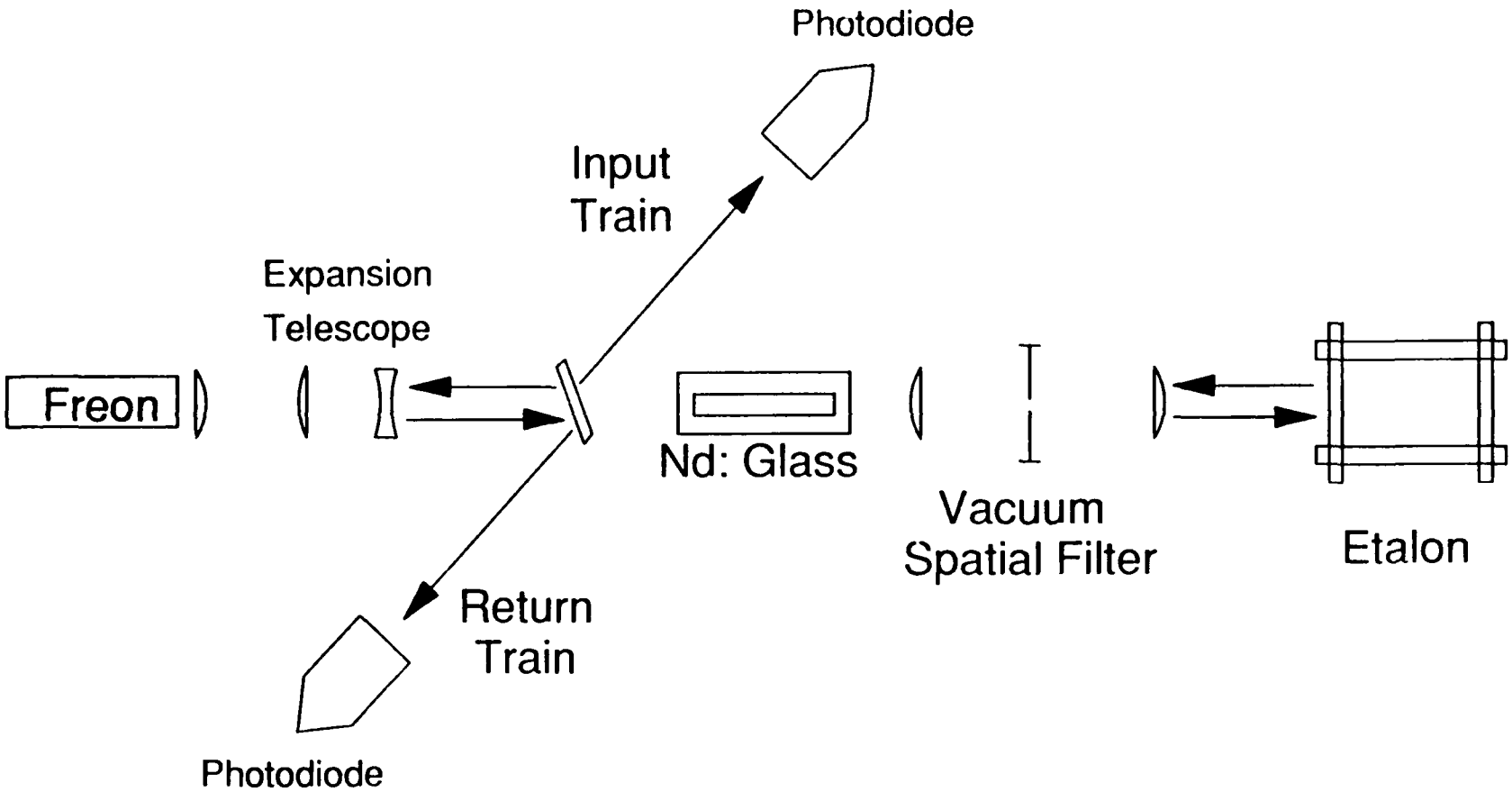

Figure 4.22 Optical layout for MECCA experiments using freon as the SBS medium

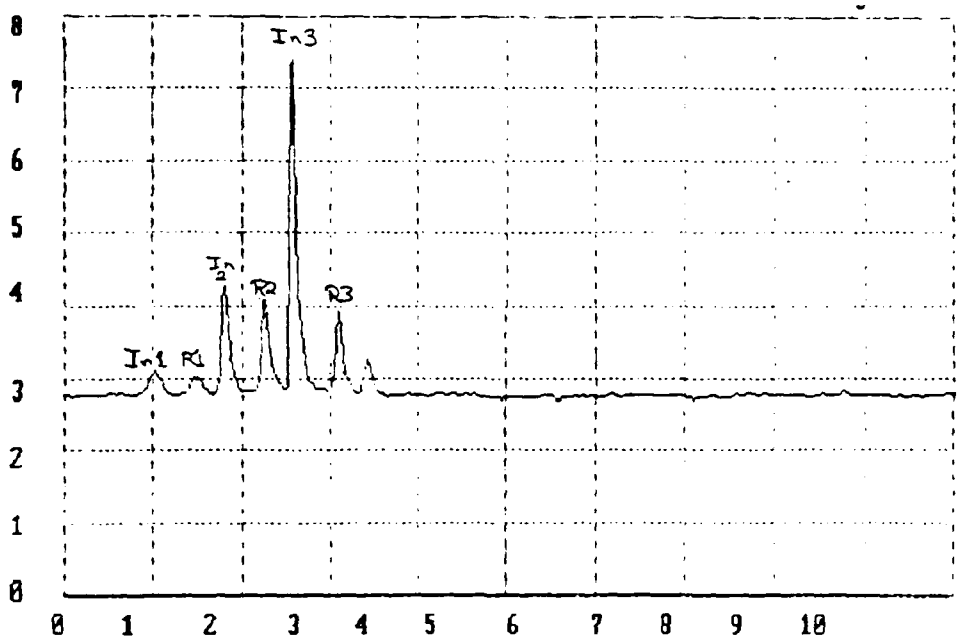

Figure 4.23 Input and reflected pulse trains from the SBS cell using the MECCA layout shown in Figure 4.23. The reflected pulses are time delayed and added to the input pulses so that each input pulse has the SBS return next to it.

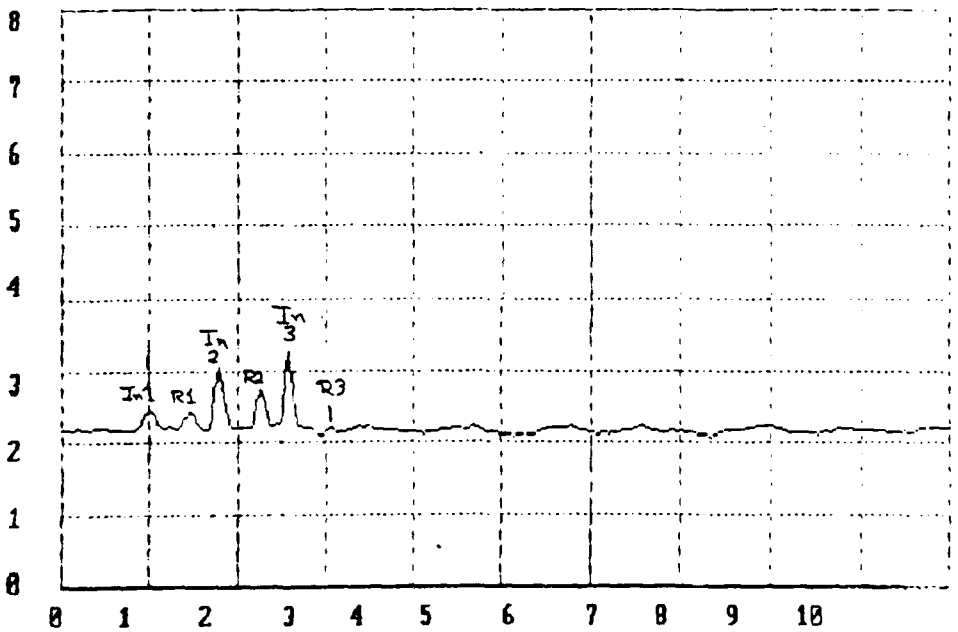

Figure 4.24 Same data as in Figure 4.24 but with a 400 μm pinhole inserted in the vacuum spatial filter

In the remainder of this section, we shall describe experiments that clarify the qualitative distinction between a single SBS reflection and repetitive, "rapid fire" SBS reflections, or reflections repeating on a 10 nanosecond timescale. It will be seen that the single pass properties reported in the previous section are alone insufficient for an understanding of the conditions created by the MECCA arrangement.

4.4.2 MECCA Cavity Characterization

This section describes key initial observations and diagnostic experiments which led to a better understanding of common focus, rapid fire, multiple pulse SBS and its implication to MECCA. These experiments in turn led to improved extraction and beam quality as described in section 4.4.3.

The experimental setup varied slightly depending on the diagnostic being performed. Figure 4.25 depicts the most general arrangement. It is similar to the arrangement shown in Fig. 4.22, with one difference being that the vacuum spatial filter has been removed; this is to allow later adjustment of the cavity length to very small values. This is not a serious problem, because all diffracting apertures have been removed from the optical train and the preliminary experiments have established that imaging is incidental to the more intrinsic difficulties of the multipass scenario, and is unable to alleviate them. The Nd:Glass amplifier is not used for most of the experiments to be described, and it too is removed if need be to achieve cavity lengths shorter than 180 cm. An f/10 focussing system is employed unless otherwise noted, and liquid freon-113 (Particulo 99.999% grade) is used as the SBS medium, contained in a pyrex cell 60 cm in length by 2 cm in diameter. Vacuum photodiodes monitor the input and reflected pulses; in addition, a vacuum photodiode is positioned alongside the cell as closely as is physically possible in order to monitor the light scattered from the focal region at 90^{o} to the optical axis of the system.

Breakdown Thresholds: The most obvious difference between single pass and multipass SBS conditions is readily evidenced in the threshold energies needed to cause optical breakdown (OBD) of the freon. Under single pass conditions, the threshold for optical breakdown is much higher than the threshold under multipass conditions. With the etalon removed from the beam path, breakdown is not observed until the input energy equals approximately 110 mJ (the maximum possible unamplified energy), and then occurs only sporadically. Breakdown is manifested as a whitish blue flash with a filamentary shape, roughly 3 cm long, located within the focal region. It produces an audible, "popping"

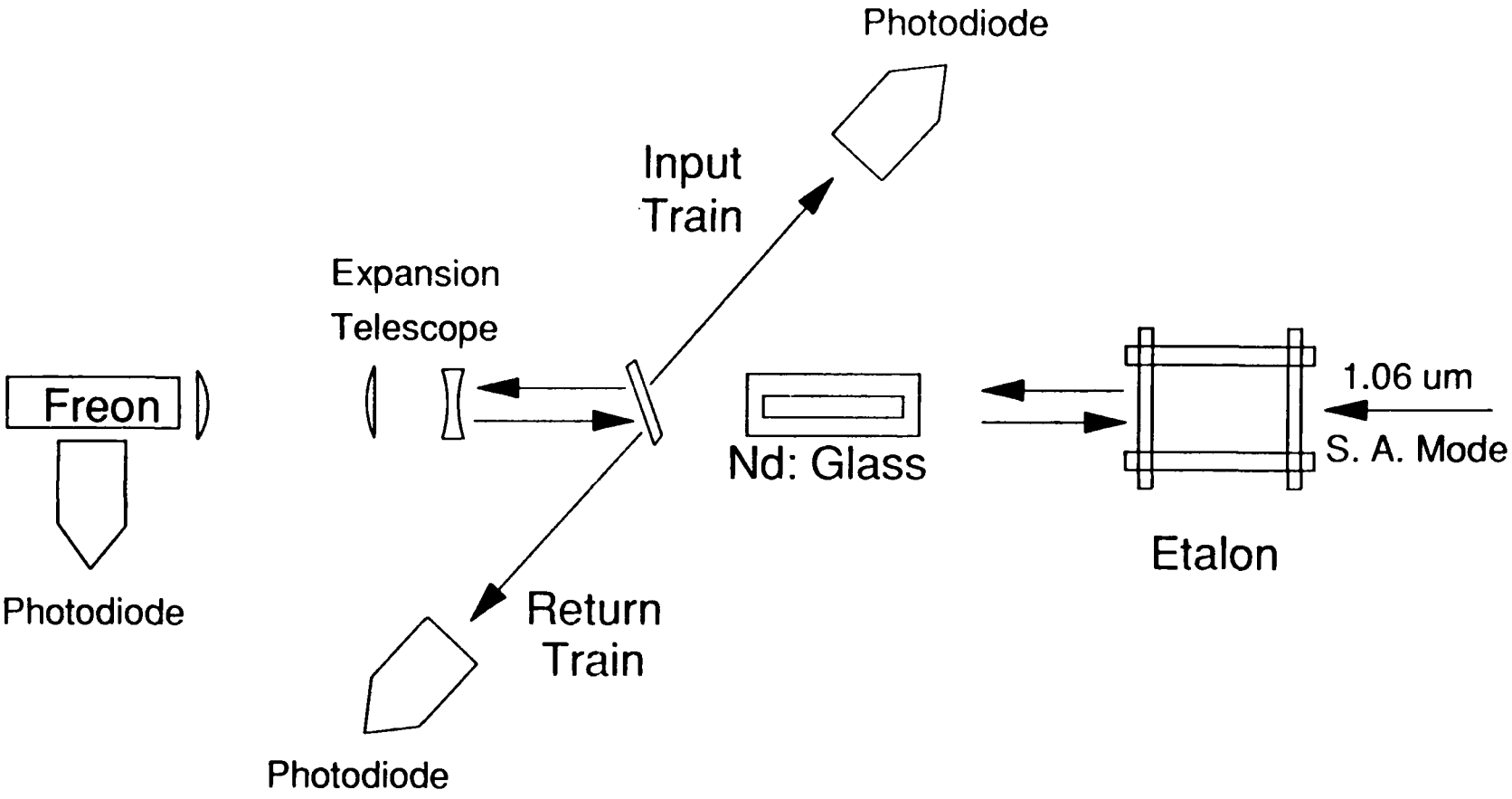

Figure 4.25 Optical layout for MECCA cavity characterization

sound and results in the evolution of gas bubbles from the focus. It thus seems likely that this phenomenon creates an irreversible change of the material; this supposition will be revisited.

With the amplifier off and the etalon in place and adjusted for three round trips, breakdown can be seen occurring in the focal volume for injected energies as small as 10 mJ. With three round trips and no amplification, the total energy incident on the focal volume, in this case, is approximately 20 mJ. Since the single pass breakdown is 100 mJ, it is certain that the first round trip cannot be responsible for breakdown; furthermore, the total energy incident for all three input pulses is also smaller than the single pass threshold. It would appear that earlier round trips leave the medium in a condition ripe for OBD by subsequent pulses.

With breakdown resulting in the production of gases within the SBS medium, one must be concerned over whether or not irreversible changes are occuring. Figures 4.26a and 4.26b adduce evidence for such a change. The upper trace of this figure shows the input and reflected pulse trains for an injected energy of 50 mJ and a freon cell that had been subjected to breakdown conditions for several hours of nearly continuous use. The cavity is set for a round trip time of 14 nsec and three round trips. The reflectivity of the first pass is down to 67%, the second pulse to 53%, and that of the third pulse is absent altogether. The lower trace shows the result of the same measurement after filling the SBS cell with a fresh batch of freon. The second reflectivity has recovered to 80%, and the third reflectivity to 58%. Thus, in investigating any of the systematic effects observed in these studies, it is important to check that they are not attributable to the aging effect of freon. It was verified, for example, that the low third pulse reflectivity seen in Figure 4.26b remains at its diminished level with a fresh fill of freon, and is not a coincidental result of a degraded medium.

1.06 μm light scattering from focal volume: Light Scattering from focal volume was monitored in a direction normal to the beam propagation. Figures 4.27a and 4.27b show traces of the three round trip input and scattered pulse trains for injected energies of 5 mJ and 10 mJ, respectively. For these traces, the amplifier flashlamps are turned on , and the flashlamp timing is adjusted so that the net round trip gain is nominally unity; the three input pulses consequently have nearly equal amplitudes. For an injection energy of 5 mJ, where no optical breakdown is observed, the amplitudes of the scattered pulses are also nearly equal (Fig 4.27a). For an injection energy of 10 mJ, where optical breakdown begins, Fig. 4.27b reveals that the amplitude of the scattered pulses increases dramatically with successive round trips. The absolute amount of energy actually lost to scattering

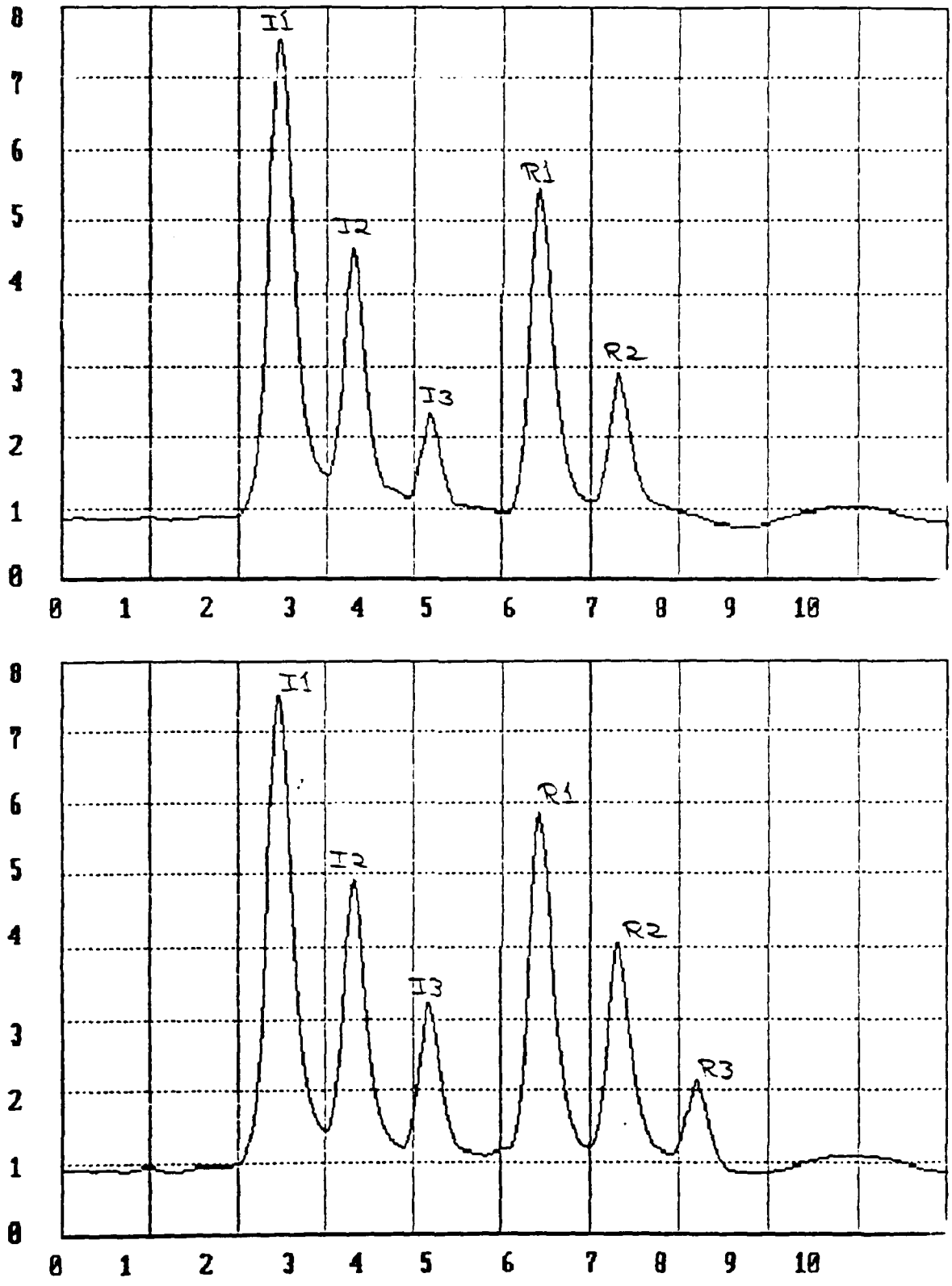

Figure 4.26 Effect of freon aging due to optical breakdown. a) intracavity pulse train with freon subjected to optical breakdown for several hours, b) intracavity pulse train with a fresh load of freon under identical conditions

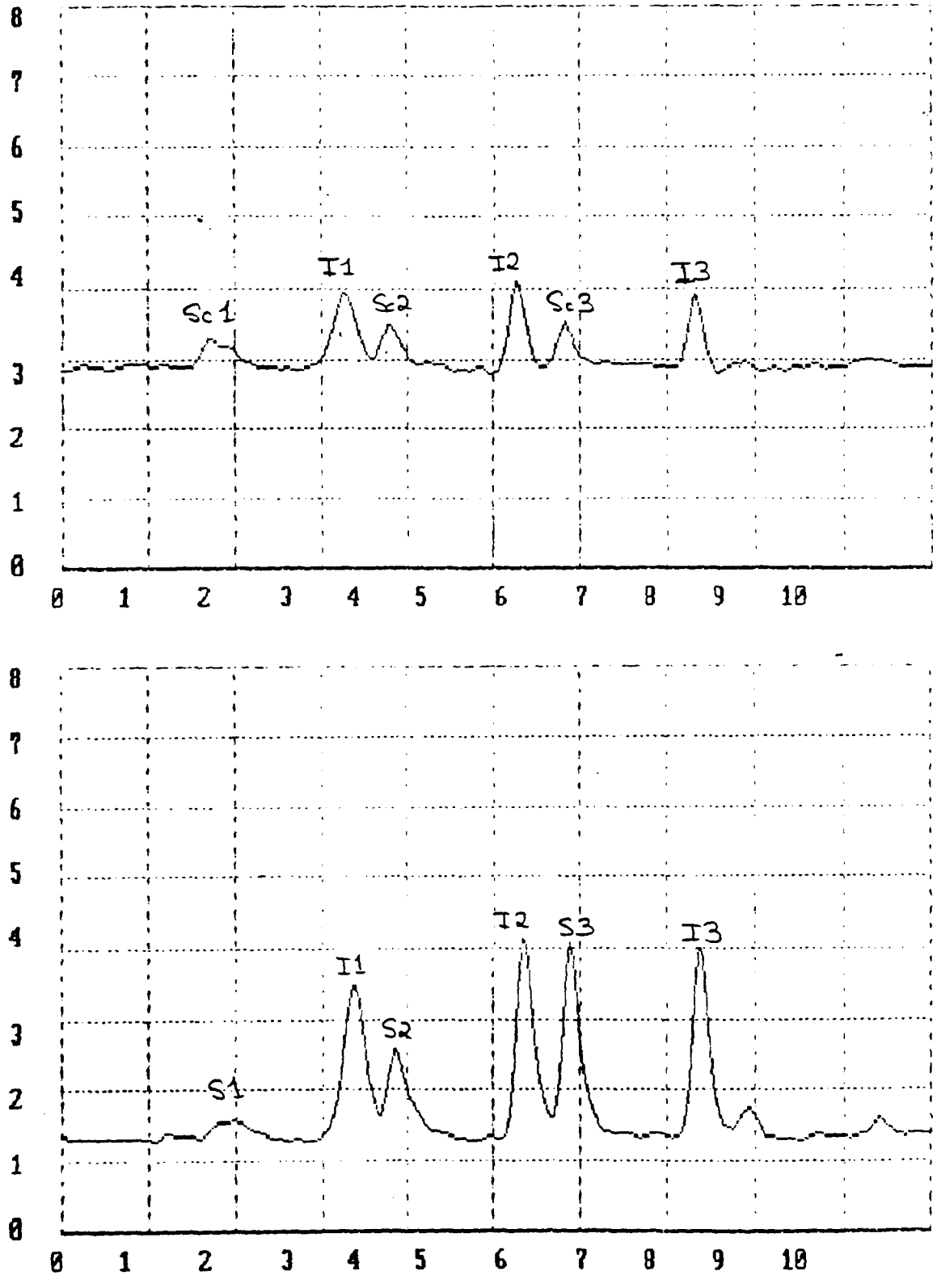

Figure 4.27 Input and scattered pulse trains from the SBS cell. The scattered pulse trains have been delayed so that each input pulse train has the corresponding scattered pulse next to it with a nominal net gain of 1. a) injected energy of 5 mJ, b) injected energy of 10 mJ.

cannot be determined from these measurements, but the trend of scattered amplitudes does confirm the hypothesis that at energies nominally above 10 mJ, earlier pulses are leaving the medium in a condition qualitatively distinct from that seen by the first pulse, or equivalently, from the condition pertinent to single-pass conditions.

Multipass Reflectivities and Two-Cell Experiments: Figure 4.28 is a trace of the input and reflected pulse trains recorded for an injection energy of 110 mJ and with the amplifier flashlamps turned off. The reflectivity of the first and second pulses both exceed 90%. The energy of the third input pulse equals 40 mJ, which under single-pass conditions would have a reflectivity of 80%; however, the third round-trip reflectivity equals 41%. This result is consistent with two general classes of interpretations. The first class holds that the degeneration of reflectivity is simply a result of a beam quality that has been sufficiently degraded so as to increase the SBS threshold and decrease the SBS reflectivity. One problem with this interpretation is that it is incomplete: it begs the question of what effect is responsible for the degradation.

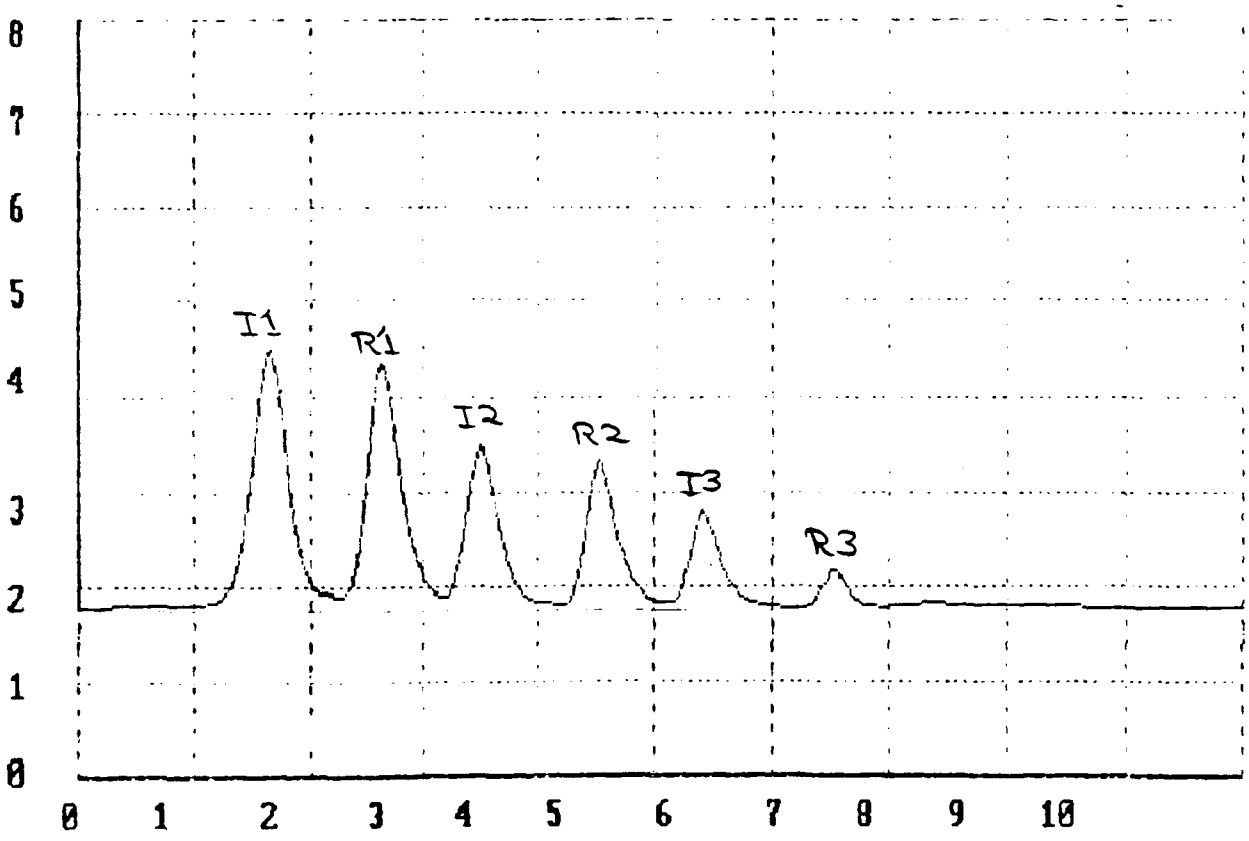

Figure 4.28 Input and reflected pulse trains from the SBS cell using the MECCA layout shown in Figure 4.23 without an amplifying medium. The reflected pulses are time delayed and added to the input pulses so that each input pulse has the SBS return next to it.

The second possible explanation for the falloff in reflectivity holds that an alteration of the medium itself is responsible. The temporal separation between pulses in Fig. 4.28 equals 38 nsec, which is much longer than the 2 nsec decay time for the SBS acoustic grating. During the "dark" period between pulses, there is no electrostrictive field present to drive the grating, so it will decay into turbulence in the manner discussed in Section 4.2. The time required for this turbulence to dissipate from the focal region will be characteristic of thermal diffusion processes, which will take much longer. Thus, according to this model, the second and third pulses will see a medium with some small scale density fluctuations. When these fluctuations become large enough, small scale lensing will occur, leading to an increase in SBS threshold, optical breakdown and a loss of SBS reflectivity and degraded SBS fidelity.

To distinguish between the effect of degraded beam quality and degraded SBS medium, a two cell experiment was conducted; the setup is shown in Figure 4.29. Two SBS cells, both filled with freon-113 are employed: one cell, termed the multipass cell, is part of the familiar multipass etalon coupled cavity, where the etalon length is now adjusted for two round trips instead of three. As in the foregoing measurement, the amplifier flashlamps are off. After two round trips in the multipass cavity, the optical pulse is extracted and polarization coupled by the quarter wave plate/polarizing beam splitter combination to a second SBS cell, termed the diagnostic cell. A sampling beamsplitter and vacuum photodiodes monitor the input and reflected beams from each cell.

With 110 mJ injected into the two round trip cavity, the final extracted pulse is reflected from the SBS test cell with a reflectivity of 81%; this is a significant improvement over the 41% value obtained when this pulse must undergo SBS reflection from the same cell as the first two pulses (Fig. 4.28). This result shows that when the third round trip pulse sees a fresh SBS medium, its reflectivity is comparable to that expected based on the single pass data. The two cell experiment militates against attributing the diminished multipass reflectivities to poor beam quality.

Cavity Length Dependence: Capsulizing the information provided by the foregoing results, it seems that in a multipass SBS setup, the reflectivity of the third pulse is degraded by some condition in the SBS focus that is created by the previous pulses. Further, the optical breakdown thresholds show that the multiple pulse failure is not energy additive: a single pulse with as much energy as the sum three input pulses has a high reflectivity. The time delay effect inherent in the acoustic grating decay model proposed above would explain both results.

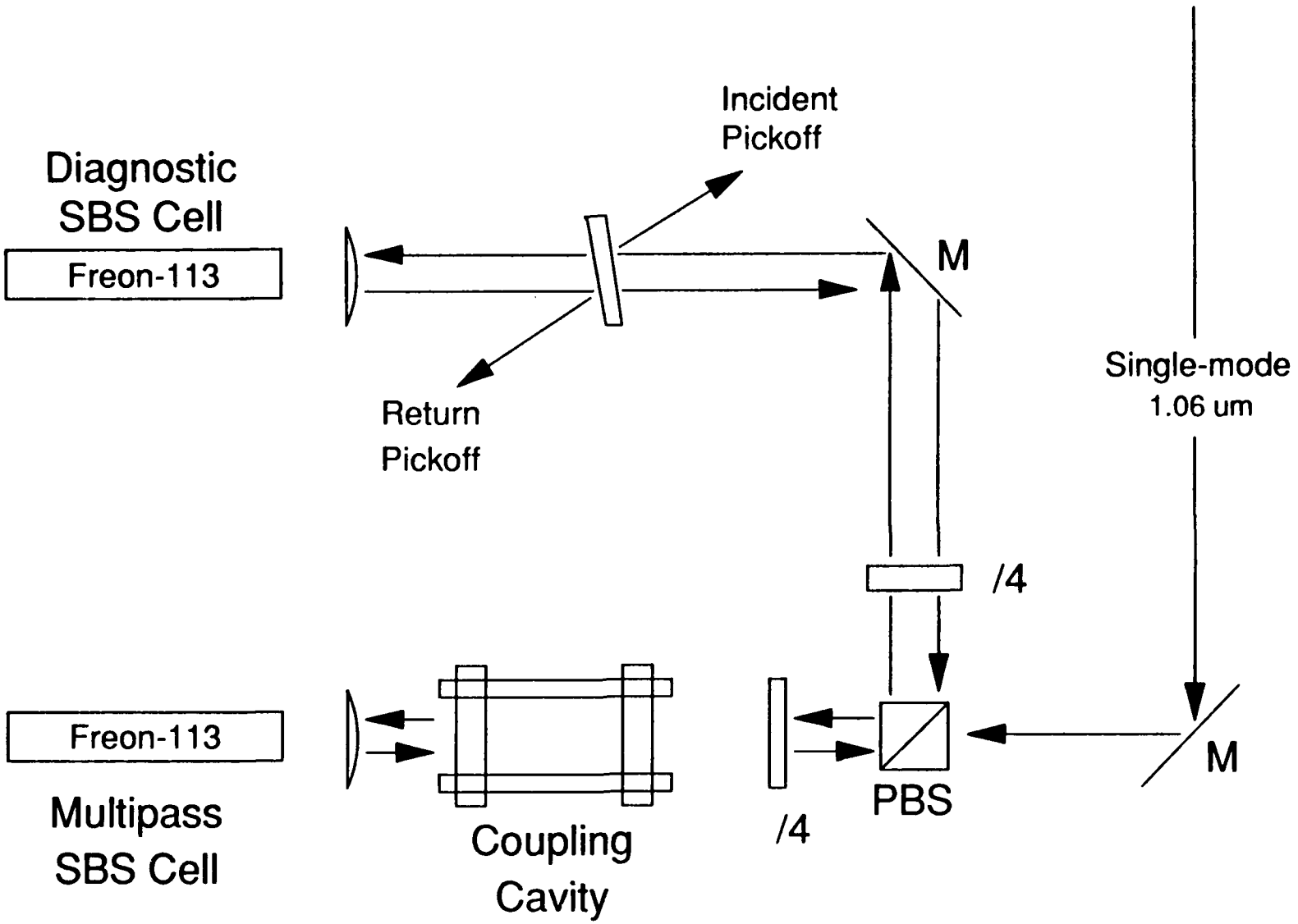

Figure 4.29 Optical layout of the two cell experiment

Acoustic-grating decay occurs because the electrostrictive driving field is absent; therefore, it should be possible to further test this hypothesis by making the cavity length so short that the successive input pulses overlap in time. For this test, we return to the standard MECCA setup; the etalon is adjusted for three round trips, and the input and reflected pulse trains recorded. Figures 4.30a and 4.30b show the results of such a measurement. The upper trace is a record of the reflected and incident pulse trains for an injected pulse energy of 60 mJ and a temporal pulse separation of 13 nsec, which results in only marginal pulse overlap. The reflectivities of the first two pulses are in the 90% range, but that of the third pulse is only 54%. The lower trace shows the incident and reflected pulses for a pulse separation of 10 nsec, for which substantial pulse overlap exists. Cursory examination reveals that the reflected pulse train is now a more faithful reproduction of the incident train than is the case for the longer interpulse separations, and the reflectivity of the third pulse has increased to 90%. As the cavity round-trip time is increased further beyond 13 nsec, the third pulse reflectivity continues to decrease until it disappears altogether. The graph in Figure 4.31 displays this dependence.

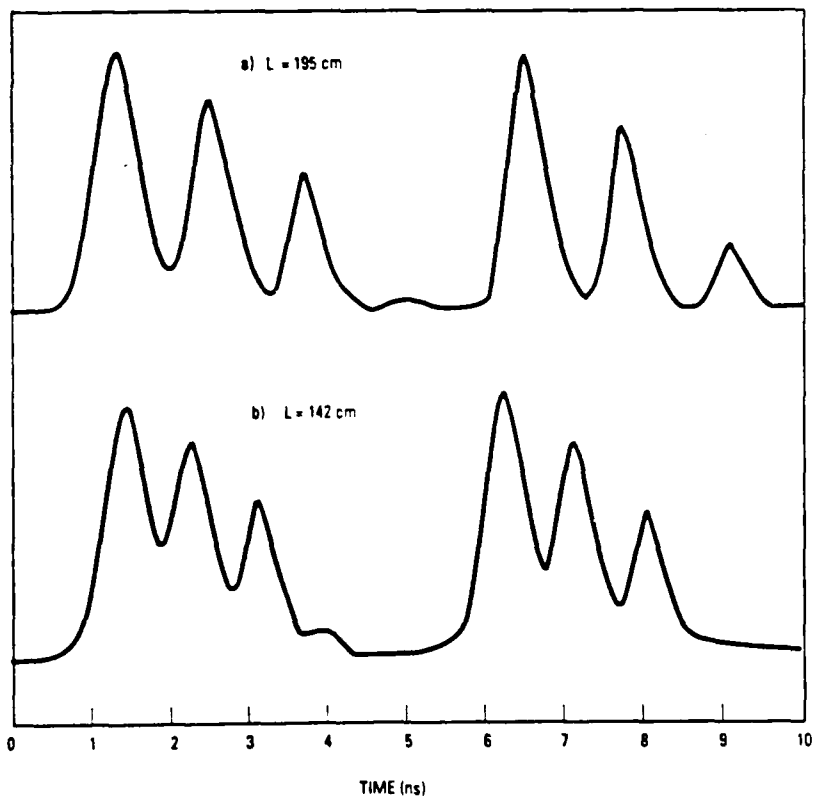

Figure 4.30 Input and reflected pulse trains from the SBS cell using the MECCA layout shown in Figure 4.23 without an amplifying medium. a) cavity round trip time 13 ns, b) cavity round trip time 10 ns

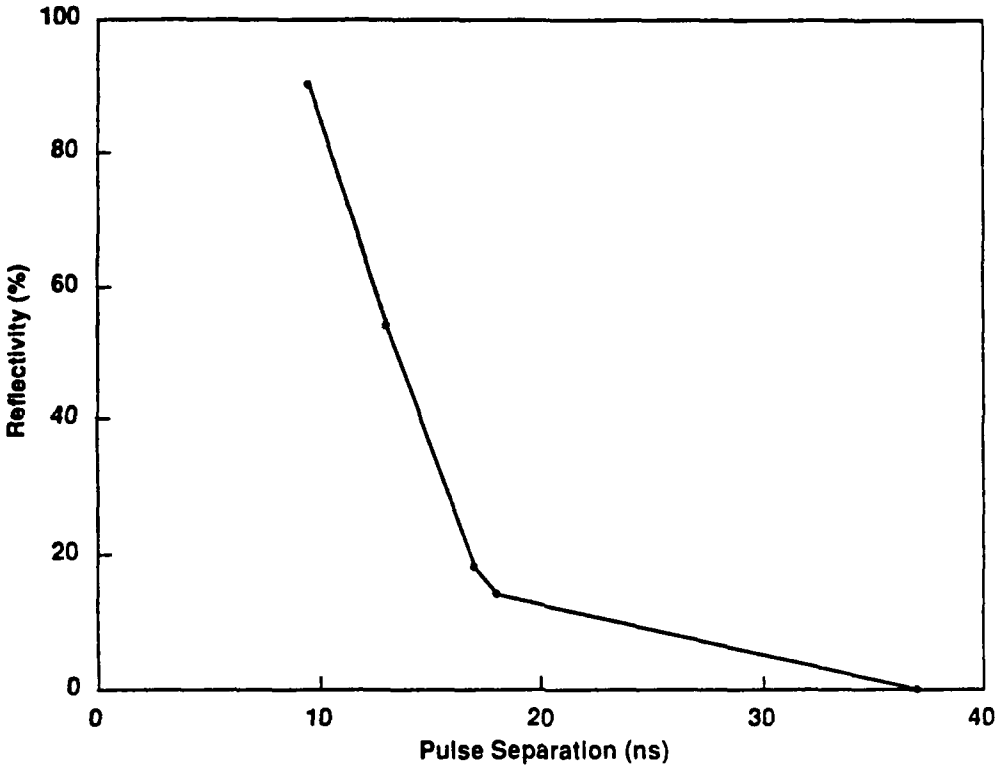

Figure 4.31 Reflectivity of the third pulse as a function of cavity round trip time

Figures 4.32a and 4.32b show the corresponding effect of the cavity-length variation on the behavior of the scattered energy. For this measurement, the etalon length was adjusted for a total of four round trips. The upper trace shows the scattered pulse energies for a cavity round-trip time of 10 nsec, and the lower trace for a round-trip time of 13 nsec. In the upper trace, the scale for the scattered pulse train is a factor of 5 more sensitive than in the lower trace as evidenced by the relative size of the first pulse. For the 13-nsec pulse separation, the amplitude of the scattered energy for the second, third and fourth pulses is disproportionately larger than that for the first pulse. In contrast, the scattered pulse energies for the case of significant pulse overlap (10-nsec separation) are nearly proportional to the corresponding input pulse energies; furthermore, the scattered amplitudes of pulses 2, 3 and 4 are smaller than in the case of the longer cavity by a factor of 5.

In general, the amplitude of scattered optical energy increases as the optical density fluctuations of a medium increase. The behavior of the scattered pulse amplitudes are thus consistent with the notion of an acoustic grating that has at least partially decayed into turbulence between the first and second input pulses. The pattern of scattered amplitudes in

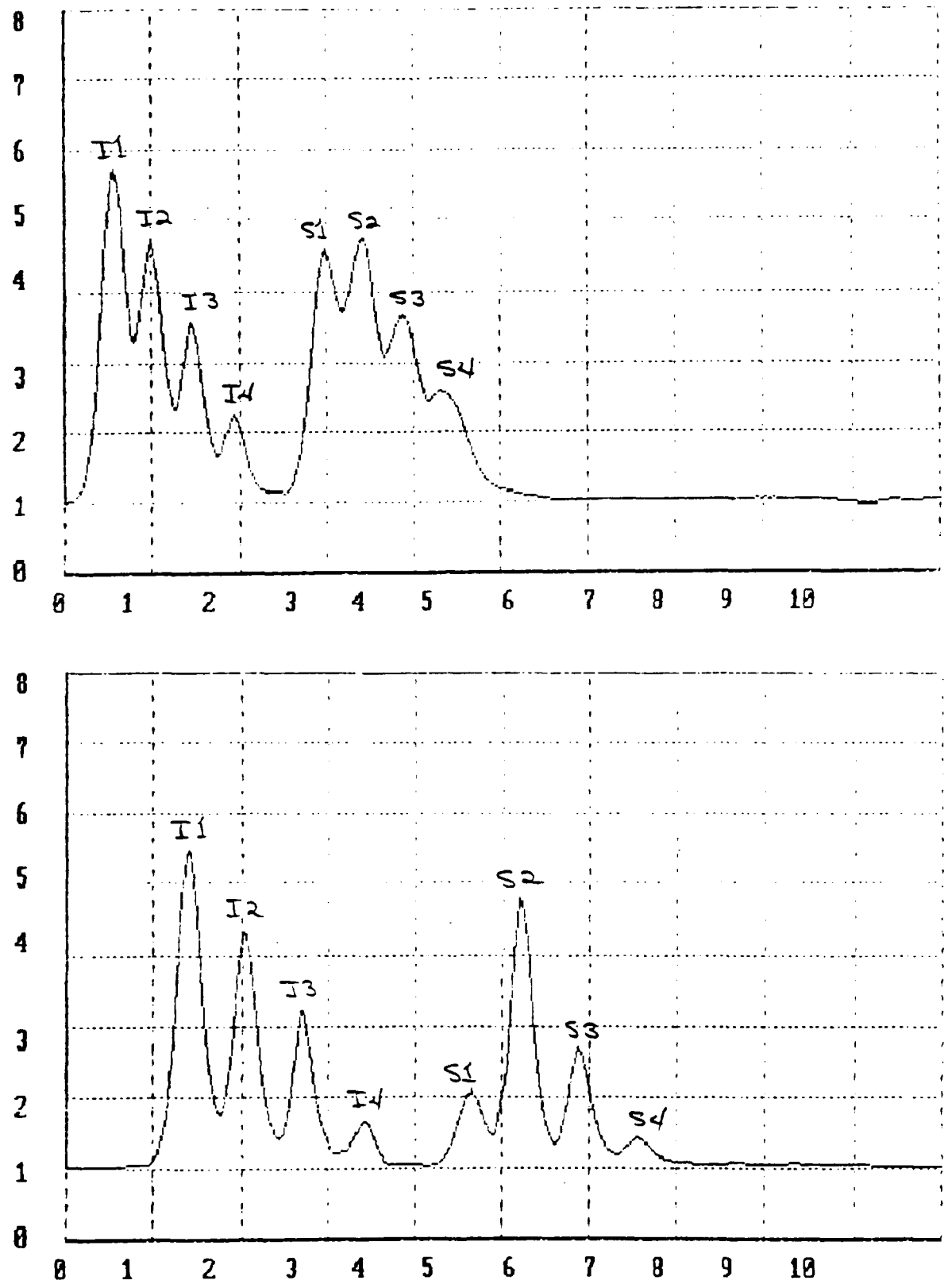

Figure 4.32 Input and scattered pulse trains from the SBS cell using the MECCA layout shown in Figure 4.23 without an amplifying medium. a) cavity round trip time 13 ns, b) cavity round trip time 10 ns

Fig. 4.32b suggests that optical density fluctuations already exist by the time the second incident pulse arrives. The two cell experiments, however, suggest that the amount of decay which occurs between the first and second pulse is only enough to slightly degrade the second pulse which typically has good reflectivity and beam quality. Within the time that two pulses have impinged on the medium, the density fluctuations are severe enough to significantly degrade the reflectivity of the third pulse. These density fluctuations are also likely to cause local small scale focusing of the beam resulting in optical breakdown.

Further evidence for the importance of the spontaneous decay of the SBS grating comes from the effect of tilting the etalon axis away from colinearity with the direction of the injected beam. With the etalon tuned for three round trips, the first and third round trip pulses will come to a focus in the same volume of the SBS medium, but the second round trip will focus at a different point (Figure 4.33). The acoustic grating created by the first round trip reflection cannot, therefore be driven by the second round trip and will decay before the arrival of the third round trip. Figures 4.34a and 4.34b show the far-field profiles of the extracted pulses for aligned and misaligned etalons, respectively; the cavity round trip time equals 10 nsec. With the etalon aligned normally, optical breakdown was observed only intermittently; Fig. 4.34a shows a relatively clean near-field profile for the extracted beam. Misalignment of the etalon results in visible and audible OBD, and a degraded near-field profile (Fig 4.34b).

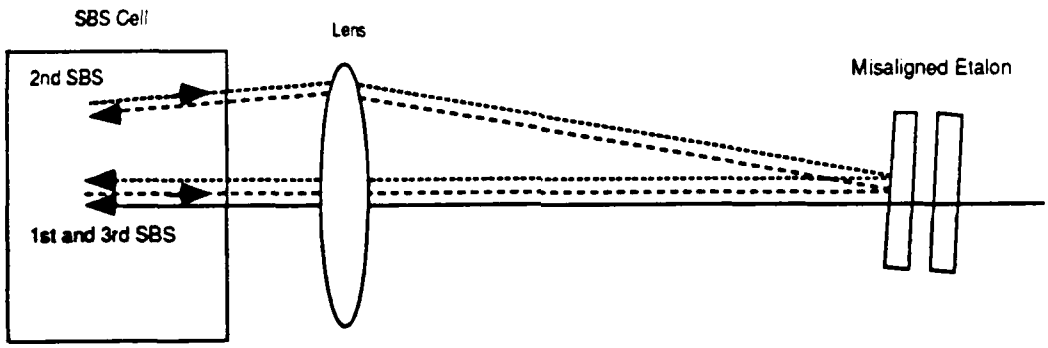

Figure 4.33 Optical drawing showing the effect of misaligning the etalon on beam path

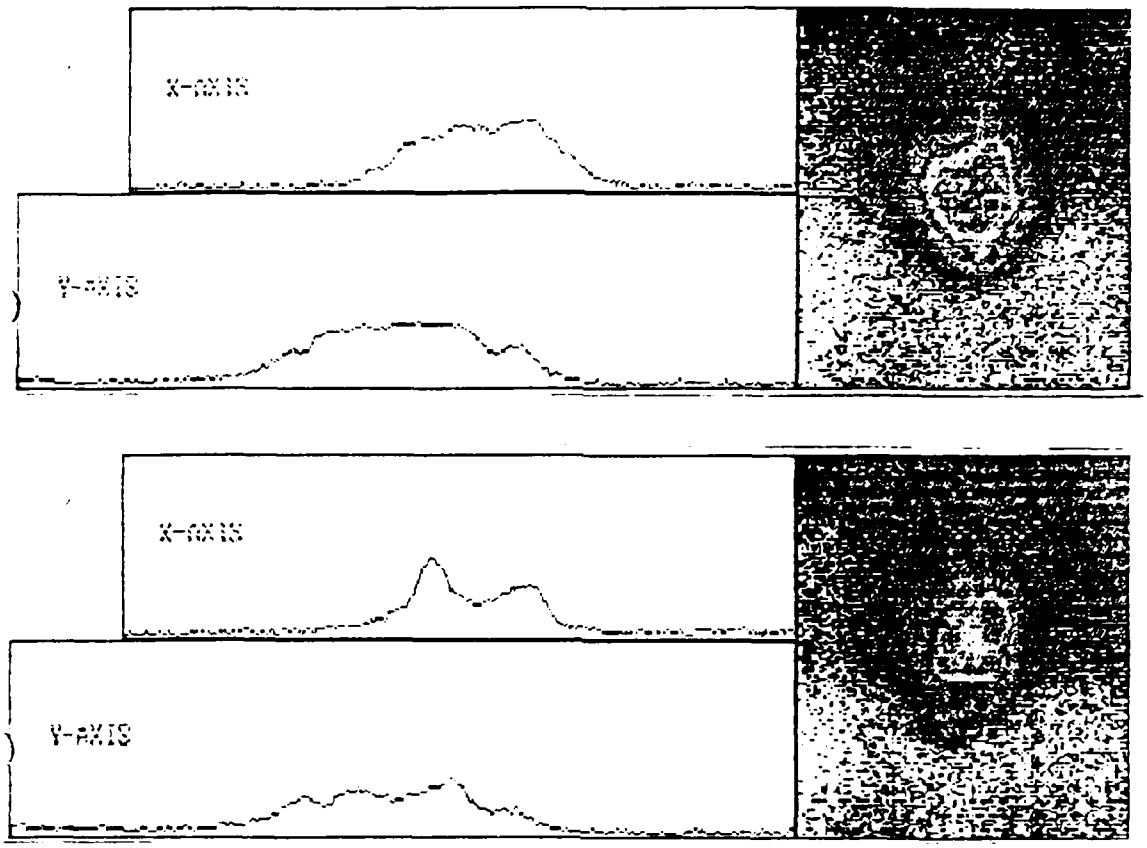

Figure 4.34 Far-field profiles of the extracted pulse under aligned (a) and misaligned (b) etalon conditions

4.4.3 MECCA Extraction

Recall that in the preliminary MECCA extraction attempts, the net gains were much smaller than what was expected from the single round-trip gain data. Reflectivity measurements showed that this is attributable in part to reduced reflectivities for round trips following the initial reflection (see, for example Fig. 4.23). The improvement in multipass reflectivities effected by the cavity-length reduction suggests attempting regenerative amplification in a short cavity.

Employing the setup shown in Fig. 4.25, a 10-mJ pulse is injected into the cavity, which is set for three round trips and a round-trip time of 10 nsec. The extracted energy measures 300 mJ, giving a net gain of 30. This represents a substantial improvement over the values obtained in the preliminary experiments using methane as an SBS medium (approximately 2) and a factor of two improvement over the estimated value of 15 obtained using freon in a longer cavity (Fig 4.30). It is, however, still substantially smaller than the factor of 125 expected based on a round-trip gain of 5.

There are at least two reasons for the lower overall gain. Figure 4.35 shows the intracavity input and reflected pulse trains under amplified conditions. First, it is evident that there is a significant amount of energy reflected back into the cavity after the third round trip. We estimate that 40 % of the third round trip pulse gets reflected back into the cavity. The cause for such poor extraction efficiency is probably attributable to the nonideal wavefront quality discussed below. An aberrated wavefront will compromise the operation of the Fabry-Perot coupling etalon, since the wavefront is now composed of a superposition of spatial frequencies that are no longer normal to the etalon mirrors as intended. Second, it can be seen in Fig 4.35 that the SBS reflectivity on the third round trip degraded to approximately 65%. This seems at first glance to contradict the short cavity reflectivity measurements reported above for the unamplified case; however, considering the role that breakdown appears to play in multipass SBS, it is not too surprising that multipass results are energy dependent.

Figure 4.36 shows the near-field profile of the extracted pulse; comparison with the experimental profile shown in Figure 4.12 qualitatively indicates substantial improvement over the preliminary methane experiments. It is also interesting to compare the near-field profile of this regeneratively amplified pulse with the extracted beam profile obtained with the amplifier turned off, for the same cavity length, shown in Figure 4.34a. As with the reflectivity performance, the beam profile for the amplified case is significantly degraded relative to the unamplified trial. Far-field power-in-the-bucket measurements give a value of 30% for the fidelity of the extracted pulse; this is a significant improvement over the value of 15% recorded for the long freon cavity described in the introduction to this section.

These improvements in extraction and beam quality, satisfying though they are, still fall short of practical requirements. The problems associated with the multipass scenario seem in part intrinsic to the nature of stimulated Brillouin scattering itself. Certainly, at some point, the inherent nonconjugate nature of SBS will become an issue, as indicated by the BRIWON simulations. There are, in addition, dynamic properties of the SBS medium that are not treated by this analysis and which we have shown play a critical role under certain circumstances, such as an unjudiciously long cavity that prevent a sustained driving field for the acoustic grating. The latter type of limitation is still amenable to certain design improvements, such as the use of longer optical pulses, which would realize a greater degree of temporal overlap for successive round trips.

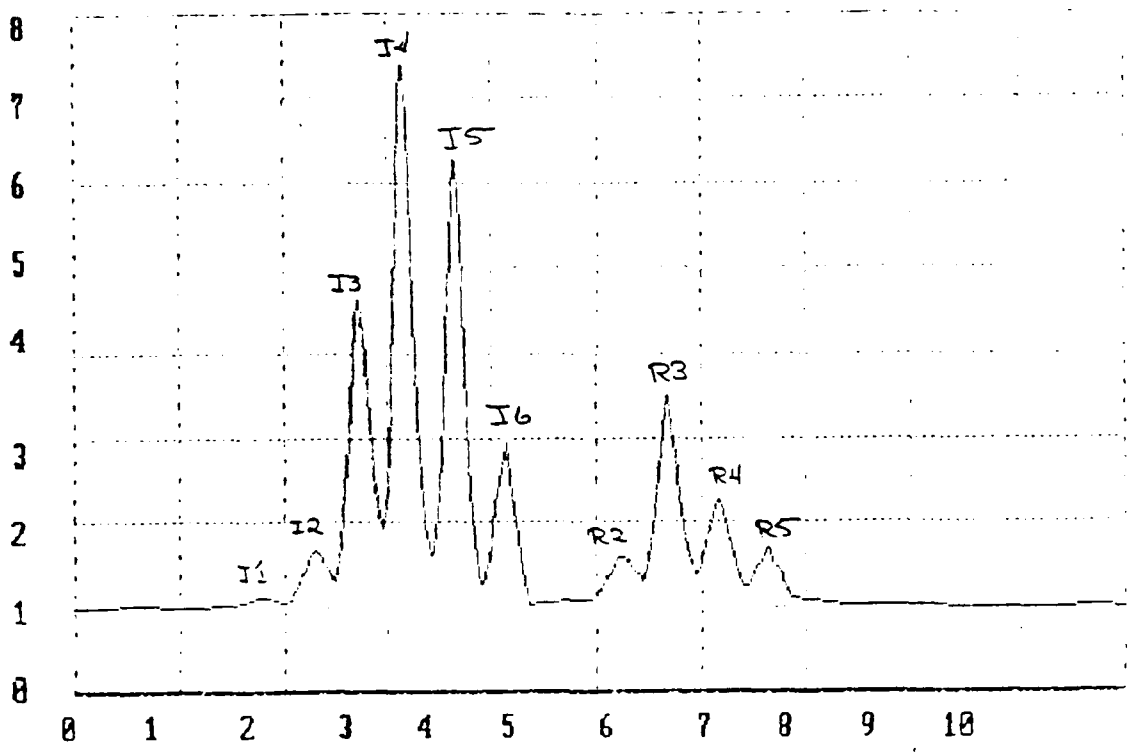

Figure 4.35 Input and reflected pulse trains from the SBS cell using the MECCA layout shown in Figure 4.23 with a nominal round trip gain of five and cavity round trip time of 12 ns.

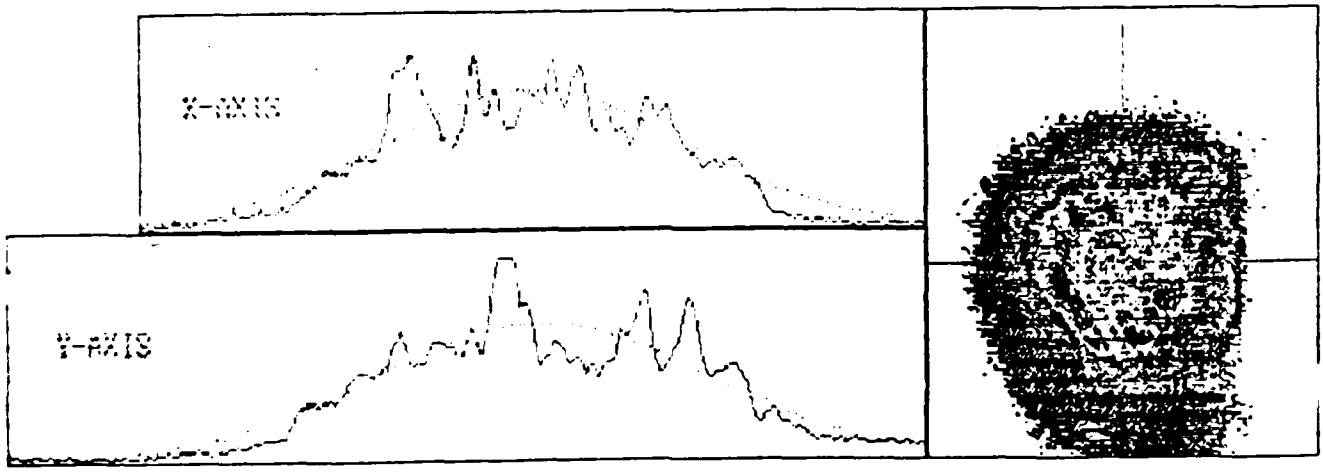

Figure 4.36 Near-field intensity distribution of the 12 ns round trip cavity extracted pulse with a factor of 30 amplification

5. ALTERNATE CONFIGURATION MECCA

The data presented in the previous Section has shown that a SBS medium with broad dynamic range, characterized under single reflection conditions, is a necessary but not sufficient condition to ensure acceptable performance of the multipass, common volume SBS feature of conventional MECCA. The decay of the acoustic grating from early pulses, which takes place on a time scale given by the acoustic phonon lifetime, forces the subsequent pulses to focus into a medium with disordered density fluctuations. This leads to progressive degradation of the SBS reflectivity and fidelity, resulting in poor extraction efficiency and beam quality. In accordance with this interpretation, we have shown that this degradation may be reduced by using shorter cavities and possibly longer pulses to sustain a driving field, but this represents a severe limitation in the applicability of the conventional MECCA.

The alternate configuration MECCA (AC MECCA) was developed to exploit the advantages of MECCA and circumvents the major handicap which limits its applicability; that of common focus multipass SBS. This section describes the AC MECCA concept, its advantages, and the experiments leading to the demonstration of an AC MECCA cavity. Overall amplification of a factor of 40 with good beam quality has been obtained during a limited series of tests.

5.1 Concept Description and Assessment

5.1.1 Design Criteria

In Section 1 we described the advantages of MECCA over other amplifier concepts, and in particular the regenerative amplifier concept developed at LLNL which we used as a standard of comparison. The following is a recollection of the advantages cited earlier:

- Coupling in and out of the cavity is performed passively without the use of an EO switch in the high power beam train
- There are no critical timing issues such as that required by an EO switch
- It can accommodate pulses of arbitrary lengths (the pulse length does not have to match the cavity round trip time)

and it is noted, that what was considered a major advantage, namely phase conjugation on every round trip, is not achieved by multiple pulse SBS and is to be avoided.

To be viable, an AC MECCA concept must continue to provide these advantages while using phase conjugation in a manner that preserves its advantages. In addition, the concept must be scalable to the multiple joule energy level without adding significant complexity to the system.

5.1.2 Concept Description

A schematic layout of the AC MECCA concept was shown earlier and is illustrated again in Figure 5.1 along with the frequency space evolution of the beam oscillating in the MECCA cavity. As with the conventional MECCA a master oscillator beam is injected in a cavity formed by an etalon and a frequency shifting element, except that in this case, the frequency shifting element is an acousto-optic (AO) modulator instead of an SBS cell, and the cavity is a ring cavity. The master oscillator beam is tuned to an off-axis transmission window of the etalon and, upon being frequency shifted, is reflected from the etalon. The beam makes several round trips while marching in frequency space, and is extracted from the cavity, as before, through the next transmission window of the etalon but into an SBS cell. The beam now reverses its path inside the cavity and is outcoupled through polarization rotation. The SBS medium in this case is selected to match an integral number of etalon FSRs so that the phase conjugated beam can reenter the cavity without attenuation. The advantage of the ring cavity now becomes apparent because it allows the beam to exit the cavity on a path different from the injection path where the SBS cell resides, and by rotating the polarization at the SBS cell using a $\lambda/4$ plate, the beam can be outcoupled with a polarizer without the use of active elements.

5.3.2 Concept Assessment

The AC MECCA concept described above is some what more complex than the conventional MECCA and raises several issues of its own. The following is a discussion of some of the issues encountered during the design and demonstration of AC MECCA.

Cavity Requirements: Given the system parameters typical of a MECCA, the off-axis operation of the etalon restricts the angles that could be used with a planar Fabry-Perot device. If the etalon finesse equals F, the etalon length L, and the incidence angle θ, then

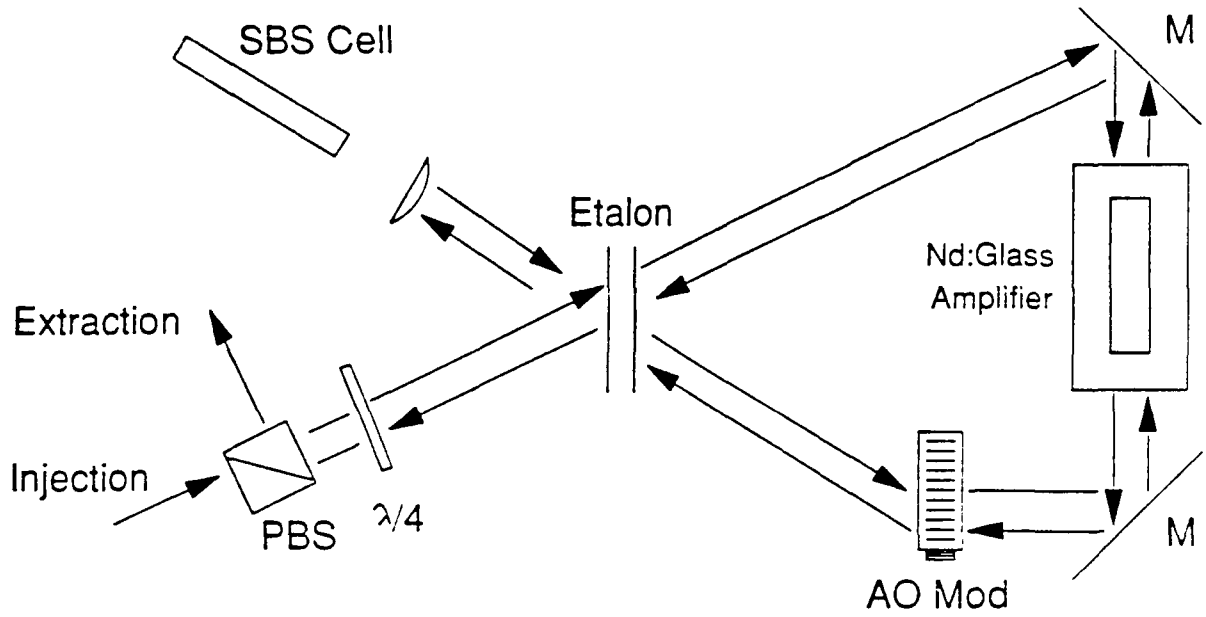

OPTICAL LAYOUT

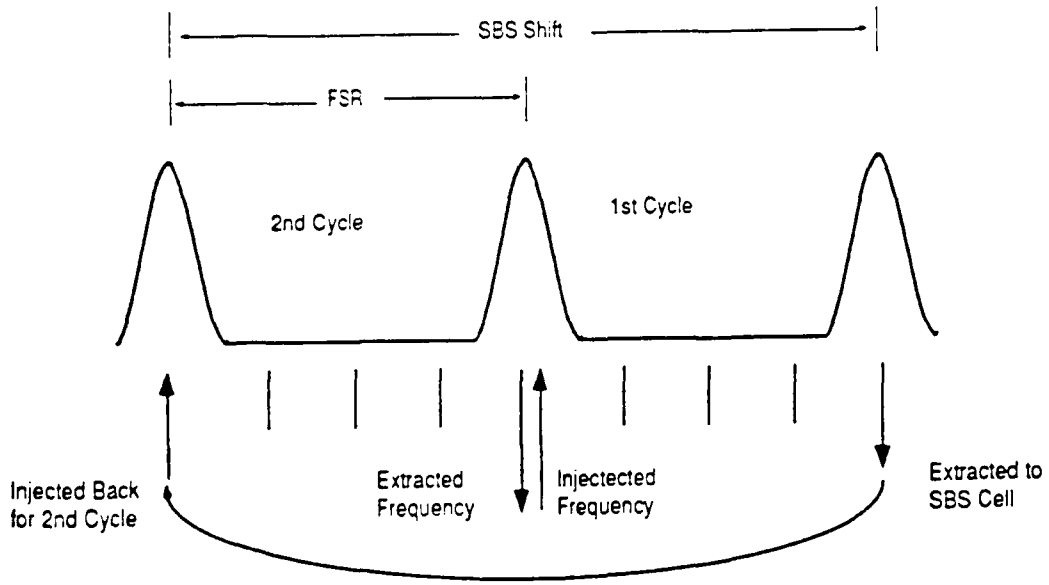

FREQUENCY EVOLUTION

Figure 5.1 Schematic layout of the alternative configuration MECCA (AC MECCA) concept

the beam will walkoff by a transverse distance upon either reflection or transmission given by:

$$d = 2LF\theta$$

To minimize losses, this walkoff must be much smaller than the beam diameter, D, such that:

$$2LF\theta << D \text{ or } \theta << D/2LF$$

A three round trip AC MECCA cavity with a modulator operating at a frequency to 200 MHz requires an etalon 25 cm in length. For an etalon finesse of 6, and a beam diameter of 1 cm, the above equation would require that the injection angle be much smaller than 3.4 mrad. This is a difficult requirement to meet, and would require critical adjustment. The best strategy for avoiding the walkoff problem inherent with a planar Fabry-Perot is to adopt a confocal etalon where the beam can be injected at an arbitrary angle. The energies present in a pulsed amplifier system would also require that the etalon contain a vacuum cell at the focal region.

The AC MECCA concept, nevertheless, can be demonstrated while avoiding the difficulties inherent in the ring cavity by using a linear cavity. The basics of such a cavity are schematically shown in Figure 5.2. The master oscillator pulse is injected into a cavity formed by the etalon and the AO modulator and is retroreflected by a mirror placed behind the modulator. This part of the cavity is functionally identical to the conventional MECCA except that the SBS cell is replaced by the AO modulator/mirror combination to provide the frequency shift that traps the beam inside the cavity. After a predetermined number of round trips, the pulse is extracted from the cavity and directed towards a SBS cell by a polarizer. To accomplish this, the extracted pulse has to have a polarization that is orthogonal to the input beam which is achieved by using one or more $\lambda/4$ plates. A more detailed discussion of the use of waveplates for this purpose is presented in section 5.3. Upon reflection from the SBS cell, the phase conjugated beam retraces its path through the cavity where the aberrations accumulated during the first set of oscillation are corrected, and is outcoupled by a Faraday rotator. As in the case of the ring cavity, the SBS frequency shift is selected to be an integral number etalon FSRs so that the phase conjugated beam can reenter the cavity without attenuation. The Faraday rotator is necessary in a linear cavity because the beam which exits the cavity after the second set of oscillations has the same polarization as the master oscillator beam.

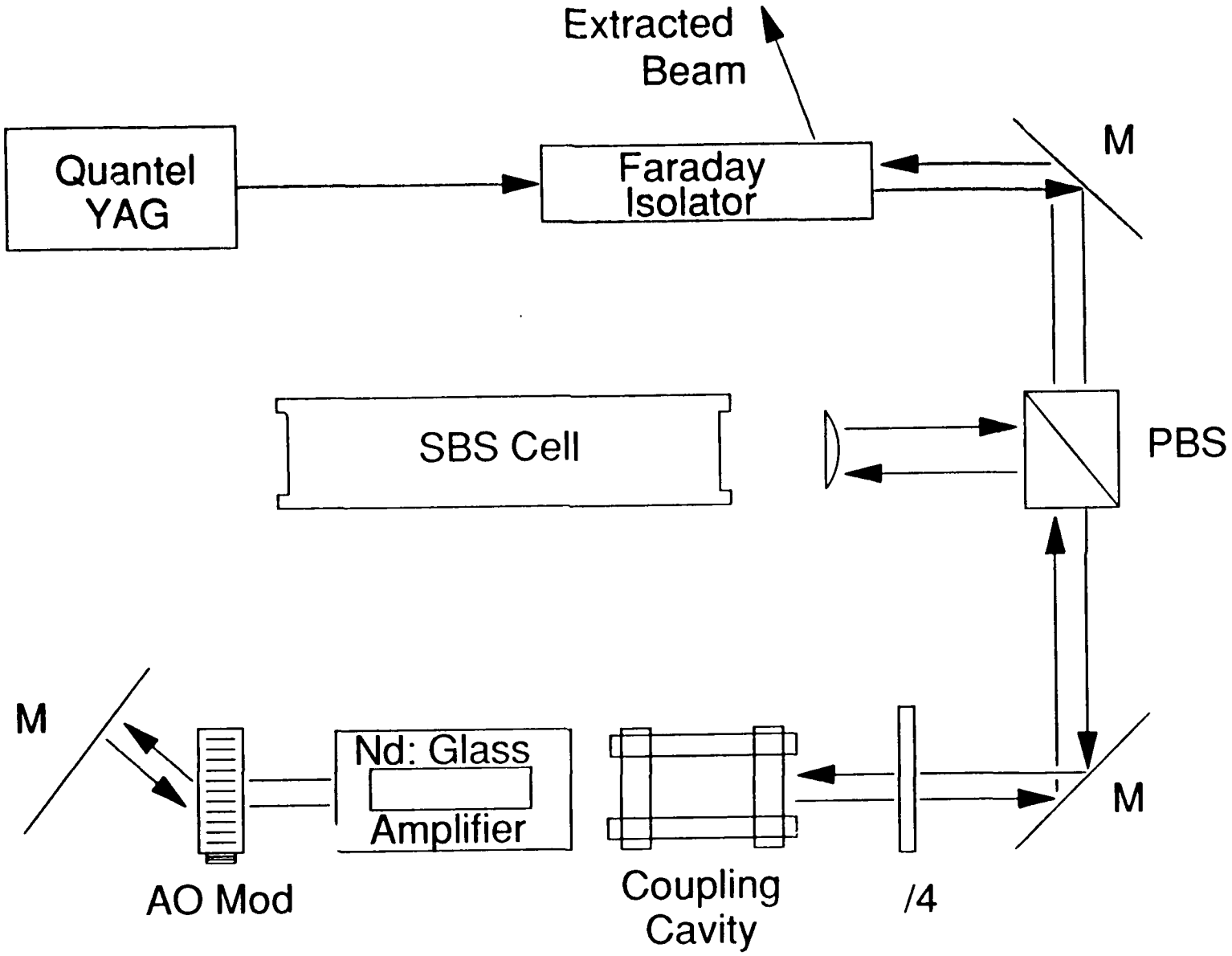

Figure 5.2 Optical layout of a linear AC MECCA demonstration cavity

Parasitic Oscillations:In the conventional MECCA configuration, the buildup of parasitic oscillations is prevented by the existence of an SBS threshold, which has an effect similar to that of a saturable absorber in making the cavity Q intensity dependent. The spontaneous emission from the glass rod is below threshold for stimulated Brillouin scattering and therefore in the absence of a master oscillator pulse, parasitic oscillations can not occur. However, an AO modulator has a diffraction efficiency that is independent of the optical intensity (no threshold). With no threshold, spontaneous emission from the glass rod can get amplified in a manner similar to that in a standard laser cavity if the gain exceeds the losses. This issue is best resolved by introducing a saturable absorber in the cavity which is bleached by the master oscillator pulse. A discussion of parasitic oscillations and other methods of suppressing them is discussed later in section 5.3.

AO Modulator Operation and Scaling: The use of the AO modulator raises two issues: the first is whether its use adds significant complexity and eliminates one of the key advantages of MECCA, that of not using active elements. The second issue is whether an AO modulator limits the scalability of the concept. Although the AO modulator is an active element, its use in AC MECCA, as described above, is very different than that of an EO switching element. In our application the AO modulator can operate in a cw or quasi-cw manner and there are no critical timing issues associated with its use. It also does not limit the beam pulse length in any way. Therefore, its implementation is much simpler than that of an EO switch. In the AC MECCA experiments described later, the AO modulator was typically turned on several μs before the injection of the pulse and was turned off approximately 10 to 20 μs after extraction. This type of operation is called quasi-cw because it appears cw compared to the time scales associated with cavity oscillation, but allows the modulator to cool between pulses. This mode of operation can accommodate rep-rates greater than 100 Hz without active cooling. A modulator that is actively cooled can operate cw without any timing requirements whatsoever.

The scalability of AO modulators is an issue when it comes to high energies only because no application has initiated the development of such a device. As the energy of the MECCA increases the modulator aperture must also increase to accommodate the higher fluences. AO modulators suitable for 1 μm operation, however, are typically made of glass or quartz and are driven by a piezoelectric driver in a direction normal to the beam propagation. Thus, they can be scaled in a manner similar to slab amplifiers (in the height dimension) by adding phased transducers to a piece of AO glass that is matched to the amplifier aperture. Cooling can also be performed in a manner similar to slabs but quasi-

cw operation can reduce the amount of heat generated by two to three orders of magnitude. Thus scaling the AO modulator, in principle, is no more an issue than scaling a glass slab amplifier.

5.2 AC MECCA Modeling And Projected Performance

A limited amount of analysis was performed to model the linear AC MECCA and assess the effect of the modulator diffraction efficiency on extraction. The model assumed a six round trip cavity (3 for each cycle), a single pass amplifier gain of 4, a modulator frequency shift of 120 MHz per pass (240 MHz round trip), an etalon bandpass of 120 MHz, and a 7 ns pulse in a nonoverlapping cavity. These parameters correspond approximately to conditions that can be achieved using our existing modulator and Nd:glass rod amplifier. Figure 5.3 shows a curve of the extraction efficiency as a function of AO modulator diffraction efficiency where the input energy has been adjusted to maximize the

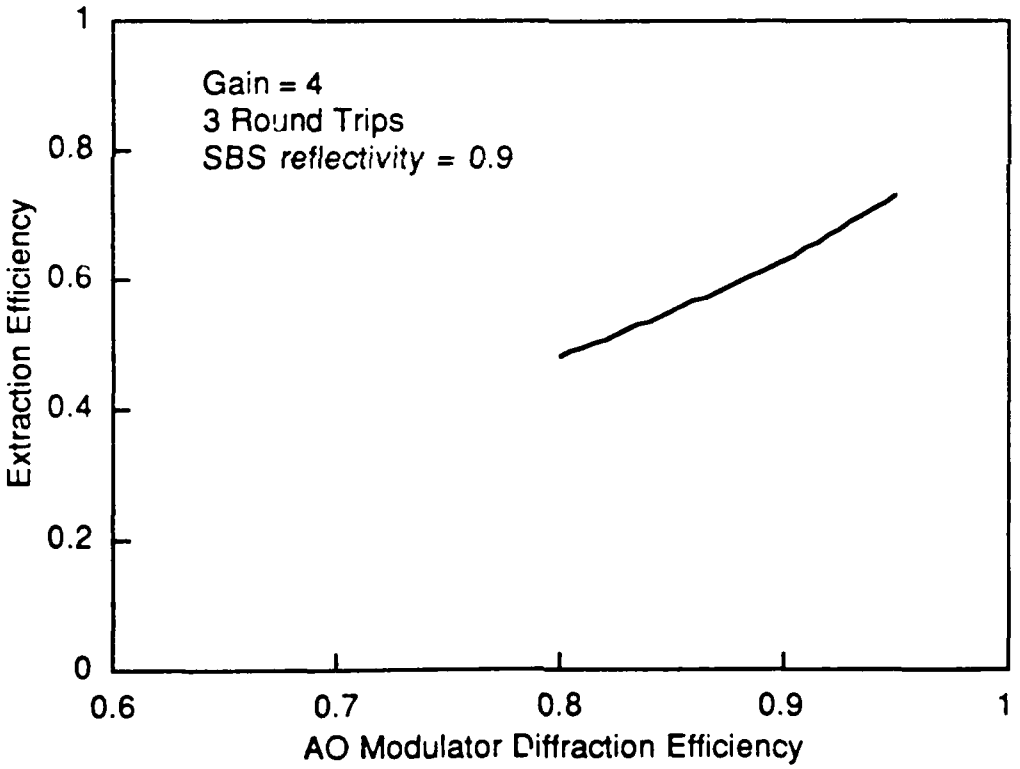

Figure 5.3 AC MECCA extraction efficiency as a function of AO modulator scattering efficiency in a six round trip cavity (three for each cycle) with a finesse of six and single pass amplifier gain of 4

extracted energy. It indicates that for these conditions, diffraction efficiencies on the order of 85% are required to provide acceptable efficiency. This is the reflectivity measured for our modulator when averaged over both polarizations; a specially designed modulator may further improve on this, resulting in extraction efficiencies greater than 60%.

5.3 Experiments

Experiments were performed to demonstrate AC MECCA and assess its performance. They included the characterization of the modulator which is critical to the operation of the cavity, demonstration of a modified linear AC MECCA cavity, and extraction experiments where the overall amplification and the beam quality of the beam were measured.

5.3.1 Modulator characterization

The results of the extraction efficiency modelling highlight the importance of the acousto-optic frequency shifter, and in particular, the diffraction efficiency required to achieve acceptable energy extraction from the amplifier medium. A frequency shifter with an operating frequency of at least 120 MHz, a diffraction efficiency of 80% or better, and an active aperture of 10 mm is indicated. The device used was fabricated by Andersen Labs of Bloomfield, CT with the goal of achieving the above specifications. The device employs SF-2 dense flint glass as the acousto-optic medium and has an optical damage threshold of over 5 J/cm^2 at 1.06 μm. Glass was used instead of quartz, another good AO material, because the diffraction efficiency is less sensitive to polarization. The modulator was designed without active cooling which limited its operation at full power (100 W of RF power) to a duty cycle of less than 6%. The modulator was supplied with a matching network whose characteristic impedance equaled 50 ohms at 120 MHz; the practical limitation to the operating frequency was the amount of power reflected back into the RF power supply at frequencies other than 120 MHz.

The acousto-optic modulator diffraction efficiency was measured at various RF frequencies and peak powers, for different optical polarization states, and also its performance in terms of the effect on the optical beam profile. Figure 5.4 depicts the optical setup used. A single frequency 1.06 μm laser pulse was collimated and directed into the modulator with vertical, horizontal, or circular polarization. The modulator was driven with RF pulses with peak powers between 10 and 100 W and frequencies from 100 to 140 MHz. At 120 MHz, the first order deflection angle equaled 31.6 mrad, so that the

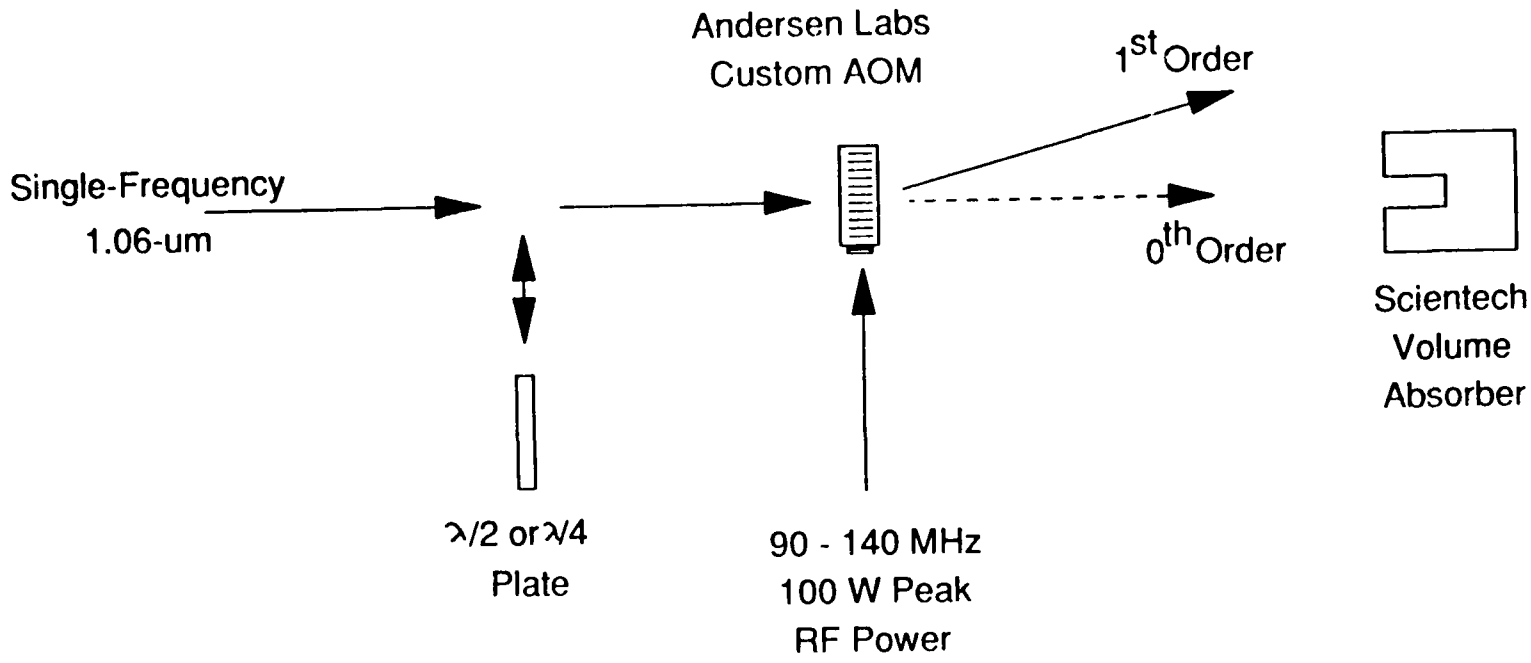

Figure 5.4 Schematic layout of AO modulator characterization apparatus

first and zeroth-order beams could be easily separated to measure the energy diffracted into first order. This was compared to the energy incident on the modulator to obtain the acoustic diffraction efficiency.

Figure 5.5 shows the RF electronics used to drive the AOM. A Q-switch timing signal from the Quantel YAG laser was used to create a 50-Hz train of 400-usec gates, which triggered a frequency synthesizer tuned to the desired AOM frequency. (The 50 Hz rate is necessary only for test purposes, in that the RF power meter will not operate reliably at lower rep rates.) This combination rep-rate and window duration constituted a 2% duty cycle, sufficiently small to avoid having to externally cool the modulator. The 400-usec RF pulses were fed to a high-power RF amplifier, then through a direction coupler and to the modulator. The direction coupler sampled 0.65% of the RF power, which was fed to an RF power meter for average power readings.

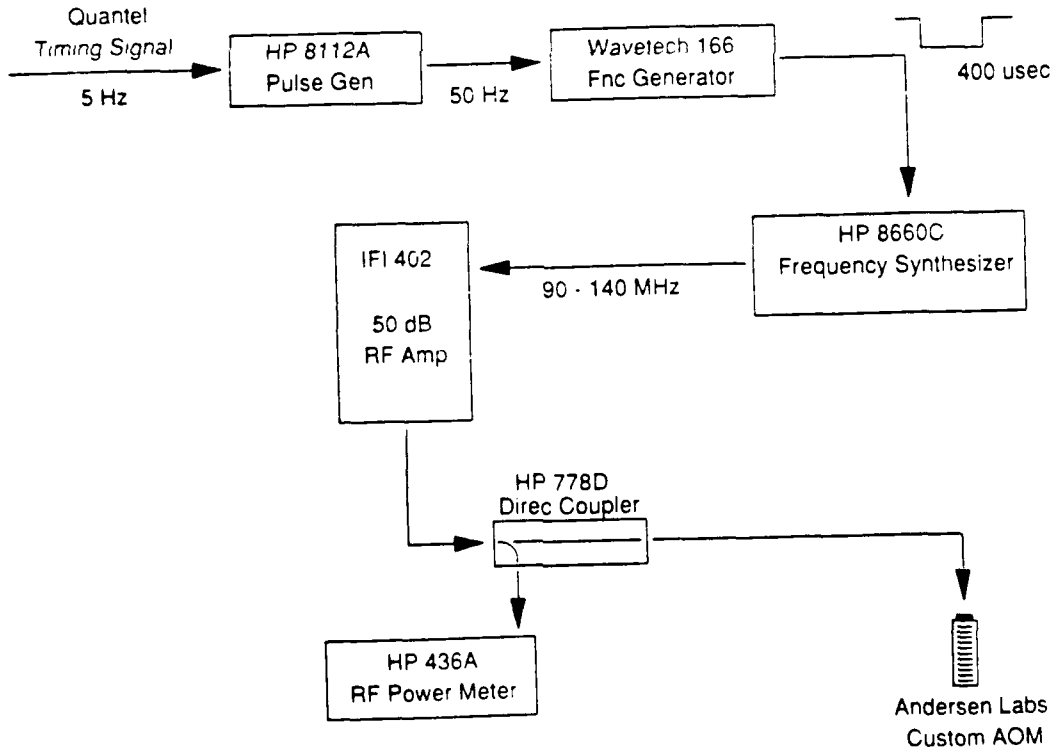

Figure 5.5 Schematic diagram of the AO modulator driver elaectronics

Figure 5.6 shows the results of the diffraction efficiencies vrs. peak RF power for vertical polarization and various RF frequencies. An RF frequency of 110 MHz results in the highest measured efficiencies; at frequencies from 100 to 120 MHz, the modulator gives efficiencies in excess of 90% at a peak RF drive power of 100 W, and efficiencies of 80% or better at all frequencies investigated. Vertical laser polarization was found to give the best diffraction efficiencies. At a frequency of 120 MHz and 80 W peak RF power applied to the modulator, the diffraction efficiency was found to be 90% for vertical polarization, 85% for circular polarization, and 77% for horizontal polarization. These efficiency measurements were repeatable to within 2%.

The first order beam, diffracted by the modulator, may be retroreflected with a mirror, frequency shifted once again, and deflected into the direction counterpropagating to the incident zeroth order beam. This arrangement was implemented on the linear AC MECCA cavity described later. It was verified that the double pass diffraction efficiency of the modulator equals the value that one expects based on the measured single pass values.

The far-field intensity patterns of the laser pulse were recorded under various conditions to ascertain the extent of aberrations imparted by the modulator. The effect of the modulator can be seen in Figure 5.7a, which shows the far-field profile for a beam that has double passed the modulator driven with a peak power of 80 W, and an average RF power of 1.6 W. The result is a vertical elongation of the far-field beam pattern; the power-in-the-bucket beam quality of this pattern is 2.6 times the diffraction limit. The distortion of the beam profile, and in particular the asymmetry is attributable to the fact that heat is being deposited into the glass medium at the sides in contact with the transducer and acoustic absorber, while the top of the glass is in contact with a heat sink. An asymmetric temperature profile therefore exists inside the modulator material. If the modulator is allowed to cool for approximately 5 minutes, the far-field beam profile assumes the shape shown in Fig 5.7b immediately following revival of the RF power.

The ability of SBS to conjugate the aberrations induced by the thermal index variations can be see in Figure 5.7c, which shows the far field profile taken with an SBS cell providing the retroreflection of the first order diffracted beam instead of a conventional mirror. Conditions are otherwise identical to those corresponding to Figure 5.7a. Depending upon the number of round trips the pulse undergoes before SBS conjugation, the distortion evident in Figure 5.7a would be further magnified. To alleviate this effect, the modulator ran with a duty cycle 10 times smaller than that used during the AOM characterization tests (2%). With such a reduced duty cycle, the double pass far-field pattern attains a power-in-the-bucket beam quality that is 1.2 times diffraction limited, resembling the profile in Figure 5.7c.

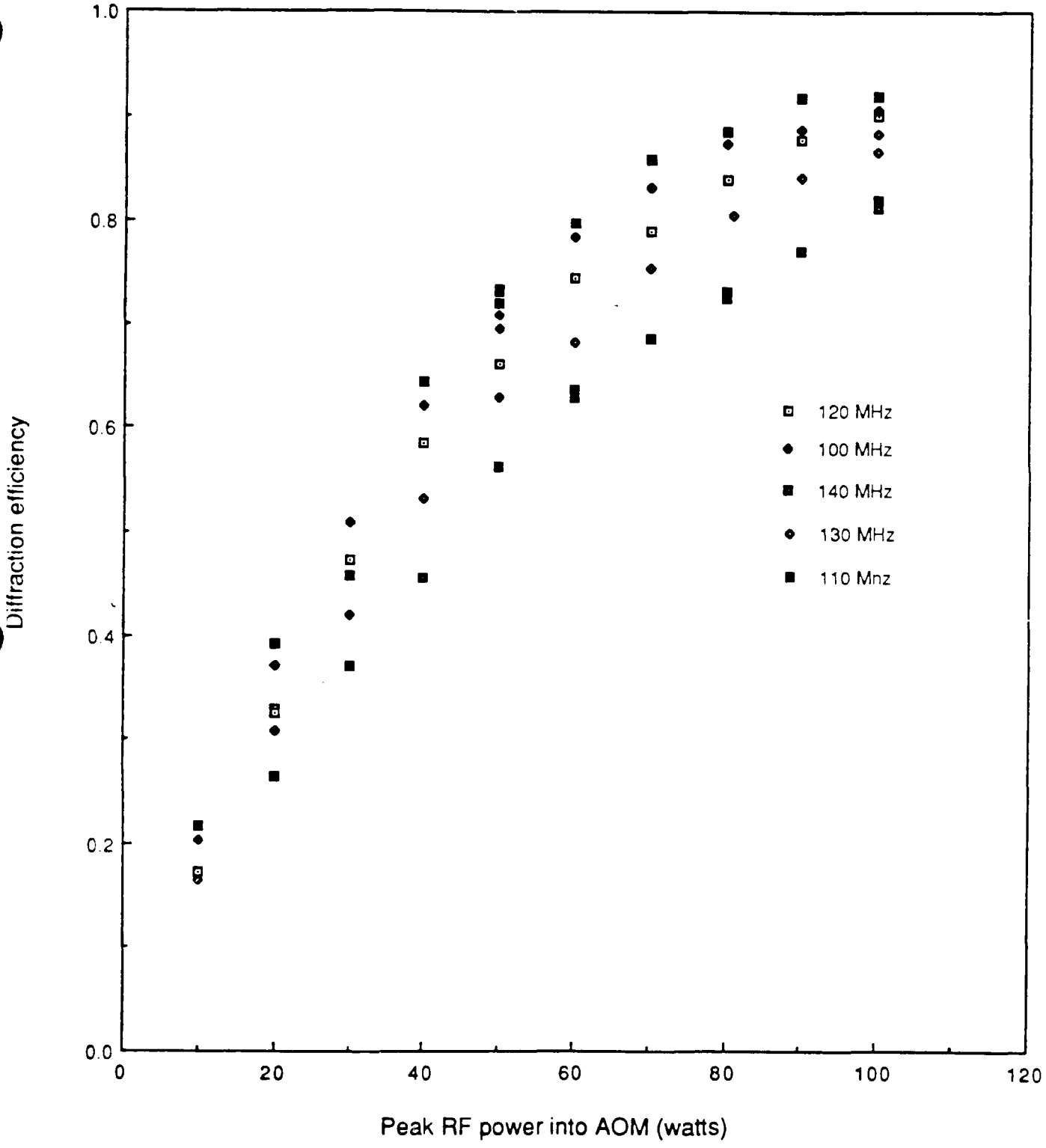

Figure 5.6 Modulator diffraction efficiency as a function of peak power for several RF frequencies

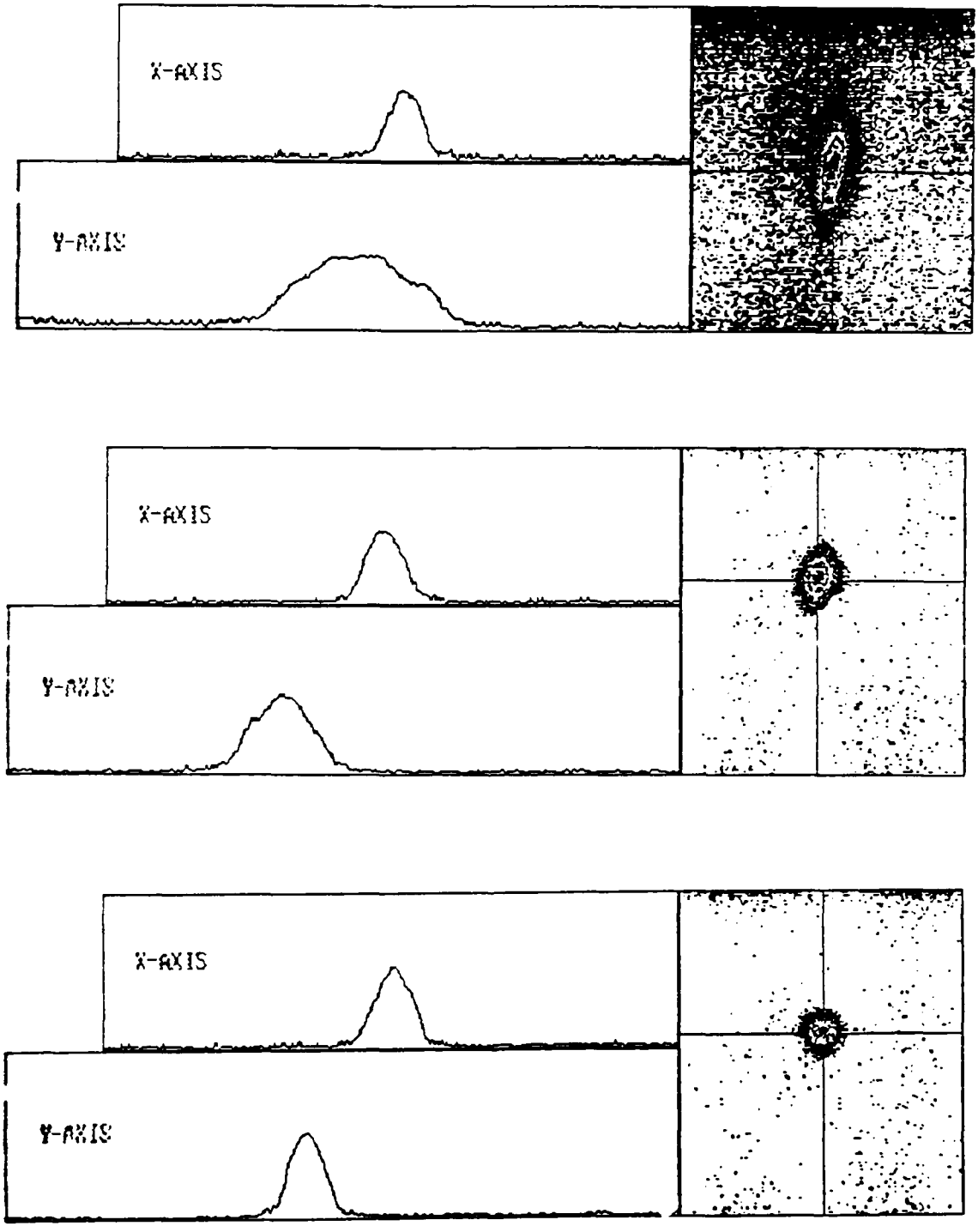

Figure 5.7 Thermal effects in the modulator. a) far-field profile of a beam making a double pass through the modulator operating with a peak power of 80 W and average power of 1.6 W. b) same conditions as a) after the modulator is allowed to cool for five minutes. c) same conditions as a) but using a SBS cell instead of a retro-mirror to correct the induced aberrations.

5.3.2 Cavity Description and Diagnostics

To avoid the difficulties associated with a ring cavity discussed earlier, the AC MECCA demonstration and extraction experiments were performed using a linear cavity similar to the one described earlier. Figure 5.8 is a schematic of the optical layout assembled. A pair of $\lambda/4$ plates, one upstream of the etalon and one inside the cavity, insure that the extracted pulse has a polarization that is orthogonal to the injected pulse, and at the same time, that the polarization of the beam diffracted through the AO modulator is always linear. This is necessary because the difference between the diffraction efficiencies of the two polarizations turns circularly polarized light into elliptical, and a single $\lambda/4$ plate outside the cavity produces circularly polarized light everywhere in the cavity. However, the addition of a second plate inside the cavity, in front of the modulator, insures that the polarization incident on the modulator is always linear but the extracted pulse polarization is orthogonal only on odd numbers of round trips. Two plates surrounding the modulator, in addition to the one outside the cavity, guarantee that both conditions are satisfied on every round trip. Our experimental arrangement used the second option with three round trips prior to extraction

Energy meter E1 samples the initially injected pulse energy, and vacuum photodiodes are positioned to monitor the intracavity pulse train. The cavity gain element was the Nd: glass amplifier rod. An imaging telescope was used to relay the etalon plane onto the cavity end mirror; the telescope employs a loose spatial filter at the focus. The SBS arm contains an expansion telescope to achieve f/10 focussing conditions; the SBS medium is freon-113.

The extracted beam quality was measured using the power-in-the-bucket method similar described earlier for the conventional MECCA. The overall amplification was measured by comparing the extracted pulse energy measured on a photodiode to a reference pulse calibrated to be equal to the injected pulse.

5.3.3 AC MECCA Demonstration and Extraction Experiments

Two frequency matching conditions must be satisfied for the AC MECCA to operate as described above: the SBS frequency shift must match an integral multiple of the etalon free spectral range, and the FSR must match an integral number of AO modulator frequency shifts. These requirements, the operating frequency range of the AOM, the number of round trips desired, and the choice of freon as the SBS medium restrict the

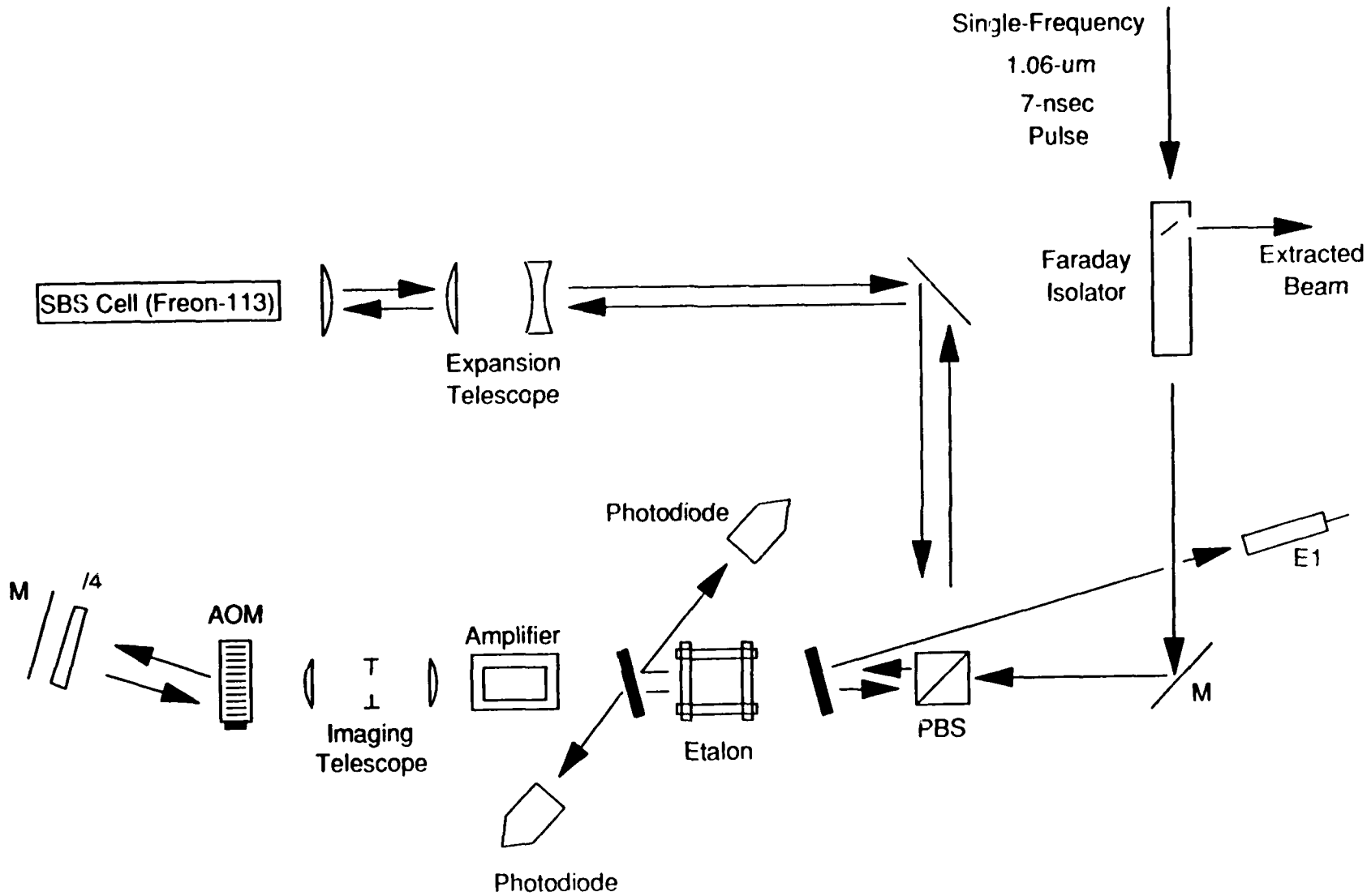

Figure 5.8 Schematic diagram of the linear AC MECCA cavity demonstration layout

selection of the etalon FSR to one of few options. By using a conventional MECCA type cavity, the SBS shift for freon-113 was measured to be 1764 MHz and the number of round trips selected was 6 (3 for each cycle). An etalon with a free spectral range of 588 MHz (25.5 cm long) which is one third the SBS shift, and an AOM frequency of 98 MHz satisfy all frequency matching requirements.

The unavailability of a suitable saturable absorber forced us to adopt several nonideal measures to eliminate parasitic oscillations in the cavity. First, the round trip gain of the cavity was kept at a modest level. The flashlamp timing was adjusted for a double pass gain of 3.7; with the AOM double pass diffraction efficiency for 65%; the etalon reflectivity of 92% (finesse of 6), resulted in a net cavity round trip gain of roughly 2.2. Second, the width of the RF pulse driving the acousto-optic deflector was adjusted to be as small as possible; this width was limited to 30 μs by the RF electronics and third, by tilting the cavity end mirror. The tilt direction was normal to the plane defined by the zeroth and first order diffracted optical beams; hence, it did not affect the diffraction efficiency of the AOM. This tilt, and the proper setting of the telescope aperture, limited the number of amplifying round trips that the parasitic oscillations could undergo. The tilt angle found necessary to suppress parasitic oscillations to an acceptable level was approximately 0.1 mrad. This meant that after three round trips, the angle at which the intended extraction pulse was incident on the etalon equaled approximately 0.6 mrad. Such an angle of incidence translates to an etalon transmission peak that is shifted by 50 MHz; with the etalon FWHM bandwidth of 96 MHz, this places the central frequency of the pulse at the 50% transmission point of the etalon. Figure 5.9a shows the sequence of intracavity pulses for the tilted cavity, in the absence of gain, with the etalon tuned so that the initial pulse is injected for optimum transmission, as usual. The reflection of a fourth pulse is evident; with gain present in the cavity, the energy of this pulse would continue to build and confuse the diagnostics. It was therefore decided to adjust the etalon for optimum transmission of the third (SBS bound) pulse, as shown in Figure 5.9b. The result is a reduced transmission both for the initially injected pulse, which is a trivial matter, but also for the final extracted pulse, which directly effects the extraction efficiency. Comparison of Figs. 5.9a and 5.9b show that the transmission of the injected and extracted pulses is approximately 75% of their ideal value; this factor should be taken into consideration in evaluating the overall gain of the system.

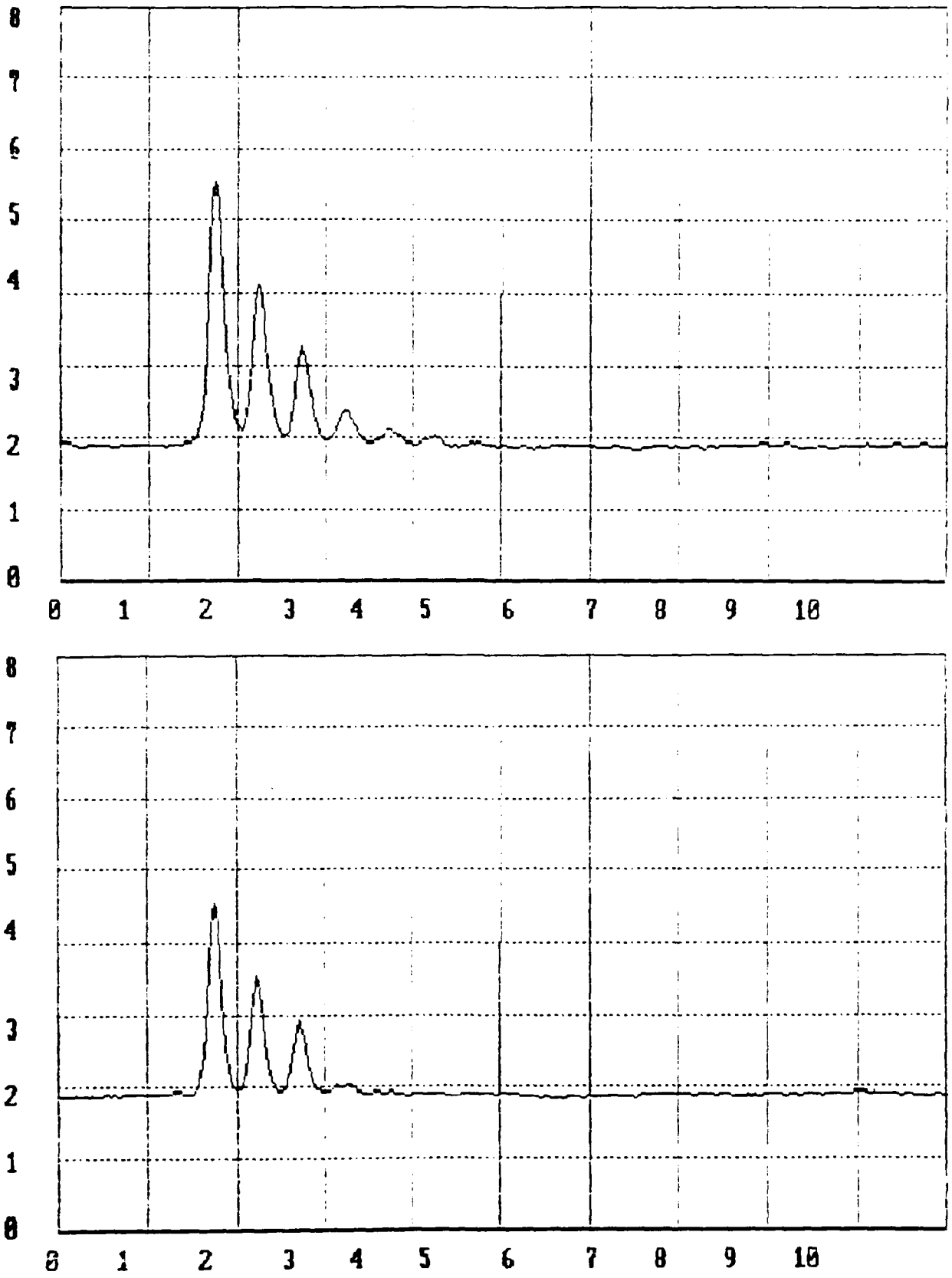

Figure 5.9 Intracavity optical train in the first cycle of the AC MECCA cavity shown in Figure 5.8 without gain. a) cavity is tuned for optimum injection, b) cavity is tuned for optimum extraction after the third round trip.

Figure 5.10 shows the far-field profile of the pulses as they couple through the etalon. With a tilted cavity, the pulse coupled into the SBS arm after three round trips is separated in direction by 2 mrad from the final outcoupled pulse, which has a direction normal to the cavity axis. Correspondingly, the pulses are separated in the far field. The lower spot seen in Figure 5.10 is a sample of the pulse as it couples from the etalon on its way to the SBS cell, while the more intense upper spot is a sample of the extracted pulse.

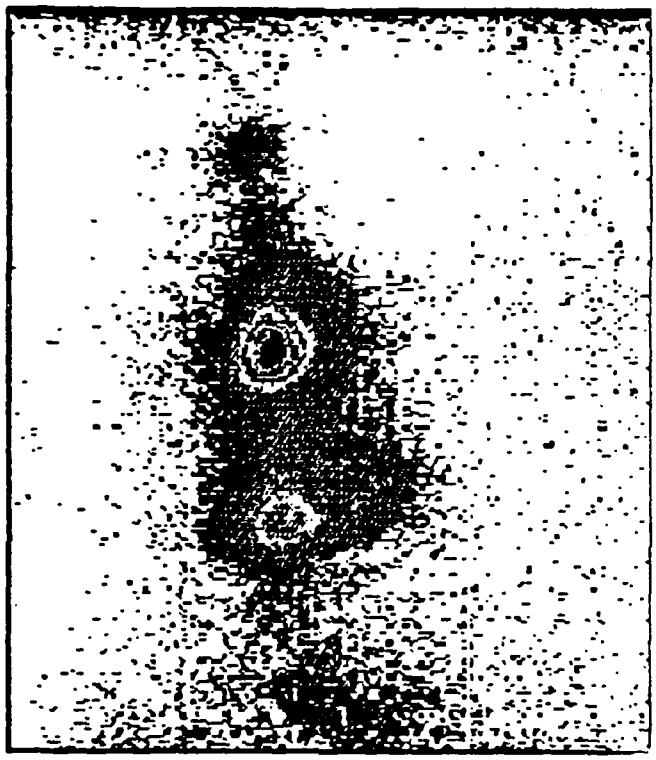

Figure 5.10 Far field intensity profile of pulses extracted from the AC MECCA cavity which is misaligned to prevent parasitic oscillations. The upper spot is a superposition of the input and the final extracted pulse, the lower spot is the pulse extracted after the first cycle

Figure 5.11 shows a digitizer trace of the beam after extraction from the Faraday isolator. This trace shows one intense pulse corresponding to the final extracted beam, along with several weaker pulses corresponding to a portion of the initial injected pulse reflected by the coupling etalon, and fractions of the various intermediate pulses that leak through the coupling etalon and polarizing beamsplitter. The initial energy injected into the coupling etalon was 3.1 mJ. The total energy present in all these pulses is recorded by energy meter E2 and is equal to 126 mJ. From the relative sizes of the pulses appearing in Figure 13, it is estimated that 85%, or 107 mJ of this energy actually resides in the

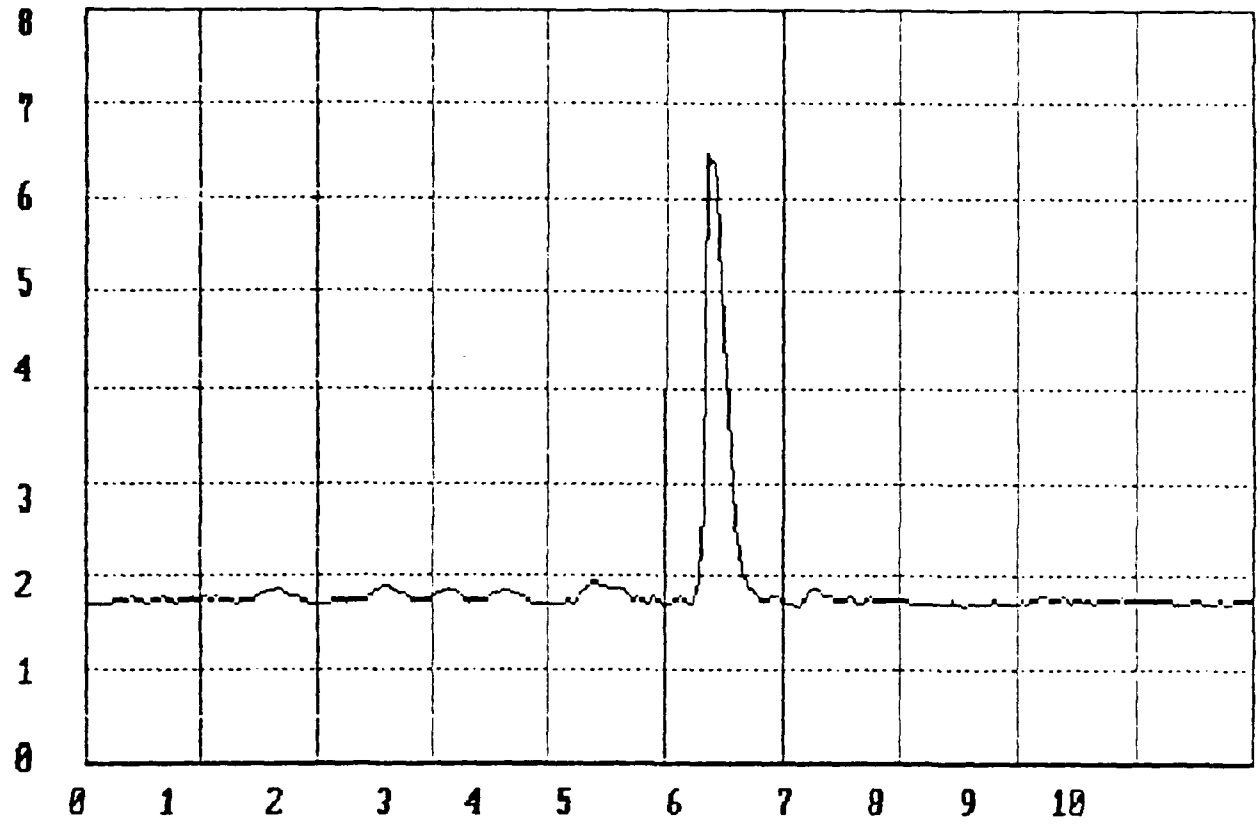

Figure 5.11 Amplification in AC MECCA ; the large pulse is the extracted pulse and on the far left, barely noticeable, is the reference pulse calibrated to match the input from the master oscillator

extracted pulse. This corresponds to a net amplification of 35. If one accounts for the fact that the tilted cavity requires that the etalon be set to transmit only 75% of the extracted pulse, then an overall gain of 46 is estimated for the system.

Similarly, energy meter E3 indicates that the energy in the extracted pulse passed through the 300-um pinhole equals 53 mJ. Since only the initial etalon reflection and the final extracted pulse appear on axis, only these pulses are able to transmit through the pinhole to meter E3. Again from the relative heights of the pulses as they appear in Figure 13, the relative fidelity of the entire AC MECCA system, after a total of six round trips with one intervening SBS reflection, was measured to be 58% corresponding to a beam quality of 1.3 times the diffraction limit. Figure 5.12 is the profile of the near-field intensity pattern for the extracted pulse and evidence of beam breakup such as that seen in the conventional MECCA scheme is absent.

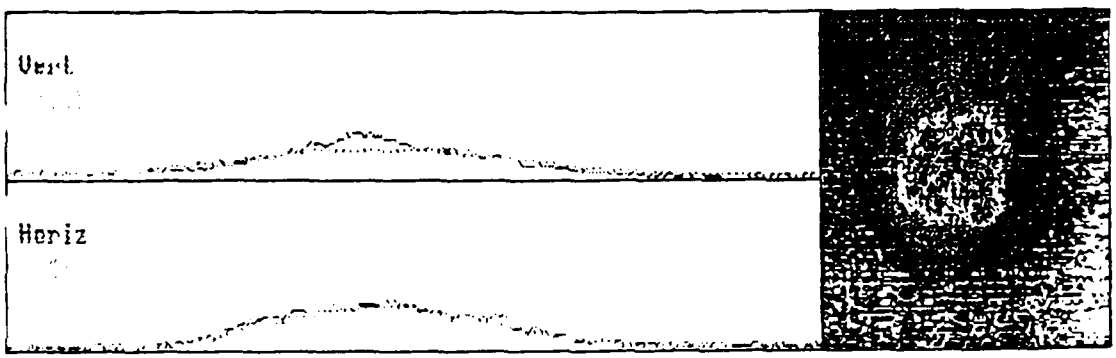

Figure 5.12 Far-field intensity distribution of the amplified pulse which corresponds to a beam quality of 1.3 x D.L.

6. CONCLUSIONS AND RECOMMENDATIONS

The MECCA regenerative amplifier concepts described in this report provide a simple and compact method to extract energy from low gain, high saturation fluence solid state media. The original MECCA concept, called the conventional MECCA, uses SBS as an integrated part of the regenerative amplifier to provide good beam quality, but also to trap the input beam in a multipass cavity formed by the SBS cell and an etalon. It was discovered, that the ability of the SBS medium to reflect pulses in the rapid fire configuration i.e. on timescales longer than the phonon lifetime, but short compared to the thermal equilibration time, is adversely affected by earlier SBS reflections. This has the effect of degrading both the SBS reflectivity and fidelity, leading to poor beam quality and low extraction efficiency. This critical timescale is related to the phonon lifetime of the material, and is the time during which the acoustic grating established by previous pulses decays into non coherent acoustic phonons or heat. Reflectivities and fidelity are observed to partially recover if the MECCA cavity is made so short that the successive pulses partially overlap and the acoustic grating is always driven by the incident fields and not allowed to decay. Short MECCA cavities employing freon as an SBS medium achieved overall gains of 30 and beam quality of 1.8 x D.L. that is a significant improvement over earlier attempts with longer cavities. These experiments also indicate that pulses which are much longer than the cavity round trip time, may provide conditions under which the problems associated with the decay of the acoustic grating may become negligibly small. The apparatus available and time constraints did not allow investigation of these conditions.

An alternate configuration MECCA (AC MECCA) was conceived and tested during the latter stages of the program which circumvents the problem of the decaying acoustic grating by phase conjugating only once, and using an acousto-optic modulator to form the etalon coupled cavity. The concept was demonstrated in the small signal gain regime and produced gains on the order of 40 with good beam quality. Although somewhat more complicated than the conventional MECCA, it is a viable alternative that showed good promise during the preliminary tests. Further experimentation is required to fully assess its potential under high energy, saturated extraction conditions.

7. REFERENCES

1. E. J. Miller, M. D. Skeldon and R. W. Boyd, Applied Optics, Vol. 28, No. 1, 92 (1989)

2. H. Brusselbach, "Near Infrared Phase Conjugate Oscillator", final report AFWAL-TR-88-1123 (1988)

3. Y. R. Shen, "principles Of Nonlinear Optics", John Wiley and Sons, Chapter 7 (1984)

4. R. A. Mullenand J.N. Matossian, Optics Lett. 15 601 (1990)

5. W-H Lee and J-H Kwon, New Phys (Kkorean Phys. Soc.) 25, 436 (1985)